



A Virtual Fixture Design for Teleoperated Vitreo- retinal Surgery: Translating iOCT Distance Measurement to Haptic Feedback

T. Shen

Technische Universiteit Delft

A Virtual Fixture Design for Teleoperated Vitreoretinal Surgery:

Translating iOCT Distance Measurement to Haptic Feedback

by

T. Shen

in partial fulfillment of the requirements for the degree of

Master of Science
in Mechanical Engineering

at the Delft University of Technology,
to be defended publicly on Wednesday October 31, 2018 at 10:00 AM.

Student number: 4620887
Project duration: December 2017 – October 2018
Thesis committee: Prof. dr. ir. D.A. Abbink, TU Delft, supervisor
Prof. dr. ir. W. Mugge, TU Delft
Dr. ir. H. Boessenkool, TU Delft

This thesis is confidential and cannot be made public until October 31, 2020.

An electronic version of this thesis is available at <http://repository.tudelft.nl/>.

Acknowledgement

Over the past two years, I underwent an intensive master training here at TU Delft. The university treated me well, and I have learned a lot. As I now look back, everything was so fulfilling but fast like a dream. However, this is just how it feels like to study at one's dream school, isn't it?

My training in the specialization - Haptics Interfaces - wouldn't be complete without the guidance of prof. David Abbink. He is always able to motivate me when I needed the most and encourage me to pursue excellence. The second year of my master training is a year enriched by Haptics. It all began from my internship at Motekforcelink. I shall not forget to thank my internship supervisor, Piet Lammartse, who taught me a lot of technical knowledge which I, later on, applied to my thesis project. As for the collaboration with PRECEYES, I am grateful for Maarten and Yannick's all-the-time supportive attitude and their critical feedback. My experiment would not be carried out without the help from my daily supervisor, Henri Boessenkool. As a specialist in teleoperation, Henri provided me with practical support with the device and rigorous training in scientific methods.

Last but not least, Delft Haptics Lab is a wonderful place to work at. It's like my second home in Delft. I shall not forget to thank Bastiaan and Timo for their support in statistics. I also gained many useful suggestions from Sarvesh and Shuai throughout my research. The master student fellows at the time is another essential part of my research life. It was very nice to have discussions and get to know what other people in the group are working on. David has supervised many students, so please allow me not to name them one by one. Anyhow, there is one name I have to mention. Although we've only met via Skype, I sincerely thank Laurens Kranendonk. His pioneering work on haptic assistance for robotic vitreoretinal surgery served as a solid foundation for my work.

T. Shen
Delft, October 2018

A handwritten signature in black ink, appearing to read 'T. Shen', with a stylized flourish at the end.

Contents

List of Figures	vii
List of Tables	ix
1 Thesis Paper	1
Bibliography	17
A Needle Steering Haptic Master & Bachmann Controller	19
A.1 Master Device	19
A.2 Bachmann Controller	20
A.3 Hardware Architecture	20
B Simulated Slave Design	21
B.1 Instrument Design	21
B.2 Two Master-Slave Mapping	22
B.2.1 MIS mapping	22
B.2.2 VN mapping	24
B.3 iOCT Simulation Design	25
C Vitreoretinal Simulator	27
C.1 Perfect Sphere as the Eye model	27
C.2 Spherical Coordinate & Target Properties	29
C.3 Peeling Mechanism Model	30
C.4 Functions for Visualization	32
C.4.1 Instrument shadow	32
C.4.2 Membrane color	32
D Virtual Fixture Design Options	35
D.1 Filtering Simulated iOCT	35
D.2 Using PDD as a Passive Virtual Fixture	35
D.3 Active Sense vs. Passive Sense of Distance	36
D.4 Soft PVF + Active Sense of Distance	37
E Extensive Metrics & Results	39
E.1 Extensive Metrics	39
E.2 Complete Paired Sample t-test Table	39
E.3 Experimental Replay	41
F Pilot Study I	43
F.1 Objective	43
F.2 Experimental Design	43
F.2.1 Part (a): Perceptual limit	44
F.2.2 Part (b): Active Sense(AS) vs. Passive Sense(PS)	44
F.3 Metrics & Data Analysis	44
F.4 Main Results	45
F.4.1 Objective 1	45
F.4.2 Additional findings	45
F.4.3 Objective 2	46
F.5 Individual Reaching Profile	47

G	Pilot Study II	55
G.1	Objective	55
G.2	Experimental Condition & Order	55
G.3	Metrics & Data Analysis	55
G.4	Results	56
G.5	Individual Peeling Raw Data	56
H	Informed Consent Forms	61
H.1	Pilot Study I	62
H.2	Pilot Study II	65
H.3	Final Experiment	69
H.4	Personal Information Sheet	74

List of Figures

A.1	CAD of the 3-DoF Needle Steering Haptic Master [1].	19
A.2	Schematic layout of the master device.	20
B.1	3D view of the instrument including its three DoFs.	21
B.2	Visualization of the home position of the instrument and the target workspace. The predefined target workspace is painted in blue, which has the central auxiliary line points from the incision to its center. The incision location is pointed with a purple vector. The α_{slave} is defined as the angle between the shaft and the x-axis.	22
B.3	[a] The 3D view of the reachable workspace using MIS mapping. [b] The top view of the MIS mapping, where the target area is plotted in blue, and the reachable workspace is colored in green.	23
B.4	[a] The 3D view of the reachable workspace of VN mapping. [b] The top view of the VN mapping, where the target area is plotted in blue, and the reachable workspace is colored in green.	23
B.5	Implementation of iOCT simulator in Simulink®.	26
B.6	The outcome of simulated iOCT using simulated true depth.	26
C.1	A 3D view of the eye model: the colored arrows indicate the origin of the global reference and point correspondingly to the direction of the axes. X is in red, y is in green, and z is in blue.	27
C.2	[a] The front view of the eye model. [b] The side view of the eye model.	28
C.3	At this position on the surgical table, a patient's right eye will have its optic disc showing on the left-hand side of the reader. The surgical simulation screen-shot on the right is modified from Eyesi® by VRmagic [2].	28
C.4	The origin of the spherical coordinate is the center of the eye model. An object in this sphere is defined by three parameters: $r, \theta, and \phi$, where θ is the zenith angle and ϕ is defined as the negative azimuth angle.	29
C.5	Criterion for θ depends on current depth. The tolerance of θ increases as current depth decreases.	29
C.6	A point light source is placed inside the eye. The simulated instrument is divided into two segments for implementing Matlab <code>surf</code> function.	32
D.1	On the left side of the figure shows the simulated noised iOCT measurement as opposed to the simulated true iOCT depth. While the outcome after moving-averaging the simulated noised iOCT depth is illustrated on the right.	35
D.2	[a] Traditional virtual fixture renders a wall with a stiff spring which starts slightly before the forbidden region to provide protection. Additional to the forbidden region colored in red, the green area is free from haptic feedback. [b] For a Position-Dependent Damping (PDD), the clear contact transition is replaced by a warning range that increases damping coefficient when approaching the forbidden region.	36
D.3	A comparison between the passive virtual fixture and the linear position-dependent damping.	36
D.4	The active sense consists of the passive virtual fixture (depicted as the blue sphere) and a spring extending from the PVF surface.	37
D.5	The passive sense consists of the passive virtual fixture (depicted as the blue sphere) and a damper extending from the PVF surface.	37
D.6	This method is a combination of AS and PS, where the spring alone is tested with two combinations with two different values of damper.	38

E.1	[a] The averaged safety margin of reaching a small target (sample size = 16). [b] The averaged safety margin of reaching a large target (sample size = 9).	39
E.2	An experimental replay of the third trial of subject 11. The time scale is ten times faster than real time. (This is an mp4 file that can only be viewed in the digital version of the report, please refer to TU Delft online repository.)	41
F.1	Puncture rate of target reaching with different ring sizes under baseline condition. . . .	44
F.2	The completion time of reaching targets with different sizes under baseline condition. .	45
F.3	[a] Precise time of reaching targets with different sizes. [b] Approach time of reaching targets with different sizes.	45
F.4	The standard deviation of the execution time in precise phase under baseline condition.	46
F.5	Puncture rate of target reaching with different haptic conditions.	46
F.6	The completion time of 0.3mm target reaching with different haptic conditions. The arrows illustrate the order of how the gains are given.	46
F.7	The approach phase time of 0.3mm target reaching with different haptic conditions. . .	47
F.8	The precise phase time of 0.3mm target reaching with different haptic conditions. . . .	47
F.9	Subject 1: Velocity profile in pilot study 1 (a).	48
F.10	Subject 2: Velocity profile in pilot study 1 (a).	48
F.11	Subject 3: Velocity profile in pilot study 1 (a).	49
F.12	Subject 4: Velocity profile in pilot study 1 (a).	49
F.13	Subject 1: [a] Velocity profile in pilot study 1 (b). [b] A zoom in of [a] with the 0.3mm target and haptic assistance visualized. The baseline condition in pilot 1 (a) is plotted as gray lines for comparison.	50
F.14	Subject 1: [a] Velocity profile in pilot study 1 (b). [b] A zoom in of [a] with the 0.3mm target and haptic assistance visualized. The baseline condition in pilot 1 (a) is plotted as gray lines for comparison.	51
F.15	Subject 3: [a] Velocity profile in pilot study 1 (b). [b] A zoom in of [a] with the 0.3mm target and haptic assistance visualized. The baseline condition in pilot 1 (a) is plotted as gray lines for comparison.	52
F.16	Subject 4: [a] Velocity profile in pilot study 1 (b). [b] A zoom in of [a] with the 0.3mm target and haptic assistance visualized. The baseline condition in pilot 1 (a) is plotted as gray lines for comparison.	53
G.1	The upper box plot shows the overall puncture rate of the two subjects. The mean values from the two trials in the four conditions of each participant are linked. The overall puncture rate can be broken down into the puncture rates of the three sub-tasks. Depicted from left to right are 'Small Target,' 'Large Target,' and 'Peeling.' The red line in the box plot represents the median.	56
G.2	[a] Depicts completion time for each sub-task under the four conditions. [b] Bar plots of precise/approach phase time for 'Small Target,' where data of the two subjects are plotted as gray dots (sample size = 2*2 for each condition). [c] Bar plots of precise/approach phase time for 'Large Target.' Note, the sample size is smaller than 'Small Target' since one of the subjects didn't penetrate the retina during peeling.	56
G.3	Subject 1: [a] Peeling data under the baseline condition. [b] Bar plots of precise/approach phase time for ted in gray dots (sample size = 16*3). [c] Bar pl	57
G.4	Subject 2: [a] Peeling data under the baseline condition. [b] Peeling data under the 'PDs' condition. [c] Peeling data under the 'PDw' condition. [d] Peeling data under the 'P' condition.	58
G.5	Subject 3: [a] Peeling data under the baseline condition. [b] Peeling data under the 'P' condition. [c] Peeling data under the 'PDw' condition. [d] Peeling data under the 'PDs' condition.	59
G.6	Subject 4: [a] Peeling data under the baseline condition. [b] Peeling data under the 'P' condition. [c] Peeling data under the first 'PDs' condition. [d] Peeling data under the second 'PDs' condition.	60

List of Tables

A.1	Master device properties	20
B.1	Slave workspace properties	21
B.2	Slave properties	22
B.3	Virtual needle properties	24
B.4	Algorithm: Gauss-Newton iteration	25
C.1	Eye model properties	28
C.2	Algorithm: Target-reached Criteria	30
C.3	Membrane model parameter settings	30
C.4	Algorithm: Membrane peeling mechanism	31
C.5	Lighting property	32
C.6	Algorithm: Instrument shadow projection	33
C.7	Function: Membrane force-color mapping	33

1

Thesis Paper

The main contribution of this thesis project is condensed in a journal paper form. Extensive information is supplemented in the appendixes, with the following structure: Appendix [A](#) describes the hardware used in this research. Appendix [B](#) and [C](#) describes how the simulator is set up. Appendix [D](#) lists several haptic feedback methods that have been tested. Extensive metrics and the corresponding results are given in Appendix [E](#). Appendix [F](#) and [G](#) documents the results of the two pilot studies. Appendix [H](#) are the inform consents used in this research.

The title of the thesis paper –*“Haptically-Augmented Telerobotic Vitreoretinal Surgery: A robust virtual fixture design for Epiretinal Membrane Peeling”*– is adjusted to be more specific than the report title for the convenience for scholars to find this paper on the search engine. The vitreoretinal surgery this project focused on is the peeling of Epiretinal Membrane (ERM) and Internal Limit Membrane (ILM). Moreover, the proposed virtual fixture design applies to noisy sensory input other than iOCT measurement. Therefore, these keywords are emphasized in the paper title.

Haptically-Augmented Telerobotic Vitreoretinal Surgery: A robust virtual fixture design for Epiretinal Membrane Peeling

T. Shen*, H. Boessenkool*, Y.G. M. Douven[†], and D.A. Abbink*,

*Cognitive Robotics Department, Delft University of Technology, Delft, The Netherlands

E-mail: T.shen@student.tudelft.nl

[†]Eindhoven University of Technology, Eindhoven, The Netherlands

E-mail: Y.G.M.Douven@tue.nl

Abstract—Epiretinal Membrane Peeling (EMP) is a common vitreoretinal surgery in clinic. Over the past twenty years, telerobotics has been developed to assist retinal surgeons. Robot-assisted surgery can aid the surgeon by motion scaling and filtering out natural hand tremor. However, the additive precision has yet to relieve the surgeon from the burdensome task entirely, and teleoperation comes with a downside of extending execution time.

One of the complicating factors in robot-assisted EMP surgery is the limited depth perception afforded by the binocular microscope, which increases the risk of inadvertent contact of the surgical tool with the retina. Recently, PRECEYES has introduced an intraoperative sensor that measures the distance to the surface of the retina to their surgical system. The master device is capable of force feedback, which can be employed to transmit distance information to the surgeon without extra burden to the already visually overwhelmed task.

This study aims to design and evaluate haptic assistance for teleoperated EMP based on noisy distance sensor. Sixteen subjects with non-medical background participated in the human factors experiment performing a simulated vitreoretinal surgery by using a 3-DoF haptic master device controlling a simulated slave robot. All subjects performed two experimental conditions (with and without haptic assistance) in a balanced order. The experimental result shows that, with haptic assistance, the overall puncture rate reduces from 9.6% to 2.8% and peeling forces are stabilized significantly. Which indicates that the proposed method utilizes distance information in a promising way, thus reducing the difficulty of the teleoperated task.

1. Introduction

Vitreoretinal surgery remains as one of the hardest surgeries at the present time. In a typical procedure, the surgeon peels off a thin membrane right on top of the retina with extremely high attention. The limited space and delicate structure of the eye restrict the maneuverability of the instrument inside the eye. Moreover, most of the forces happening are below the $7.5mN$ perceptual threshold [1]. These difficulties make qualified retinal surgeons hard to train and limit their career lifetime to their 50's. Despite their

skill and experience are still improving, the physiological tremor due to aging forces them to stop.

Two decades ago, the Jet Propulsion Lab in the US carried out micro-surgery using a telerobot [2]. Since then, surgical robots have been developed to assist vitreoretinal surgeries but remained in the stage of animal or in vitro testing. In June 2018, PRECEYES achieved the world's first human test with their teleoperated system [3]. PRECEYES Surgical System enhances the surgeon's skill with additive precision, while the surgeon can still guide the surgery leveraging their knowledge and experience [4], which has a great potential to extend the boundary of what current medical technology can achieve.

This master thesis project is in collaboration with PRECEYES B.V., a spin-off company at Eindhoven University of Technology, aimed to explore promising human-machine interfaces for PRECEYES Surgical System.

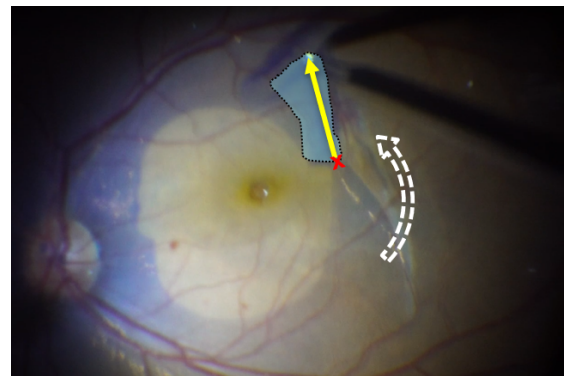


Figure 1. A screenshot of Dr.Sandeep Bachu manually performing an Internal Limit Membrane (ILM) peeling surgery. The red 'x' marks the attaching point of the membrane being peeled (the highlighted blue area), and the yellow arrow is an approximated line of action of the force applied to it. The circular peeling motion spiraling around the fovea is illustrated with the white dashed arrow. The image is retrieved and modified from Prime Retina™ Eye Care Centre [5].

1.1. ERM & ILM Peeling

The growth of Epiretinal Membrane (ERM) is an age-correlated retinopathy. ERM is a scar-like tissue that de-

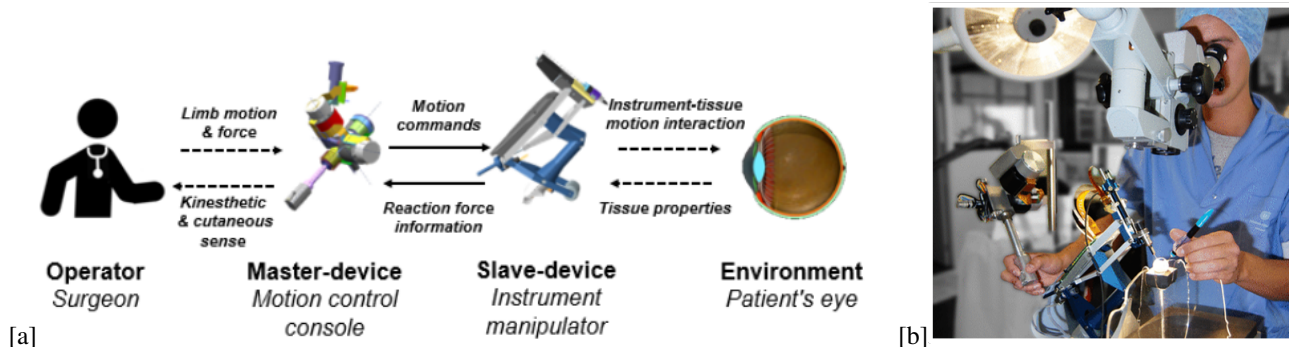


Figure 2. [a] Human in the loop teleoperation block diagram of PRECEYES Surgical System. [b] Image of a surgeon operating PRECEYES Surgical System ©PRECEYES BV.

velops in response to changes in the vitreous humor, which might distort vision and, in some extreme, detach the retina.

Epiretinal Membrane Peeling (EMP) has become a routine procedure to cure this disease since the 1980's. To guarantee a complete removal, a normal retinal layer underneath ERM called Internal Limit Membrane (ILM) is suggested to be delaminated. ILM is a $5\mu\text{m}$ -thick membrane that separates the retina from vitreous humor. Risk of complication and ERM regeneration are reported lower with the combination of ERM and ILM peeling. Figure 1 shows an image of ILM peeling. Generally, ERM and ILM peeling surgery consist of three steps:

Step 1: Vitrectomy

Most of the vitreoretinal surgeries start with vitrectomy (i.e., vitreous + removal), and EMP is no exception. Three incisions are made to insert an intra-illuminator to light up the posterior eye, a vitrector to cut out the gel-like vitreous (humor), and a cannula to transport the replacement for vitreous and maintain the pressure to support the eye. At the end of vitrectomy, ILM is dyed with indocyanine green or membrane blue for better visibility.

Step 2: Flap Initiation

Next, the vitrector is replaced with a pick to initiate an edge for peeling. A pick is a probe with a curved tip which is attached with a sharp blade. By a back and forth cutting motion, the ERM (with a medium thickness of $60\mu\text{m}$) is elevated from the retina (with thickness $100 - 320\mu\text{m}$) until the flap is large enough to be grabbed using forceps. Some advanced forceps have a blade at the tip, so there is no need to switch between a pick and forceps.

Step 3: Membrane Peeling

Although the purpose of peeling is to remove ERM covering the fovea, which is the most light-sensitive part of the retina, starting a flap right on the fovea could risk causing irreversible damage. Therefore, a widely accepted technique is to initiate the flap a few (optic) disc diameters from the fovea and to peel off the membrane with a circumferential motion [6]. This motion is highlighted in a white dashed arrow depicted in Figure 1. In typical

cases, peeling involves several repetitions of releasing and re-grabbing the flap, such that the membrane can be peeled at a small angle (as opposed to perpendicular to the retinal surface). Distance to the retina is suggested to be kept smooth and constant around 0.5mm during peeling [7].

1.2. PRECEYES Surgical System

PRECEYES Surgical System is a teleoperated robot designed for vitreoretinal surgery. It features a remote center of motion such that the instrument can pivot around the incision without scratching the sclera. The surgeon holds the motion control console (master device) to control the slave robot called the instrument manipulator on the remote side. Figure 2 [a] shows the block diagram of the human-in-the-loop teleoperated vitreoretinal surgery.

1.2.1. Teleoperation. Tremor filtering is not a feature exclusive for PRECEYES Surgical System. However, compared to its counterparts at the time (the hand-held robot, Micron [8], and the co-operative Steady-Hand Eye Robot [9]), the physical separation of the instrument from the surgeon's hand facilitates motion scaling (by a factor of 10) and opens up design opportunity for better ergonomics. The shortcoming of the disconnection of a sense of maneuvering can be compensated or even overturned by restoring force feedback to the control console. Two mainstream concepts in the field of haptic feedback for teleoperation are natural force feedback and augmented (artificial) force feedback. The original design of the control console of PRECEYES Surgical System is capable of providing force feedback on all of its controllable DoFs [7].

1.2.2. OR Setup. In the Operation Room (OR), the base of the surgical system is anchored to a standard surgical table. The instrument manipulator can be rotated and flipped over to approach the patient's eye. Once the adjustment is made, this rotation will be fixed, leaving no relative motion of the remote center of motion. PRECEYES Surgical System is operated in a hybrid manner, where the surgeon controls the robot with the motion control console with one hand and holds an intra-illuminator with the other. Figure

2 [b] shows an image of a surgeon operating the system. Beneath the surgical table are foot pedals for microscope and vitrectomy. Medical staffs can switch between different control modes and functions using the touchscreen mounted with the electronics cabinet near the surgical table. Based on the patient (cases), a successful vitreoretinal surgery takes around 1–3 hours, including sterilization, anesthesia, setting up the system, and the actual operation.

1.2.3. Intraoperative Optical Coherence Tomography.

Vitreoretinal surgeries are performed by surgeons looking into the posterior eye through the pupil using a stereomicroscope. Depth perception is limited and not solved by the intervention of robotic systems [10]. Optical Coherence Tomography (OCT), is an interferometry technology that uses light as sonar to measure the distance to the retina. It has been employed in ophthalmology for 25 years. Once used as a diagnostic tool from outside the eye, OCT is now capable of real-time measurements inside the eye.

An intraoperative OCT (iOCT) has been installed on PRECEYES Surgical System. The sensor probe is attached to the instrument with a negligible tilting angle, which measures distance in the shaft direction up to a range of 3mm. With a machine learning method trained by an off-line database and the $5\mu\text{m}$ precision of the robotic system, an accuracy of $40\mu\text{m}$ within 99% of scans is achieved [11]. Based on these specifications, the iOCT simulator is built in section 2.1.1.

Visual display as feedback for sensory information does not comprehensively reduce the workload of the already visually occupied task. Auditory feedback is one of the options, but it is not optimal, for the background of the operation room is noisy [12], and the medical staffs have to communicate with each other. Haptic feedback is a prospective method surpassing the two perceptual channels [13], is exclusively applicable to teleoperation, which will be discussed in the following sub-section 1.3.

1.3. Related Work on Haptic Assistance

The scope of this research focuses on artificial force feedback as opposed to natural force feedback. For the purpose for installing an iOCT sensor probe is to prevent retinal puncture, haptic assistance is meant to provide support before surface contact. Therefore, restoring or magnifying tissue interaction forces are not of interest. Early in the 90's, Rosenberg proposed Virtual Fixture (VF) to aid teleoperation [14]. VFs are basically abstract perceptual overlays imposed on top of the task environment. In teleoperated EMP, VF can be a protection for the retina. However, traditional VF renders a solid wall by a stiff spring, which requires a sensory input with high signal-to-noise ratio; otherwise, the wall will vibrate and lead to contact instability. This is not feasible with the current iOCT precision.

Instead of using a distance sensor, Steady-Hand Eye Robot built at John Hopkins University uses a force sensor built-in at the tool tip. Leveraging its admittance-typed robot feature, a virtual fixture protecting the retina is achieved

by variable admittance (damping) and cutting off command force [15]. Similarly using damping, a linearly increasing damper field (depicted in Figure 3) using iOCT information was designed by Laurens and tested with human factors experiment at Delft Haptics Lab [16]. Laurens' experimental result showed that participants use the Position-Dependent Damping (PDD) to sense the distance while approaching the retinal surface. Inspired by "variable admittance" used

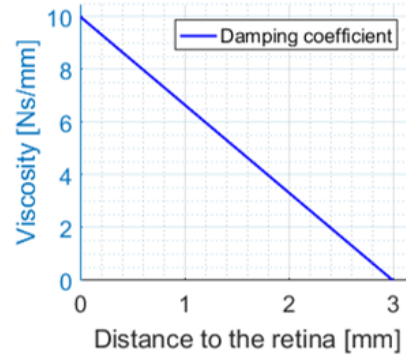


Figure 3. The Position-Dependent Damping (PDD) in Laurens' research [16] is a (one-sided) damper field in the axial direction of the iOCT sensor probe, which linearly increases the damping coefficient after entering the 3mm range.

by Steady-Hand Eye Robot, rendering a wall with PDD is feasible by ramping up the damping coefficient when approximating the virtual fixture. Nevertheless, this approach raises safety concern that a damper cannot provide a solid stop. Especially for PRECEYES, the feedback force of the impedance-controlled motion controller is limited by the maximum output of the device.

In a research study on teleoperation for ophthalmology [17], a method called "feature extraction" is suggested by the authors. By altering the 'force feeling' passing through different impedance bound, the effect of haptic assistance can be enhanced. In one of their proposed methods, an enlarged virtual fixture was imposed on the workspace to predict an event before a collision and to provide haptic cues accordingly. The virtual fixture used in this master thesis project is designed based on these methods described in literature [18].

1.4. Problem Statement & Research Objective

The primary problem is the difficulty of current teleoperation for EMP. Despite the benefit of motion scaling and tremor filtering brought by telerobotics, the risk factors of the task environment have not been ameliorated. To what extent depth can be perceived dictates the difficulty of the task. Hence, PRECEYES integrated an iOCT sensor probe to their system. However, how this additional information can be fed-back to the surgeon remains unresolved. A secondary problem is time. Execution time is reported 2 – 3 times longer with teleoperation [10], [19], which is a consequence

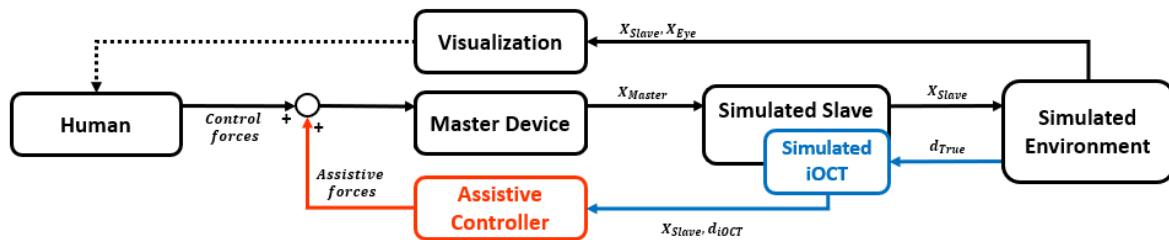


Figure 4. Block diagram of the used test-setup: The operator interacts with the simulator with visualization on the desktop computer and the force feedback from the haptic master device. The assistive controller calculates assistive forces using the states of the simulated slave and the iOCT signal (d_{iOCT} is generated using the simulated true distance measurement d_{True} in the simulated environment). The simulated environment consists of the retina and a simplified membrane in an eyeball.

of motion scaling. The operator has to scale up his/her motion compared to that during manual vitreoretinal surgery.

To continue Laurens' research, the Vitreoretinal Simulator has been extended by including a membrane peeling model, and the effect of iOCT variance has been incorporated. The objective of this research is to realize and evaluate a robust virtual fixture design (against noisy sensory input) for PRECEYES Surgical System. A human factors experiment is conducted to answer the following research question: "To what extent does the Virtual Fixture (VF) improve teleoperated Epiretinal Membrane Peeling (EMP) in terms of performance, workload, and execution time?" It is hypothesized that with the aid of VF: 1. The puncture rate decreases; 2. The peeling force is more stabilized; 3. The workload reduces; 4. The execution time shortens.

1.5. Approach & Outline

A simulation of retina surgeons performing teleoperated EMP surgery is established using the model architecture shown in Figure 4. The proposed haptic assistance is tested by participants operating the haptic master device controlling a simulated slave robot in a simulated EMP surgical context. The research approach consists of four parts described in the following sections:

- 2.1 Simulation Development
- 2.2 Simulation Validation
- 3 Haptic Assistance Design
- 4 Human Factors Experiment

The experimental results are given in section 5. Followed up, in section 6, is the discussion regarding the statistical analysis of the experimental results. The outcome of this research is bullet-pointed in section 7.

2. Simulation of Teleoperated EMP

2.1. Simulation Development

For accessibility, the subject group was predetermined to be people without medical background. Therefore, apart from the selection of the haptic master, the development of

the EMP Simulator (i.e., simulated slave + simulated environment + visualization) is where the main design activity is undertaken. The EMP Simulator has to be easy enough for subjects to learn and trigger the key motions that the surgeon would perform in the real surgery. After the frame of the EMP simulator was carried out, model parameters and haptic assistance method were determined by iteration. Self-experiments and two pilot studies were conducted before the final experiment.

Pilot study 1 consists of two parts (a and b) which both focus on target reaching task. The purpose of the two parts are: (a) The determination of a critical target size for the baseline condition; (b) The first selection round for haptic assistance. Pilot study 2 was conducted for fine tuning the model parameters and haptic gains. The design considerations and simplification of the simulated EMP are as described:

Close to Retina

In real EMP surgery, the surgeon has to interact with tissue that is close to the retina constantly. To meet this design specification, two mechanisms are implemented. Ring-shaped target is designed to trigger the motion of flap initiation and re-grabbing flaps. While to motivate participant to stay close to the retina during peeling, a simplified peeling model is implemented (see next point). The mechanism restricts the participant to peel off the membrane at a small angle. Thereby, forcing them to stay close to the retina.

Peeling Motion

Peeling motion is the most characteristic motion to be simulated. Due to the complexity and variation between patients, a realistic ERM model has yet been developed. However, within the scope of this research, a model of a thin polymer (as described in section 2.2.2) is sufficient to trigger the desired motion. Moreover, the peeling motion has to follow a circular path. Therefore, a simple circular visual path guide is given to trigger a circular motion.

Depth Perception

The accessibility to depth information determines the difficulty of current robotic-aided EMP. However, this does

not imply there is no way to perceive depth. Surgeons have developed techniques using light and shadow to precisely estimate depth inside the eye [7]. Therefore, a simple point light shadow mechanism is implemented in the simulator to provide quasi-equivalent depth perception.

Microscopic Force

Although 75% of forces happened during vitreoretinal surgery are below human perceptual limit [20], the surgeons also developed ways to estimate applied force. One of which is by visual cues. The subtle change in appearance and deformation of the tissue reveal force information [21]. Retinal surgeons use the vascular movement as a warning signal to release and re-grasp the membrane [6]. To provide equivalent visual information, membrane force is reflected on the color change of the membrane. The visualization design is described in section 2.1.4.

2.1.1. Master Device. The Needle Steering Haptic Master [22] was used for this research. It has 3 degrees of freedom (2 rotation, 1 translation) with appropriate operation range (rotation: $\pm 20^\circ$; translation: $300mm$). PRECEYES Surgical System has 4 DoFs to manipulate the instrument. The fourth DoF is the rotation of the shaft in its axial direction, which enables finer surgical motion. However, the simplification of not including this DoF reduces variability in participation behavior, which is beneficial to human factors experiment where participants are not medical professions.

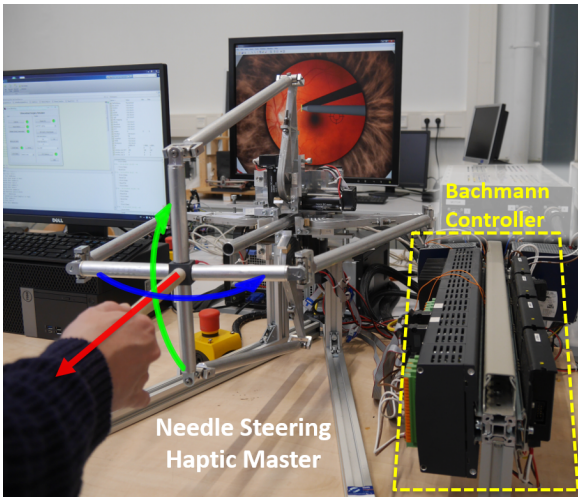


Figure 5. An overview of the experimental set-up. The Needle Steering Haptic Master has three DoFs that can be manipulated by the operator. The Bachmann controller (of the haptic master) is on the right side.

2.1.2. Simulated Slave with iOCT. The simulated slave is a retinal pick inserted into the eye with three degrees of freedom: a translation in shaft-direction, two rotations: α and β . Instead of a direct scaling from the master to the corresponding DoFs of the slave, a position mapping

leveraging the vantage point of Needle Steering Haptic Master is used. First, the tip position of a hypothetical needle on the master-device is scaled down in Cartesian space. Next, the tip position is aligned with the instrument tip of the slave in the simulated environment. Through the end-point position, the orientation and translation of the simulated slave are solved by Gauss-Newton iteration. This mapping is much similar to PRECEYES' master-slave mapping, where the inverse motion due to minimally invasive surgery (MIS) is solved, and the motion scaling factor is decoupled from depth.

Compared to the $1000Hz$ update rate of the haptic master, iOCT sensor probe updates typically with $20Hz$. Therefore, the simulation of iOCT signal starts by zero-order-holding (ZOH) the simulated true depth every other 50 updates on the Bachmann (haptic master) controller. By assuming the noise to be normally distributed within the range of $\pm 40\mu m$, where we have the target membrane $10 - 100\mu m$, Gaussian noise spanning between ± 0.5 small target size is added to the ZOH depth to simulate iOCT signal. The outcome of the simulated signal is plotted in red in Figure 9.

2.1.3. Simulated Environment. The eye is modeled as a perfect sphere, which brings the benefit of defining objects in its spherical coordinate system and reduces complexity when calculating the normal vector of the surface. Peeling

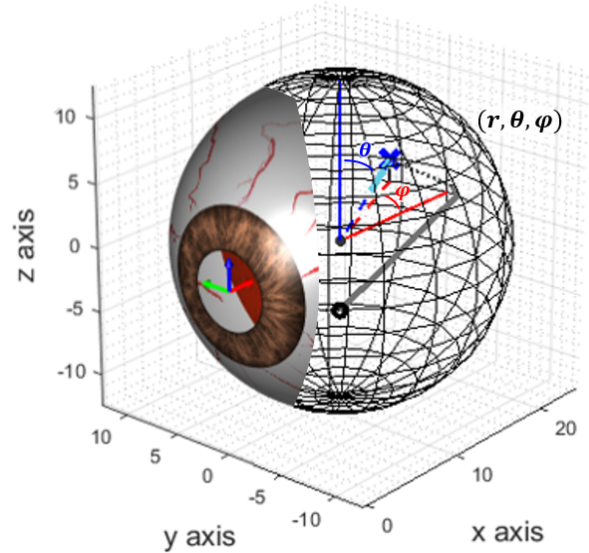


Figure 6. A sectional view of the eye model. With radius, zenith angle θ , and horizontal angle ϕ , the peeling proxy (blue 'x') is defined. The surface normal vector of the proxy is colored in light blue, which always points to the center of the sphere. The colored arrows indicate the origin of the Cartesian global reference, where the x-axis is in red, y-axis in green, and z-axis in blue.

proxy and ring targets are placed according to the spherical

coordination. Figure 6 illustrates a sectional view of the eye model. Angle θ is defined as the zenith angle in the sphere, while angle ϕ is defined relative to x-axis with right-hand rule. Also, the instrument in gray indicates where the incision is made. An experimental simplification for peeling proxy is that it moves only towards right-half sphere (in negative ϕ direction).

2.1.4. Visualization. Materials from section 2.1.1 to 2.1.4 build up a simulator for teleoperated EMP. To provide a convincing environment, a real retina image is used as a static background. The scale is adjusted referring to surgery videos and commercial simulators. As for dynamic visual cues, the shadow of the instrument and a color change of the membrane are implemented. The shadow is generated by a point light source inside the eye using ray tracing. Figure 11 shows the outcome of the shadow generation. The color of the membrane reflexes the applied force. To reduce the learning process for participants, the color-mapping is a simple "blue-to-red" transition, which is made more obvious. Figure 7 shows the relation between peeling angle to minimum peeling force and the force-color mapping as a bar on the side.

2.2. Simulation Validation

Combining the key features of EMP (section 1.1) and the design specifications of the simulator (section 2.1), the validation of the simulation focuses on three aspects:

2.2.1. Target Reaching. There are two different sizes of rings for target reaching. The small ring (radius: $0.25mm$) is designed to simulate the flap initiation process, where the target membrane is still attaching to the retina. The large ring, having a radius of $0.5mm$, is to simulate the re-grabbing motion after releasing the membrane, where the membrane has some edges been made easier to grasp. The dimensions of the target are determined by pilot study 1 (a), where various sizes of rings (from $0.6 - 0.2mm$) were tested under baseline condition. The result indicates that $0.3mm$ is a performance threshold using pure visual perception. Conducted with pilot study 1 (a), pilot study 1 (b) tested the first few candidates for haptic assistance, where the participants were asked to reach $0.3mm$ targets with several haptic conditions. The participant behavior of reaching the target was validated in pilot study 1 (a and b). The task instruction was tested to be clear, and the desired behavior was triggered.

2.2.2. Constant Distance. The peeling model used in this research simplifies ERM to a long thin rectangular polymer membrane. As visualized in Figure 7, the minimum force required to overcome the adhesion increases as the peeling angle approximates 90° , i.e., pulling the membrane vertically. The threshold breaking the membrane is set to $7.5mN$ —the same force level as the perceptual limit. Therefore, the safety margin of the peeling force is larger when the peeling angle is kept small ($< 60^\circ$). This mechanism restricts the

participants to stay close to the retinal surface, and together with the lower bound for penetration detection, the distance is forced to be kept between the two bounds. The peeling model has the following equation [23]:

$$\left(\frac{F}{b}\right)^2 \frac{1}{2dE} + \frac{F}{b}(1 - \cos(180 - \theta)) - R = 0 \quad (1)$$

, where the experimental constant R is used for fine-tuning after setting the dimension of the membrane (width: $b = 10^{-3}mm$; thickness: $d = 10^{-4}mm$) with a reasonable Young's modulus $E = 9 * 10^5 N/mm^2$ for a polymer.

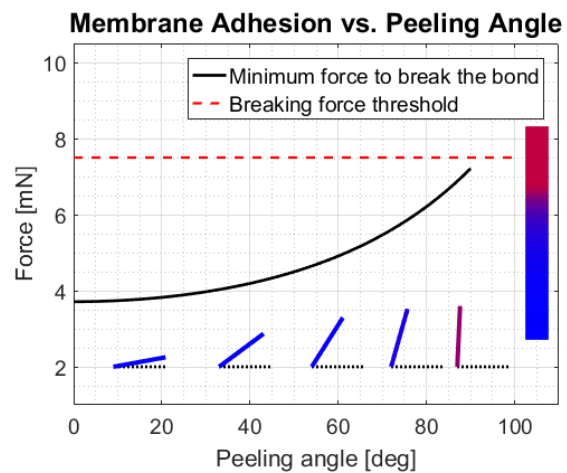


Figure 7. The outcome of peeling model. Five peeling angles are illustrated as example of the force-color mapping. A full spectrum is depicted in the color bar on the right.

Validation of the motion maintaining constant distance during peeling was assessed in pilot study 2. The task for pilot study 2 extends the target reaching motion to membrane peeling, which is identical to the final experiment, with only some difference in model parameters. Although the desired peeling motion is observed, the simulated membrane was extremely delicate when the membrane is short such that the peeling process was too frustrating to reach enough repetitions. Therefore, the calculation of membrane force is adjusted in the final experiment. When the membrane length is under 30% of its full segment length, the applied membrane force is discounted by a factor.

2.2.3. Circular Motion. The circular motion used in the experiment is based on the actual circular movement during eye surgery. Therefore, to trigger the desired motion from subjects with no medical background, a path guide and a target aim are displayed on the screen (as depicted in Figure 11 [b], [c]).

Circular peeling motion was validated in pilot study 2 by examining the trajectory history of the membrane proxy. The results of all trials of all participants in the final experiment are visualized in Figure 8: Baseline condition on the top and VF condition at the bottom.

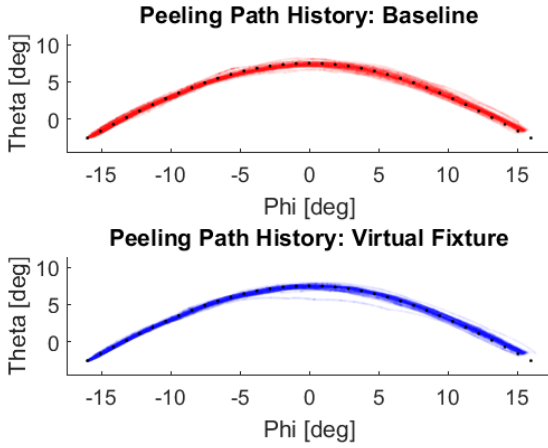


Figure 8. The path history of the peeling proxy of all participants recorded in the final experiment. There are 16*3 traces for each condition: Baseline condition plotted in red on the top, and VF condition plotted at the bottom.

3. Haptic Assistance Design

The main contribution of this study is to translate the noisy iOCT signal into haptic force feedback to assist the operator in performing a telerobotic vitreoretinal surgery. A virtual fixture modeling the $60\mu\text{m}$ membrane with sensor information fluctuating between $(\pm 40\mu\text{m})$ is established. In the block diagram depicted in Figure 4, the assistive controller uses the simulated iOCT signal and the states of the slave as input, and outputs the calculated force feedback to the operator.

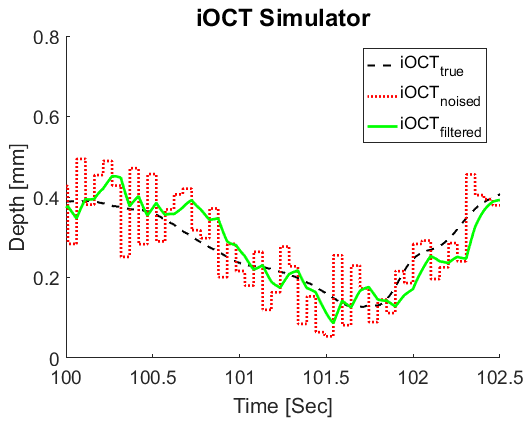


Figure 9. Simulated true iOCT depth, noised iOCT signal, and the filtered iOCT signal using a weighted moving average filter.

3.1. Development

A weighted moving average filter with proper window size (i.e., large enough to smooth out the noised ZOH nature but small enough such that the phase delay will

not lead to instability of the haptic assistance) facilitates the implementation of haptic feedback. The outcome of the filtered iOCT signal is plotted in green in Figure 9. Although the phase lag hinders the realization of a traditional virtual fixture, damping with high coefficient and springs with subtle stiffness can now remain stable.

On the basis of Steady-Hand Eye Robot using "variable admittance," a damper with high damping coefficient is implemented as a passive virtual fixture to generate surface contact force. To provide a sense of distance while approaching the virtual fixture, permutations combining subtle springs and dampers were added and tested. Corresponding to "feature extraction," the combination of springs and dampers highlight the haptic perception in terms of impedance transition. Although the scope of this research does not cover optimizing haptic assistance, the final haptic assistance design is relatively more promising than other permutations tested in pilot study 1(b) and pilot study 2.

A design that overturned the limited sensory dimension (1D) to create a feeling of a virtual fixture in 3D is by applying force feedback in the axial direction of the instrument – from a local perspective.

3.2. Final Virtual Fixture Design

The final virtual fixture design is a one-sided position-dependent (including velocity) force field having the property depicted in Figure 10, which consists of: 1. A damper field with two phases. The damping coefficient increases

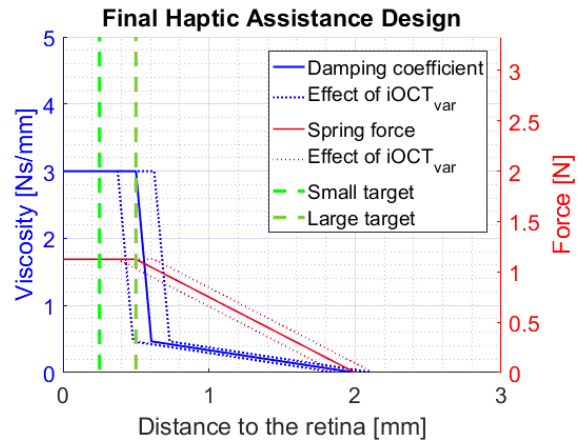


Figure 10. The final design of the haptic assistance, with the small and large target visualized in green dash lines. The left y-axis reads the value of the damping coefficient corresponding to the damper field colored in blue. The y-axis on the right reads the force of the spring colored in red.

subtly as the distance draws closer to the retina, and until contacting the passive virtual fixture with 0.5mm offset, the damping coefficient ramps up to 3Ns/mm . The 0.5mm offset does not hinder the instrument from reaching the 0.25mm small target since the phase lag of the filtered iOCT signal delays the force feedback to kick in. 2. The

second component of the final virtual fixture is a subtle spring starting off from $2mm$, which provides a reference of distance even staying static.

This method is robust in the sense that the haptic feedback force is less sensitive to the variation of the input signal. Corresponding to the statement that "The surgeons dislike losing control over the surgical robot." in Griffin et al.'s review paper [24], the design concept behind the virtual fixture is kept simple and less interrupting. The final virtual fixture design is expected to function as a passive virtual fixture that protects the retina from being damaged by unintended motion and a spring that provides a reference of a sense of current distance to the retina within the $2mm$ range.

4. Experimental Methods

A within-subject design (two conditions) is employed for the human factors experiment. The performance metrics are calculated from the experimental data, which are averaged over all three trials and analyzed using statistical methods (section 4.6) for the hypothesis test.

4.1. Participants

The experiment is approved by Delft University of Technology Human Research Ethics Committee, and all participants are given and signed the informed consent. Sixteen healthy participants between 22 and 31 years old ($M=25.13$, $SD=5.11$, nine female, seven male) volunteered the experiment. To unify the participants' knowledge and experience in teleoperated surgery, the selection criteria of this research are as follows: 1. Non-medical background; 2. No previous experience operating the Needle Steering Haptic Master.

4.2. Experiment Walk-through

The overview of the task is to peel off a simplified membrane following the given visual guiding path until the peeling proxy reaches the goal. The task consists of three sub-tasks:

Sub-task 1: Small Target Reaching

Each trial begins with reaching a small target, which represents the flap initiation motion in membrane peeling surgery. As depicted in Figure 11 [a], the participants always start from the home position and are asked to place the tool tip within the space of the $0.25mm$ ring-shaped target and hold for 0.5 second. All participants achieve the same amount of successful reaches, i.e., three times in total for each experimental condition. Any penetration in this sub-task leads to a re-start from the home position.

Sub-task 2: Membrane Peeling

Followed up by the completion of sub-task 1 is the second sub-task— '(Membrane) Peeling.' As depicted in Figure 11 [b], the visual cue for circular motion will immediately

appear. During peeling, the subjects are asked to peel (pull) the membrane proxy towards the goal.

Sub-task 3-1: Large Target (init.)

Any penetration during peeling leads to a $0.5mm$ large target reaching task from the home position. Therefore, sub-task 3-1 is denoted with (init.), which represents reaching a large target from "initial" position. Depending on individual performance, the number of this sub-task differs. If a participant has no puncture during peeling, then there is no large target (init.).

Sub-task 3-2: Large Target (arb.)

The membrane detaches from the retinal pick whenever the applied force is excessive, or a $2.2mm$ full-length membrane segment is completed. The participants are asked to reach a large target from the position he/she left. Hence sub-task 3-2 is denoted with (arb.), which stands for reaching a large target from "arbitrary" positions (see Figure 11 [c]). In reality, peeling ERM involves several release and grasp. The $2.2mm$ length is designed according to the re-grab number in typical EMP surgeries, which also regulates the minimum number of 'Large Target (arb.)' to be at least five times. After the completion of either sub-task 3-1 or 3-2, the task switches back to peeling (sub-task 2).

4.3. Task Instruction & Gamification

All participants are instructed with the following rules: 1. Avoid penetration; 2. Peel the membrane with a small peeling angle. 3. No time pressure but the faster in peeling motion, the higher the score. Besides the aforementioned subjective instructions, objective gamification is implemented in the EMP Simulator to enhance participation. The gamified settings are meant to motivate the desired motion and reduce participants' variability in behavior. The settings focus on the following aspects:

Avoid punctures: The consequences of penetration are: 1. 10-point deduction from the score; 2. Reset of the haptic master handle to the home position and followed by a target reaching task. These settings demotivate the participants from penetration.

Small peeling angle & Time:

Besides the instruction of maintaining a small peeling angle, an immediate reward by this desired behavior is given by the scoreboard displaying on the middle top of the screen (see Figure 11 [b]). The smaller the peeling angle and the faster the peeling motion, the faster the score accumulates.

Peeling on the track:

In reality, there is no optimal path available. Therefore, how accurate the path is followed is not of interest in this study (not included as one of the performance metrics).

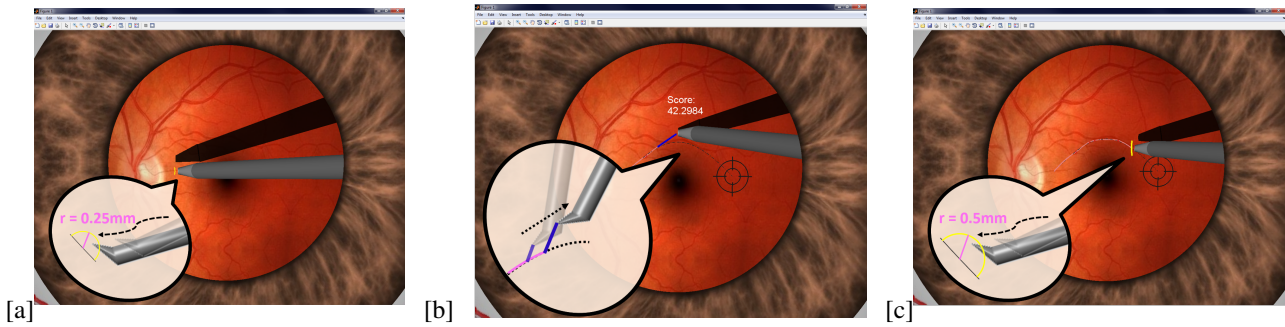


Figure 11. Illustrations of the experimental sub-tasks: [a] Sub-task 1: Small Target Reaching; [b] Sub-task 2: (Membrane) Peeling; [c] Sub-task 3-1 (and 3-2): Large Target Reaching (init. & arb.).

However, whether the path is followed is essential for assessing training and controlling the participant behavior, so it accounts for accumulating the score.

Full segment bonus:

A 25-point bonus is granted whenever a membrane segment with 2.2mm length is completed. The bonus motivates the participants to pay extra attention to the applied force on the membrane and to avoid penetrating the retina.

4.4. Experimental Protocol

The experiment consists of two different conditions: A baseline condition without haptic assistance and a condition with virtual fixture assistance. All participants perform three trials per condition. To balance the learning effect on the order the haptic assistance is given, subjects are divided into two groups. Participants in group one (upper part in Figure 12) are trained first with baseline condition. Only until the minimum completion time is within 2:30 minutes can they proceed on training for VF condition. To begin the actual measurement, the second condition also must be completed within 2:30 minutes, and the total training session has to last at least 20 minutes.

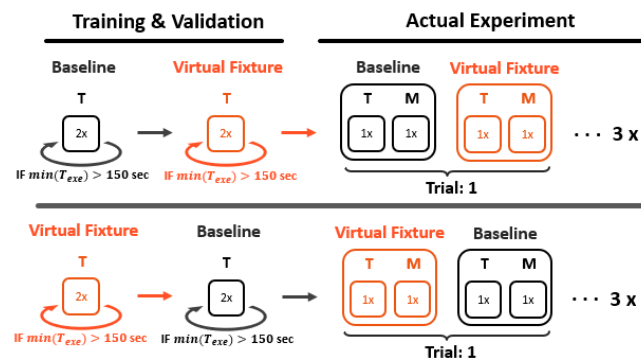


Figure 12. Flowchart of the experiment: The upper group is treated first with the baseline condition, while the other group experiences the opposite order. 'T' stands for training, and 'M' is measurement.

The order of the condition during actual measurement is the same as training. In one trial, the participant in group one are asked to complete two runs with baseline condition, then two runs with VF. The first run of each condition is meant to wash out the confusion due to transition. In the second run, the data are collected. This procedure repeats until the participants complete three trials. On the contrary, participants in group two undergo the opposite order. At the end of the experiment, the participants are asked to fill out the NASA-TLX task load questionnaire to report their subjective workload.

4.5. Data Acquisition & Metrics

Data (including the states of the simulated slave and the simulated membrane) are sampled at 1000Hz on Bachmann controller (of Needle Steering Haptic Master) and downloaded to the desktop computer at the end of every trial. Metrics used in this study are categorized into four aspects:

Puncture Rate

Puncture rate is calculated by dividing the accumulated puncture number by the total number of attempts of each sub-task throughout three trials. The overall puncture rate can be further decomposed into individual puncture rate of the three sub-tasks (3-1 and 3-2 are counted together as one): 'Small Target,' 'Large Target (init.),' 'Large Target (arb.),' and 'Peeling.'

Peeling Quality

In reality, retinal surgeons are trained to maintain constant distance (around 0.5mm) to the retina when peeling off ERM. To evaluate how steady this constant distance is maintained, the standard deviation of the simulated perfect iOCT depth during peeling is used. Moreover, the mean value and the standard deviation of the membrane force throughout the entire peeling process are used as metrics to reflect the steadiness of the performance of peeling.

Figure 13 uses the data of a typical subject to illustrate how peeling performance is recorded. Instead of looking at these values in time domain, the perfect iOCT depth and the membrane force are (semi-)normalized between

each subject by assigning one value to one length on the discretized proxy path. If multiple values coincide at a certain length, which happens when the subject idles for some period of time, the value is chosen with the time index that corresponds to the smallest peeling angle.

Execution Time

Although, compared to the entire one-hour setup time, the three-minute operation time could be negligible. Execution time is an indicator of how intuitive the teleoperation is [25]. Extra execution time often implies either the master-slave mapping or the assistive method is ill-designed. The overall

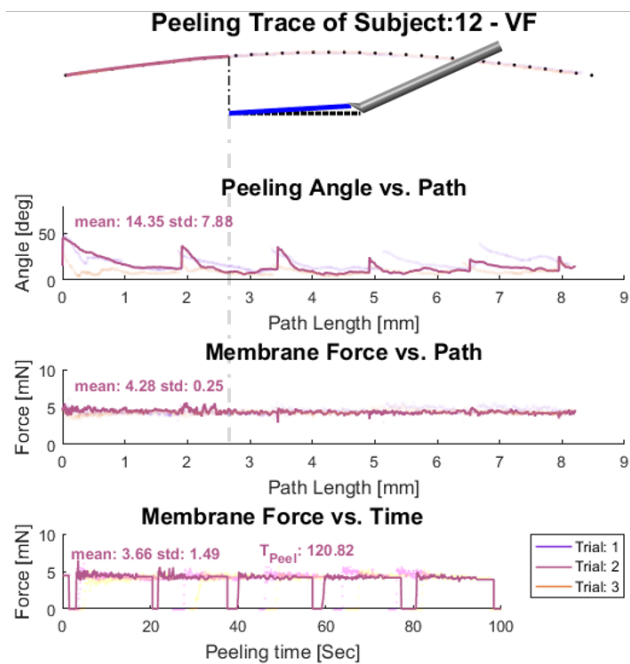


Figure 13. The second trial of subject number twelve under virtual fixture condition is highlighted to demonstrate how peeling data is measured. The top subplot shows the history trace of the membrane proxy following the dotted visual suggestion path. At this certain length on the trace, the corresponding peeling angle and the membrane color are visualized with a retinal pick. The bottom subplot is the simulated membrane force recorded in time domain. The two subplots in between are peeling angle and the membrane force assigned to the proxy path length.

execution time consists of the total completion time of all sub-tasks. For instance, in one trial, there are one 'Small Target,' one 'Peeling' (divided into several fragments), and several 'Large Target (init./arb.)' in between. The timer is suspended during the master device's initialization to the home position. Time is recorded only when the participants execute the task.

Workload

The NASA-TLX questionnaire [26] is employed to measure the subjective workload, which evaluates the operator's workload based on six questions regarding the feeling of

the task. A scale of 0 to 100 is used, where a higher scale signifies higher workload.

4.6. Data Analysis

The performance metrics obtained in each experimental condition are averaged over three trials. A paired sample t-test is performed, using two-tailed hypothesis. The significance level is set to $\alpha = 0.05$. The statistical results for every metric are listed in Table 1.

5. Results

5.1. Puncture Rate

Figure 14 depicts the observed puncture rates of the overall membrane task (on the top) and the three sub-tasks (at the bottom). The overall puncture rate [%] has significantly decreased from Baseline ($M=9.61$, $SD=6.82$) to VF ($M=2.80$, $SD=2.94$), with $t(15) = 5.3$, $p = 8.9 \times 10^{-5}$, $d = 1.32$. As for the three sub-tasks, the puncture rate for 'Large Target' and 'Peeling' show significant decreases with large effect sizes (Cohen's $d > 0.8$) under VF condition. Note that, due to the nature of the task design, not all participants experienced 'Large Target (init.)'—subject 4, 6, 7, 12, 13, 15, and 16 didn't. Therefore, the two 'Large Target' sub-tasks (3-1 and 3-2) are jointly examined. There is no significant

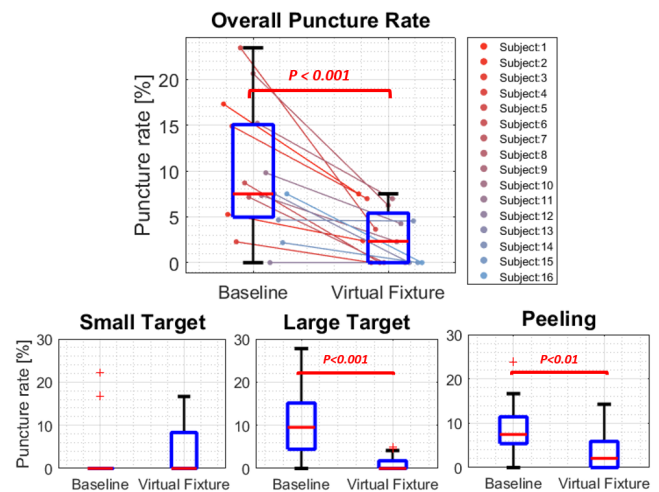


Figure 14. The upper plot shows the overall puncture rate of all subjects. Individual raw data are plotted as color dots and linked between two conditions. The lower plots depict the puncture rates during the reaching of the small target, large target and during peeling. Similar to the overall puncture rate, the sample size is $n = 16 \times 1$. The upper and lower whiskers are the upper bound and lower bound of the data. The outliers in red '+' are defined by exceeding 2.7σ . The blue boxes cover the 25 – 75% of the sample.

difference in 'Small Target.' Most of the participants had zero puncture rate in both conditions. A few participants improved with the virtual fixture, while the other performed worse.

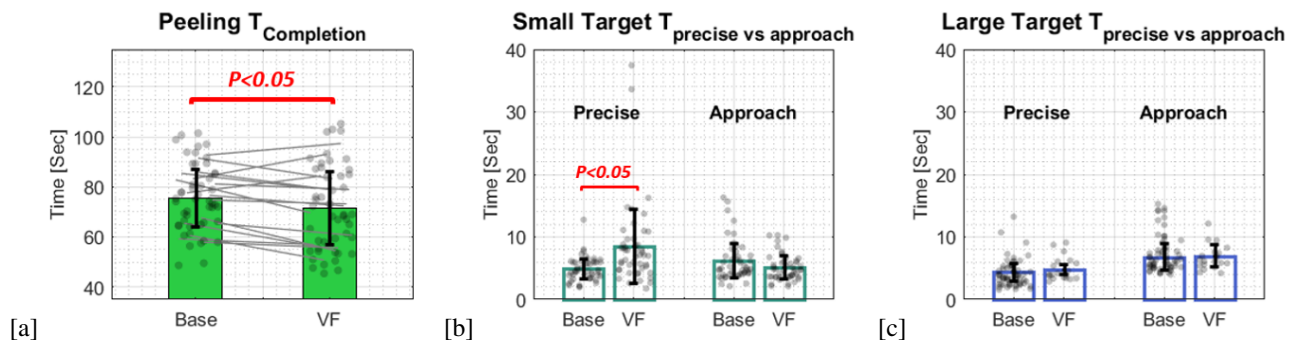


Figure 15. Execution time for three sub-tasks: [a] Completion time for 'Peeling'; [b] Execution time for 'Small Target' in precise/approach phase; [c] Execution time for 'Large Target' in precise/approach phase. The bars represent the mean values of all participants' averaged data over three trials, while the whiskers show the standard deviation of which. Individual data are plotted as gray dots (sample size $n = 16 * 3$ for [a] and [b]; sample size $n = 9 * n$ for [c]). In [a], the averaged peeling time for each subject in the two experimental conditions are linked with gray lines.

5.2. Peeling Quality

The standard deviation of the simulated true iOCT depth and the simulated applied membrane force are analyzed based on the metrics evaluating peeling quality. The standard deviation of depth [mm] during peeling has significantly decreased from Baseline ($M=0.27$, $SD=0.11$) to VF ($M=0.23$, $SD=0.09$), with $t(15) = 3.43$, $p = 3.7 * 10^{-3}$, $d = 0.86$, with a large effect size.

The simulated applied membrane force [mN] shows no significant difference in mean value while a significant reduction is observed in standard deviation from Baseline ($M=0.60$, $SD=0.12$) to VF ($M=0.54$, $SD=0.10$), with $t(15) = 4.05$, $p = 1 * 10^{-3}$, $d = 1.01$, which is a large effect.

5.3. Execution Time

Although there is a significant difference in the overall execution time, owing to the nature of the task design, the reduction in time is not entirely contributed due to faster completion of individual sub-tasks. A more direct way is to look into individual sub-task completion time. Peeling completion time [Sec] shows significant difference with a medium effect size, from Baseline ($M=75.51$, $SD=11.48$) to VF ($M=71.58$, $SD=14.50$), with $t(15) = 2.37$, $p = 0.03$, $d = 0.59$. Figure 15 [a] depicts the recorded execution time for peeling, where the trend of reducing peeling time can be seen from the linked gray lines.

Since the number of 'Large Target (init.)' each participant experienced differs, the completion time for Large Target (init.) is averaged over the available data set. That is, seven of the subjects (4, 6, 7, 12, 13, 15, and 16) who did not experience Large Target (init.) are removed. Therefore, the statistic test only performs over nine subjects for Large Target (init.), which makes comparing the completion time between the small and large target not possible.

No significant difference is observed in completion time for reaching the small and large target. Upon a closer look with the precise/approach phases defined by the distinction of $1.5mm$ depth, a significant difference in the

precise phase of the small target reaching is identified. With no difference in the small target puncture rate, under VF condition, the precise time has increased from Baseline ($M=4.88$, $SD=1.65$) to VF ($M=8.48$, $SD=5.92$), with $t(15) = 2.60$, $p = 0.02$, $d = 0.65$ (medium effect). Figure 15 [b] and [c] depict the precise/approach phase time of the small target and large target reaching. Individual raw data are plotted as gray dots.

5.4. Subjective Workload

The subjective workload is significantly reduced with the aid of virtual fixture. The scores reported by the NASA-TLX questionnaire are: Baseline ($M=61.63$, $SD=9.78$); VF ($M=54.37$, $SD=12.20$), with $t(15) = 3.06$, $p = 0.0079$, $d = 0.77$, which is a medium effect.

6. Discussion

6.1. Main Result

Based on the statistical results discussed in section 5, the virtual fixture did reduce the puncture rate and stabilize peeling motion as we hypothesized. The subjective workload of teleoperating an EMP surgery in the simulator is also reduced with the assistance of the virtual fixture. Interestingly, not all the completion time for each sub-task improved with the aid of the virtual fixture. '(Membrane) Peeling' is the only sub-task that improved in completion time with medium effect. Additionally, a significant increase in time spent in the precise phase of 'Small Target' is observed. Hence, all of the null hypothesis can be rejected except the one regarding execution time.

6.2. A Closer Look at Target Reaching

To further inspect the target reaching tasks, the completion time is divided into approaching phase and precise phase based on the perpendicular distance of the tool tip to the retinal surface (within or above $1.5mm$). Corresponding

to Laurens' research [16], 'Large Target' shows no significant difference in time for both approaching and precise phase. It is as expected since a strong sense of contact with the virtual fixture only happens entering the $0.5mm$ offset. Therefore, due to the effect of iOCT variance and the phase lag caused by filtering, 'Large Target' is more likely to be reached before the influence of the haptic feedback.

In 'Small Target,' where the iOCT variance approximates half the target size, the mean execution time of all subjects in precise phase has increased by 3.60 seconds with the support of virtual fixture. The result depicted in Figure 15 [b] indicates that the proposed VF seems to confuse the depth perception. As a consequence, time spent in precise phase increases but the penetration rate fails to decrease. This is an interesting observation beyond the scope of Laurens' research, which implies the joint precision of the teleoperation requires further study regarding the influence of dynamic model error.

6.3. Is Small Target Easier?

Due to the difference in sample size between 'Small Target' and 'Large Target (init.),' comparing these two sub-tasks based on completion time is not recommended. However, by comparing the puncture rate of all the sub-tasks ('Small Target,' 'Large Target,' and 'Peeling'), it is found that the puncture rate of 'Small Target' is the lowest. This is surprising because a ring with a smaller diameter is expected to have a higher risk of puncture than the one with a larger diameter. Why is reaching a small target easier in terms of puncture rate?

In pilot study 1 (a), rings from $0.6-0.2mm$ are consecutively generated at a random location on the simulated retina. For each participant, the ring shrinks by $0.1mm$ in size after every five accumulated reaches. The sample size of each condition for all participants are identical. Thus a repeated measures analysis of variance (ANOVA) is performed. The result indicates that the smallest target ring is significantly harder than the largest ring in terms of precise phase time.

An explanation for puncture rate is that 'Small Target' always generates the small ring at the same position in every trial. On the contrary, 'Large Target (init.)' generates the large ring at the place where the membrane is released (after puncture). Open-loop strategies could have been developed by the participants, thus affecting the result. The conclusion that 'Small Target' has a lower puncture rate is not made because the nature of the task is different from 'Large Target.' Additionally, comparing the difficulty between the two is not possible.

6.4. Experimental Set-up Limitation

The balance of the experimental conditions described in section 4.4 is to single out the effect of learning. Instead of intersecting the two experimental conditions, an alternative design could be switching only once after all the trials in the first condition are completed. By doing so, the washout

runs (training) required in the adopted approach are not necessary. Hence, the alternative approach could achieve twice amounts of repetitions within the same amount of time. The benefit of the adopted method is an early evaluation of the learning effect for both conditions. Additionally, the 2:30-minute minimum requirement is set up to guarantee that all the subjects reach a certain level of proficiency of the task. The alternative approach could lead to uneven exposure time to one of the two conditions during learning, and thus being hard to control the total time of the experiment.

Having their pros and cons, both methods are reasonable choices to deal with the learning effect of the complicated EMP surgery. However, how much can a subject thoroughly learn to execute a task during a given training session determines how complex can the task be designed. Therefore, the scope is limited to a simplified version of the real EMP surgery. This might reduce the transferability to reality had it not been for a keen identification of what are the essential factors in real surgery. For future study testing subjects with no medical background regarding more complicated procedures, the training session is recommended to be extended (, or even separated into days). Otherwise, retinal specialists should be recruited for the human factors experiment.

6.5. EMP Simulator Limitation

The membrane model employed in this study is rather simplified. Due to the breaking force threshold, potential force peaks that could have accounted for a higher standard deviation of the peeling force were saturated. Therefore, the peeling force we can observe is limited to peeling motion but not after (and right at) the instance when the membrane breaks. Nevertheless, within the scope of this research, the quality of peeling is sufficiently evaluated. It is reasonable that the averaged peeling force has no significant difference between the two conditions since the proposed VF is not designed to affect the membrane force explicitly. Based on the consistency of keeping the $0.5mm$ distance and the stabilization of the (saturated) membrane force, the virtual fixture can be concluded to be useful for EMP motion.

Another limitation of the EMP Simulator is the limited dimension the iOCT sensor probe can sense (see section 1.2.3). This implies the haptic assistance provided by the virtual fixture is restricted to the instrument's local perspective. In other words, the haptic force feedback can be felt differently at different locations in the eye. The force is more sensitive when the sensor probe points perpendicularly to the retinal surface. Correspondingly, punctures during peeling are self-reported by some subjects to be higher after 3/4 of the path, where the retina surface curves towards the instrument, resulting in a large tilting angle in the measuring direction.

For a future study, it is strongly recommended to implement a more complex membrane model, where the dynamics of the tissue-instrument interaction can be taken into account. It would also be interesting to investigate haptic feedback that deals with the complexity of the environment,

e.g., the occlusion of iOCT sensor caused by the floaters inside the eye.

6.6. Future Work

During the time this study was carried out, PRECEYES developed an assistive method called "Sensor-Based Bound," which decouples the instrument manipulator from the motion control console when the iOCT sensor senses the distance to be closer than a given lower bound. This method is extremely safe in the sense that the retina will never be punctured.

However, the variance of the iOCT signal makes Sensor-Based Bound too conservative to reach a target on the retina, thus extending the execution time even more. This problem is encountered in this study too. The next step of this research would be including Sensor-Based Bound as a baseline condition and, on top of that, develop virtual fixtures, or other haptic assistance that can combine Sensor-Based Bound.

7. Conclusion

The purpose of this research is to enhance teleoperated Epiretinal Membrane Peeling (EMP) with haptic assistance utilizing the state-of-the-art distance sensing technology. A proof-of-concept facilitating a virtual fixture in spite of noisy sensory information is tested with human factors experiment ($N = 16$). Overall, the experimental result indicates that the proposed method successfully translates iOCT distance information to depth perception via force feedback and reduces the difficulty of the teleoperated task.

- The overall puncture rate has reduced from 9.6% to 2.8% with a large effect size.
- Peeling quality has been improved by reducing 9.4% variance of the peeling force.
- Not all sub-tasks shortens execution time. Only the completion time for peeling decreases from 75.5 to 71.6 seconds with a medium effect size.
- The subjective workload has decreased from 61.64 to 54.37 with a medium effect size.

References

- [1] S. Sunshine, M. Balicki, X. He, K. Olds, J. U. Kang, P. Gehlbach, R. Taylor, I. Iordachita, and J. T. Handa, "A force-sensing microsurgical instrument that detects forces below human tactile sensation," *Retina (Philadelphia, Pa.)*, vol. 33, no. 1, 2013.
- [2] H. Das, H. Zak, J. Johnson, J. Crouch, and D. Frambach, "Evaluation of a telerobotic system to assist surgeons in microsurgery," *Computer Aided Surgery*, vol. 4, no. 1, pp. 15–25, 1999.
- [3] U. of Oxford, "First human test of robotic eye surgery a success," 2018. [Online]. Available: <http://www.ox.ac.uk/news/2018-06-18-first-human-test-robotic-eye-surgery-success>
- [4] T. Meenink and I. Thijs, "Vitreo-retinal eye surgery robot: sustainable precision," Ph.D. dissertation, Technische Universiteit Eindhoven, 2011.
- [5] S. Bachu, "Macular hoe ILM PEELING 4K," 2017. [Online]. Available: <https://www.youtube.com/watch?v=0smRqwnf4c>
- [6] S. J. HAUG and H. R. McDonald, "Clinical Pearls for Performing ILM Peeling in Vitreoretinal Surgery," *Retinal Physician November/December*, pp. 53–57, 2014.
- [7] R. Hendrix, "Robotically assisted eye surgery: A haptic master console," Ph.D. dissertation, Technische Universiteit Eindhoven, 2011.
- [8] S. Yang, "Handheld micromanipulator for robot-assisted microsurgery," 2015.
- [9] X. He, M. Balicki, P. Gehlbach, J. Handa, R. Taylor, and I. Iordachita, "A multi-function force sensing instrument for variable admittance robot control in retinal microsurgery," in *Robotics and Automation (ICRA), 2014 IEEE International Conference on*. IEEE, 2014, pp. 1411–1418.
- [10] H. Yu, J.-H. Shen, R. J. Shah, N. Simaan, and K. M. Joos, "Evaluation of microsurgical tasks with OCT-guided and/or robot-assisted ophthalmic forceps," *Biomedical optics express*, vol. 6, no. 2, pp. 457–472, 2015.
- [11] R. J. Samplonius, Y. G. M. Douven, M. J. G. van de Molengraft, and M. Steinbuch, *Distance Measurement and Retinal Recognition from A-scans using an OCT Probe*, 2017.
- [12] M. Balicki, A. Uneri, I. Iordachita, J. Handa, P. Gehlbach, and R. Taylor, "Micro-force sensing in robot assisted membrane peeling for vitreoretinal surgery," in *International Conference on Medical Image Computing and Computer-Assisted Intervention*. Springer, 2010, pp. 303–310.
- [13] A. M. Okamura, "Methods for haptic feedback in teleoperated robot-assisted surgery," *Industrial Robot: An International Journal*, vol. 31, no. 6, pp. 499–508, 2004.
- [14] L. B. Rosenberg, "The Use of Virtual Fixtures as Perceptual Overlays to Enhance Operator Performance in Remote Environments." Tech. Rep., 1992.
- [15] P. Marayong, M. Li, A. M. Okamura, and G. D. Hager, "Spatial motion constraints: Theory and demonstrations for robot guidance using virtual fixtures," in *Robotics and Automation, 2003. Proceedings. ICRA'03. IEEE International Conference on*, vol. 2. IEEE, 2003, pp. 1954–1959.
- [16] L. Kranendonk, *Applying Dynamic Damping to Robotic Vitreoretinal Surgery*, 2017.
- [17] K. W. Grace, P. Jensen, J. E. Colgate, and M. Glucksberg, "Teleoperation for ophthalmic surgery: From the Eye Robot to feature extracting force feedback," *Automedica*, vol. 16, no. 4, pp. 293–310, 1998.
- [18] T.-K. Shen, *Haptic Feedback providing a Sense of Distance for Telerobotic Vitreoretinal Surgery: A Literatur Study*, 2018.
- [19] M. Nambi, P. S. Bernstein, and J. J. Abbott, "A Compact Tele-manipulated Retinal-Surgery System that Uses Commercially Available Instruments with a Quick-Change Adapter," *Journal of Medical Robotics Research*, vol. 1, no. 02, p. 1630001, 2016.
- [20] P. K. Gupta, P. S. Jensen, and E. de Juan, "Surgical forces and tactile perception during retinal microsurgery," in *International Conference on Medical Image Computing and Computer-Assisted Intervention*. Springer, 1999, pp. 1218–1225.
- [21] B. Gonenc, M. A. Balicki, J. Handa, P. Gehlbach, C. N. Riviere, R. H. Taylor, and I. Iordachita, "Preliminary evaluation of a micro-force sensing handheld robot for vitreoretinal surgery," in *Intelligent Robots and Systems (IROS), 2012 IEEE/RSJ International Conference on*. IEEE, 2012, pp. 4125–4130.
- [22] A. G. L. Hoevenaars, P. Lambert, and J. L. Herder, "Kinematic design of two elementary 3dof parallel manipulators with configurable platforms," in *Computational Kinematics*. Springer, 2014, pp. 315–322.
- [23] K. Kendall, "Thin-film peeling-the elastic term," *Journal of Physics D: Applied Physics*, vol. 8, no. 13, p. 1449, 1975.

TABLE 1. RESULTS OF THE PAIRED SAMPLE T-TEST

Small Target		Baseline		Virtual Fixture		p – value <i>t</i> (15)	Cohen’s d	Effect size <i>r</i> ²
		M (SD)	M (SD)					
<i>Puncture Rate</i>	(%)	3.4722 (7.5564)	4.1667 (7.4536)	0.8198 <i>t</i> = 0.2319	0.0580	0.0598 ²		
<i>T_{completion}</i>	(Sec)	11.0311 (3.8194)	13.6238 (6.7623)	0.1121 <i>t</i> = 1.6878	0.4219	0.3995 ²		
<i>T_{approach}</i>	(Sec)	6.1482 (2.7488)	5.1391 (1.7846)	0.054 <i>t</i> = 2.0904	0.5226	0.4750 ²		
<i>T_{precise}</i>	(Sec)	4.8830 (1.6468)	8.4847 (5.9240)	0.02 * <i>t</i> = 2.6031	0.6508	0.5578 ²		
Large Target		Baseline		Virtual Fixture		p – value <i>t</i> (15)	Cohen’s d	Effect size <i>r</i> ²
		M (SD)	M (SD)					
<i>Puncture Rate</i> (<i>Large</i>)	(%)	10.4986 (8.7915)	1.0802 (1.9512)	5.26e-04 *** <i>t</i> = 4.3910	1.0977	0.75 ²		
Large Target (Initial Position)				p – value <i>t</i> (8)				
<i>Puncture Rate</i>	(%)	5.2800 (9.6529)	0 (0)	0.1394 ¹ <i>t</i> = 1.6410	0.5470	0.5018 ²		
<i>T_{completion}</i>	(Sec)	11.5466 (3.3662)	11.6875 (2.0384)	0.8878 <i>t</i> = 0.1456	0.0485	0.0514 ²		
<i>T_{approach}</i>	(Sec)	7.0342 (2.5913)	6.9112 (1.7630)	0.8586 <i>t</i> = 0.1840	0.0613	0.0649 ²		
<i>T_{precise}</i>	(Sec)	4.5123 (1.4142)	4.7763 (0.7260)	0.6547 <i>t</i> = 0.4645	0.1548	0.1620 ²		
Large Target (Arbitrary Position)				p – value <i>t</i> (15)				
<i>Puncture Rate</i>	(%)	14.4048 (12.4082)	1.3715 (2.4958)	8.18e-04 *** <i>t</i> = 4.1717	1.0429	0.7329 ²		
Membrane Peeling		Baseline		Virtual Fixture		p – value <i>t</i> (1,15)	Cohen’s d	Effect size <i>r</i> ²
		M (SD)	M (SD)					
<i>OCT Depth AVG</i>	(mm)	0.6307 (0.1953)	0.6032 (0.2009)	0.3324 <i>t</i> = 1.0017	0.2504	0.2504 ²		
<i>OCT Depth STD</i>	(mm)	0.2762 (0.1149)	0.2290 (0.0915)	0.0037 ** <i>t</i> = 3.4298	0.8574	0.6630 ²		
<i>Peeling Force</i> (<i>AVG</i>)	(mN)	4.8983 (0.2383)	4.9393 (0.2908)	0.3434 <i>t</i> = 0.9784	0.2446	0.2449 ²		
<i>Peeling Force</i> (<i>STD</i>)	(mN)	0.5969 (0.1212)	0.5405 (0.1024)	0.0010 ** <i>t</i> = 4.0549	1.0137	0.7231 ²		
<i>Puncture Rate</i>	(%)	8.7089 (5.9809)	3.9215 (4.7954)	0.0042 ** <i>t</i> = 3.3739	0.8435	0.6569 ²		
<i>T_{peeling}</i>	(Sec)	75.5067 (11.4830)	71.5780 (14.5025)	0.0315 * <i>t</i> = 2.3713	0.5928	0.5222 ²		
Overall		Baseline		Virtual Fixture		p – value <i>t</i> (1,15)	Cohen’s d	Effect size <i>r</i> ²
		M (SD)	M (SD)					
<i>Puncture Rate</i> (<i>overall</i>)	(%)	9.6132 (6.8189)	2.7996 (2.9448)	8.9e-05 *** <i>t</i> = 5.3006	1.3251	0.8074 ²		
<i>T_{execution}</i>	(Sec)	149.1209 (48.9609)	126.1862 (28.4806)	0.0133 * <i>t</i> = 2.8063	0.7016	0.5867 ²		
<i>Workload</i>	(–)	61.6354 (9.7784)	54.3687 (12.1978)	0.0079 ** <i>t</i> = 3.0625	0.7656	0.6203 ²		

†: Although the original data set passed the Kolmogorov-Smirnov normality test, the puncture rates of VF condition are all zeros (pushed to one side). Additionally, a rank transformed t-test is performed, and the result: *t*(8) = 2.4954, *p* = 0.0372* is obtained

P < 0.05 *
P < 0.01 **
P < 0.001 ***

[24] J. A. Griffin, W. Zhu, and C. S. Nam, “The Role of Haptic Feedback in Robotic-Assisted Retinal Microsurgery Systems: A Systematic Review,” *IEEE transactions on haptics*, vol. 10, no. 1, pp. 94–105, 2017.

[25] H. Boessenkool, “Haptic assistance for teleoperated maintenance of fusion plants: task analysis, design and evaluation,” Ph.D. dissertation, 2017.

[26] E. A. Bustamante and R. D. Spain, “Measurement invariance of the Nasa TLX,” in *Proceedings of the Human Factors and Ergonomics Society Annual Meeting*, vol. 52, no. 19. SAGE Publications Sage CA: Los Angeles, CA, 2008, pp. 1522–1526.

Bibliography

- [1] V. J. Kalas, *Assesment of influence of play in joints on the end effector accurcay in a novel 3DOF (1T-2R) parallel manipulator*, Tech. Rep. (2016).
- [2] VRmagic, *Eyesi Surgical*, (2018).
- [3] A. G. L. Hoenenaars, P. Lambert, and J. L. Herder, *Kinematic design of two elementary 3dof parallel manipulators with configurable platforms*, in *Computational Kinematics* (Springer, 2014) pp. 315–322.
- [4] Wiki, *Line-sphere intersection*, (2017).
- [5] R. J. Samplonius, Y. G. M. Douven, M. J. G. van de Molengraft, and M. Steinbuch, *Distance Measurement and Retinal Recognition from A-scans using an OCT Probe* (2017).
- [6] K. Kendall, *Thin-film peeling-the elastic term*, *Journal of Physics D: Applied Physics* **8**, 1449 (1975).
- [7] Wiki, *Ray tracing (graphics)*, (2018).
- [8] L. M. Kranendonk, *What haptic technologies could improve robotic vitreoretinal surgery, and which are the most promising?* (2017).
- [9] T.-K. Shen, *Haptic Feedback providing a Sense of Distance for Telerobotic Vitreoretinal Surgery: A Literatur Study* (2018).
- [10] L. Kranendonk, *Applying Dynamic Damping to Robotic Vitreoretinal Surgery* (2017).



Needle Steering Haptic Master & Bachmann Controller

This appendix expands paper section 2.1.1 with the detail of the hardware device employed in this master project. The mechanical configuration, output capabilities, and the controller architecture are described.

A.1. Master Device

The Needle Steering Haptic Master was originally built for controlling steerable needles in MIS application [3]. Consisting of four arms, the manipulator forms a parallel mechanism that gives it 3 DoFs (2 rotations and 1 translation). As illustrated in Figure A.1, the α_{master} angle rotates about Y-axis, and the β_{master} angle rotates about minus X-axis. Both rotations have workspace ranging from -20 to 20 degrees. The translation happens along Z-axis. Starting from home (neutral position for both rotations; minimum position for translation), the manipulator can move up to 300 mm in Z-direction. Each arm

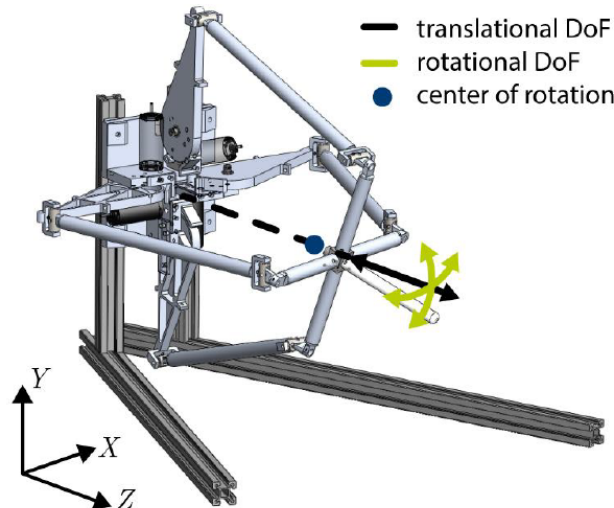


Figure A.1: CAD of the 3-DoF Needle Steering Haptic Master [1].

is actuated by a DC motor mounted with an encoder. The haptic master is an impedance-controlled robot. Through position feedback from the encoders, the device can move its handle to the desired position or express desired forces depending on applications. The overall properties of the master device are listed in Table.A.1.

Table A.1: Master device properties

Property	[unit]	Value
α_{master} range of motion	[deg]	[-20, 20]
β_{master} range of motion	[deg]	[-20, 20]
z_{master} range of motion	[mm]	[0, 300]
Max. force (translation DoF)	[N]	10
Max. torque (rotational DoF)	[Nm]	0.3
Encoder resolution	[PPR]	4000

A.2. Bachmann Controller

The Haptic Master Device is controlled using a real-time Bachmann® controller [?]. The controller reads the digital signals from the four encoders, and generate analog signals to control the DC motors. Moreover, through Ethernet, the digital signal can be communicated at 1000Hz sampling rate. The control architecture inside the Bachmann controller is programmable and compatible with Matlab® Simulink®. The M-Target® developed by Bachmann electronic compiles the Simulink model to the Bachmann controller.

A.3. Hardware Architecture

The schematic layout is shown in Figure A.2.

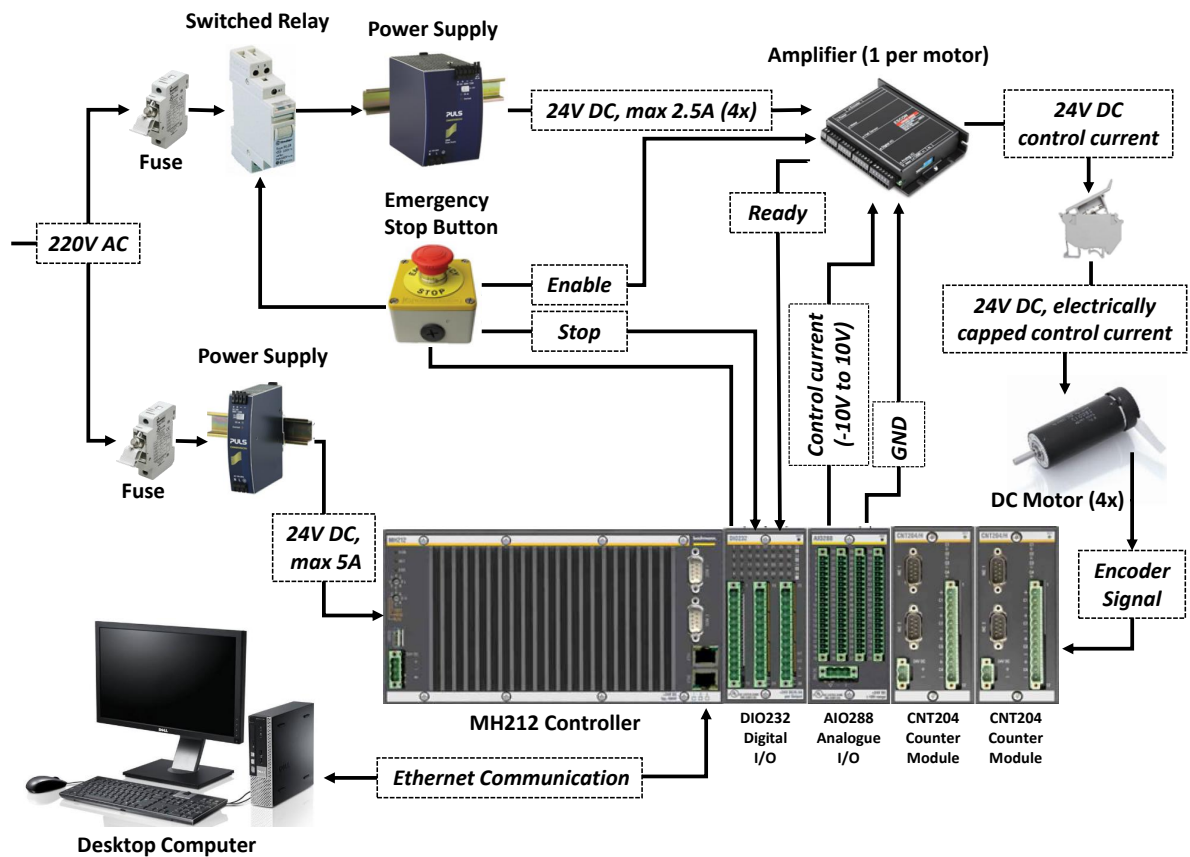


Figure A.2: Schematic layout of the master device.

B

Simulated Slave Design

This appendix describes the model behind the simulated slave and iOCT sensor probe, which serves as the supplement information for paper section 2.1.2. During the design phase, two master-slave mapping methods were tested. The disposed method called "MIS" mapping is a direct scaling inspired by Minimally Invasive Surgery (MIS). The adopted method, abbreviated as "VN" mapping, stands for virtual needle mapping. VN mapping leverages the strength of the Needle Steering Haptic Master. Both mapping methods are elaborated in Appendix B.2. The iOCT simulator is introduced in Appendix B.3.

B.1. Instrument Design

The simulated slave in this experiment is a retinal pick, which is an instrument with a bent tip. A 3D view of the pick plotted in its body fixed coordinate is depicted in Figure B.1. The surgical pick has three degrees of freedom with a center of rotation overlapping the incision of the eye. The operational range

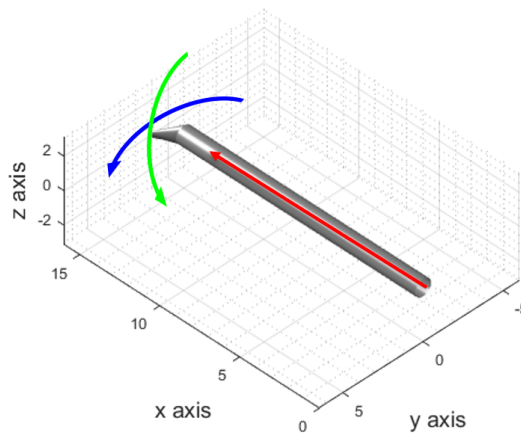


Figure B.1: 3D view of the instrument including its three DoFs.

on the retinal surface and the location of the incision are defined based on typical surgical condition. The home position of the pick is chosen such that the tip position starts at 16mm away the incision and

Table B.1: Slave workspace properties

Property	[unit]	Value
Incision point ($X_{incision}$)	[mm]	[2.53, -8, 0]
Predefined target diameter	[mm]	10'
Initial depth	[mm]	16

points towards the center of the target area. Table B.1 lists the properties of the predefined workspace

for the slave. Figure B.2 visualizes the definition of the slave's workspace. Table B.2 lists the properties of the simulated pick.

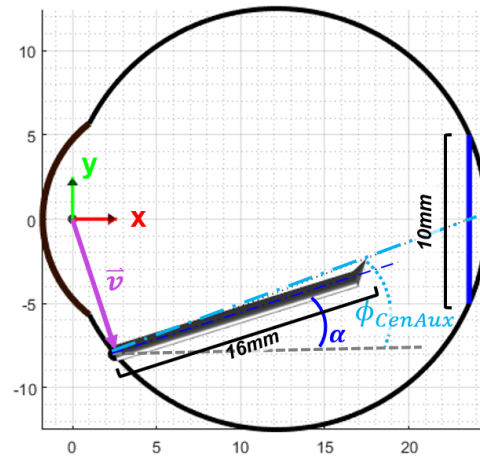


Figure B.2: Visualization of the home position of the instrument and the target workspace. The predefined target workspace is painted in blue, which has the central auxiliary line points from the incision to its center. The incision location is pointed with a purple vector. The α_{slave} is defined as the angle between the shaft and the x-axis.

B.2. Two Master-Slave Mapping

B.2.1. MIS mapping

The MIS master-slave mapping is a linear one-to-one mapping in joint space, i.e., from each DoF of the master device to the corresponding DoF of the slave. Rotations are scaled down with the rotational scaling factor $SF_{angular}$, while the translation uses a finer scaling factor $SF_{translation}$. To set the instrument at home position, constants for the neutral position are applied to the mapping equation as follows:

$$\alpha_{slave} = \alpha_{master} * SF_{angular} + \alpha_0 \quad (B.1)$$

$$\beta_{slave} = \beta_{master} * SF_{angular} \quad (B.2)$$

$$x'_{slave} = (z_0 - z_{master}) * SF_{translation} \quad (B.3)$$

The pick properties and the constants used in master-slave mapping are listed in Table B.2. The

Table B.2: Slave properties

Property	[unit]	Value
Shaft diameter	[mm]	1
Center of rotation	[mm]	[0; 0; 0]'
Shaft length (no tip)	[mm]	14.97
Tip coordinate X'_{tip0}	[mm]	[15.97; 1; 0]'
Tip radius	[mm]	0.2
α_0	[deg]	17.22
z_0	[mm]	45
$SF_{rotation}$	[-]	0.6
$SF_{translation}$	[-]	0.06
α_{slave} range of motion	[deg]	5.22 to 29.22
β_{slave} range of motion	[deg]	-12 to 12
x_{slave} range of motion	[mm]	2.7 to 20.7

reachable workspace employing MIS mapping is visualized in Figure B.3. The current state of the

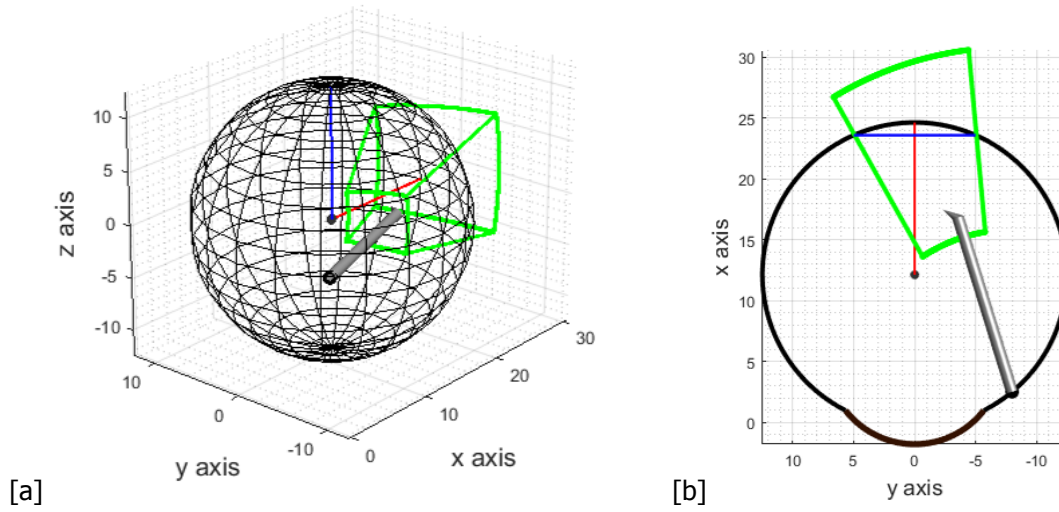


Figure B.3: [a] The 3D view of the reachable workspace using MIS mapping. [b] The top view of the MIS mapping, where the target area is plotted in blue, and the reachable workspace is colored in green.

simulated slave has the tool tip X_{tip} , the normal vector of the pick shaft \vec{n}_{pick} , and the moment arm r_{MIS} :

$$r_{MIS} = X_{tip} - X_{incision} \quad (B.4)$$

The calculated force feedback at the simulated tool tip (F_{tip}) is transferred to the master via equations:

$$Fz'_{master} = F_{tip} \cdot \vec{n}_{pick} \quad (B.5)$$

$$M_{master} = r_{MIS} \times F_{tip} \quad (B.6)$$

Fz'_{master} is the transnational feedback force on the master. Since α_{master} rotates about z-axis, the α feedback torque $T_\alpha = M_{master}(3)$. Similarly, β_{master} rotates about y-axis, so the β feedback torque $T_\beta = M_{master}(2)$.

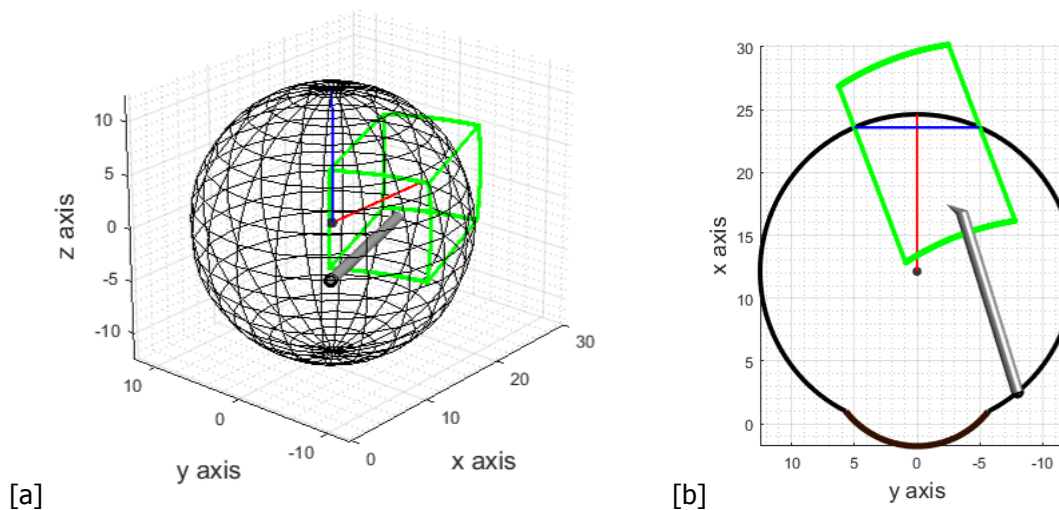


Figure B.4: [a] The 3D view of the reachable workspace of VN mapping. [b] The top view of the VN mapping, where the target area is plotted in blue, and the reachable workspace is colored in green.

B.2.2. VN mapping

Pointing from the incision to the center of the predefined circular target area is an auxiliary line. The virtual needle mapping can be considered as placing a scaled down master on that auxiliary line. As its name suggests, VN mapping assumes there is a needle with adjustable length attached to the master handle. Once the length of the virtual needle and scaling factors are set, the factor of motion scaling is determined. This method leverages the inherent mechanical feature of the Needle Steering Haptic Master, a virtual needle with three DoFs (2 rotations, 1 translation) can be realized by simple scaling. The end-point of the needle in the simulated environment can be calculated with the following equations:

$$\alpha_{needle} = \alpha_{master} * SF_{angular} + \phi_{CenAux} \quad (B.7)$$

$$\beta_{needle} = \beta_{master} * SF_{angular} \quad (B.8)$$

$$x'_{needle} = (z_0 - z_{master}) * SF_{translation} \quad (B.9)$$

From the three states of the virtual needle, the end-point position in global coordinate can be calculated by rotation and translation of the body-fixed coordinate:

$$X_{needle'_{tip}} = [L_{needle}; 0; 0] \quad (B.10)$$

The Remote Center of Motion (RCM) of the virtual Needle moves along the center auxiliary line, which has the direction vector, \vec{n} , from Incision to Workspace_Target. The position of the remote center of motion is calculated by:

$$Needle_{RCM} = (||X'_{tip0}|| - L_{needle} + x'_{needle}) * \vec{n} + X_{incision}; \quad (B.11)$$

The Needle tip is the result of rotation with respect to this RCM

$$X_{needle_{tip}} = Rotate_{\alpha}(\alpha_{needle}) * Rotate_{\beta}(\beta_{needle}) * X_{needle'_{tip}} + Needle_{RCM}; \quad (B.12)$$

The constants used in VN mapping are given in Table B.3.

Table B.3: Virtual needle properties

Property	[unit]	Value
L_{needle}	[mm]	22.48
ϕ_{CenAux}	[deg]	20.80
α_{needle} range of motion	[deg]	8.8 to 32.8
β_{needle} range of motion	[deg]	-12 to 12
x'_{needle} range of motion	[mm]	2.7 to 20.7

The final step is by using this end-point position to solve the orientation and translation of the retinal pick. The workspace is selected such that the singularity point is avoided, so it can be solved by Gauss-Newton iteration. The outcome of VN mapping is visualized in Figure B.4. Table B.4 shows the algorithm of Gauss-Newton method. The geometric constraint D (equation B.13) is the alignment of the virtual needle tool tip with the simulated pick:

$$Rotate_{\alpha}(\alpha_{slave} - \phi_{CenAux}) * Rotate_{\beta}(\beta_{slave}) * (X'_{tip0} - [z_{master}; 0; 0]) + X_{incision} = X_{tip} \quad (B.13)$$

The equation D_{kj} is the result of taking Jacobian of D with respect to three states of the slave:

$$D_{kj} = J_D(\alpha_{slave}, \beta_{slave}, z_{slave}) = \left[\frac{\partial D}{\partial \alpha_{slave}}; \frac{\partial D}{\partial \beta_{slave}}; \frac{\partial D}{\partial z_{slave}} \right] \quad (B.14)$$

The calculated force feedback at the simulated tool tip has a slightly different transformation with VN mapping. The RCM moves along the central auxiliary line, hence the moment arm r_{VN} becomes:

$$r_{VN} = X_{tip} - Needle_{RCM} \quad (B.15)$$

, and the inner product of the axial force on the master device is now calculated with the normal vector of the virtual needle \vec{n}_{needle} , which is the unit vector of equation B.15 by:

$$Fz'_{master} = F_{tip} \cdot \vec{n}_{needle} \quad (B.16)$$

$$M_{master} = r_{VN} \times F_{tip} \quad (\text{B.17})$$

Identical to MIS mapping, Fz'_{master} is the transnational feedback force on the master. $M_{master}(3)$ and $M_{master}(2)$ are the rotational feedback forces for α and β .

Table B.4: Algorithm: Gauss-Newton iteration

Algorithm: Gauss-Newton method
<pre> % Geometric constraint: D($\alpha_{slave}, \beta_{slave}, -Z_{slave}, X_{tip}$); % Jacobian wrt state variables: $D_{kj}(\alpha_{slave}, \beta_{slave})$; % load initial value from last slave state Initial_guess = [$\alpha_{slave}, \beta_{slave}, -Z_{slave}$]; set iteration = 1; set tol=1 e-12; set maximum iteration = 10; % Calculate residual of the geometric constraints D_eval = D(Initial_guess, X_{tip}); Dx = D_{kj}(Initial_guess); while(abs(D_eval)>tol) && (iteration<maximum iteration) % Increment based on residual dx=-Dx.'*((Dx*Dx.)\D_eval); % Update states Initial_guess = Initial_guess + dx.'; D_eval = D(Initial_guess, X_{tip}); Dx = D_{kj}(Initial_guess); iteration = iteration + 1; </pre>

B.3. iOCT Simulation Design

The iOCT sensor probe measures the distance to the retina (and a few retinal sub-layers underneath) in the axial direction. In reality, there could be a tilting angle between the instrument and the sensor probe due to mounting such that the measured distance has to be corrected according to this geometric relation. For simplicity, the tilting angle is neglected, hence the simulated iOCT measures the distance in the direction from the incision to the tool tip. Leveraging the benefit of approximating the eye as a perfect sphere (correspond to paper section 2.1.3 and Appendix C.1), the distance d from the incision to the retinal surface can be calculated using line-sphere intersection equations [4]:

$$\vec{l} = (X_{tip} - o) / \|X_{tip} - o\| \quad (\text{B.18})$$

$$d = -(\vec{l} \cdot (o - c)) + \sqrt{(\vec{l} \cdot (o - c))^2 - \|o - c\|^2 + r^2} \quad (\text{B.19})$$

, where c is the center of the sphere, r is the eye radius, and o is the incision of the instrument. \vec{l} is the vector of the measuring direction. Note that the largest square root of equation B.19 has been used. For the tip position is inside the sphere, the intersection is in the positive direction. Therefore, the true depth is calculated as:

$$depth = d - \|X_{tip} - o\| \quad (\text{B.20})$$

As addressed in paper section 2.1.2, the 20Hz iOCT signal has to be simulated on the 1000Hz master controller. This is achieved by zero-order-holding (ZOH) the perfect depth every other 50 updates. The Simulink® model used for iOCT simulator is given in Figure B.5. The left top block calculates the perfect depth, and by using this value, the simulated iOCT signal is generated in the following blue block. The

hold operators regulate the update every other 50 iterations. ZOH has the mathematical expression as equation B.21.

$$depth_{ZOH}(t) = depth(kT), \quad kT \leq t < kT + T \quad (\text{B.21})$$

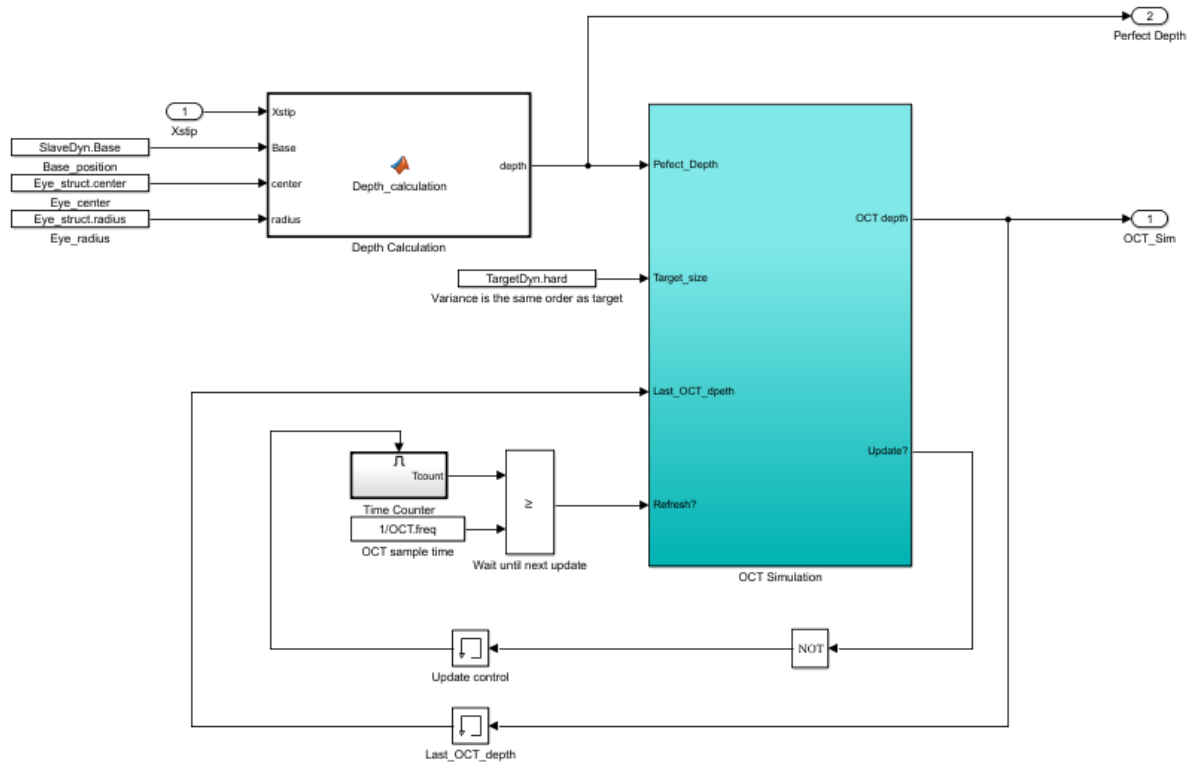


Figure B.5: Implementation of iOCT simulator in Simulink®.

The motivation behind the design of noise is based on the latest research of PRECEYES' iOCT sensor technology [5]. The accuracy of state-of-the-art filtering technique can achieve accuracy within $40 \mu\text{m}$ in 99% of the scans. The noise level approximates half the size of the target membrane. By assuming the noise to be normally distributed, the ZOH true depth is added Gaussian noise with the amplitude half the size of the small target. The outcome of the simulated iOCT signal depicted in Figure B.6.

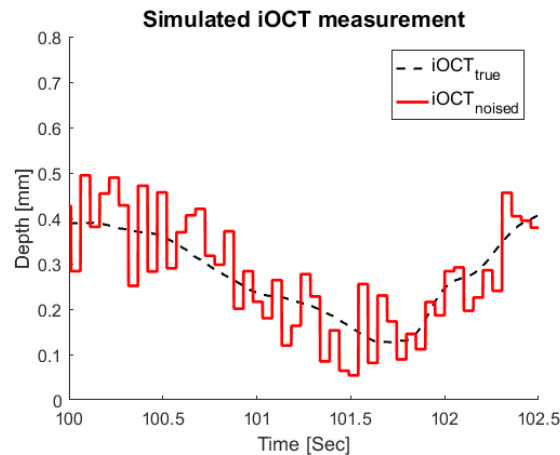


Figure B.6: The outcome of simulated iOCT using simulated true depth.

C

Vitreoretinal Simulator

This appendix provides supplemental information about the Vitreoretinal Simulator employed in the thesis project. Appendix C.1 describes the properties of the eye model in paper section 2.1.3. Appendix C.2 describes the set-up of the spherical coordinate and design of the ring-shaped target along with its reaching criteria, which corresponds to paper section 2.1.3 and 2.2.1. The membrane model and the corresponding peeling mechanism which are discussed in paper section 2.2.2 are explained and provided with detail algorithms in Appendix C.3. The last part of this appendix documents the visualization of the Vitreoretinal Simulator, which corresponds to paper section 2.1.4.

C.1. Perfect Sphere as the Eye model

In Vitreoretinal Simulator, the eye is modeled as a perfect sphere in Cartesian space. The location of the center, the radius of the eyeball, iris, and pupil determine the spatial property of this eye model. For convenience, the coordinates of the simulated eye are chosen to adapt to Matlab `plot3` function,

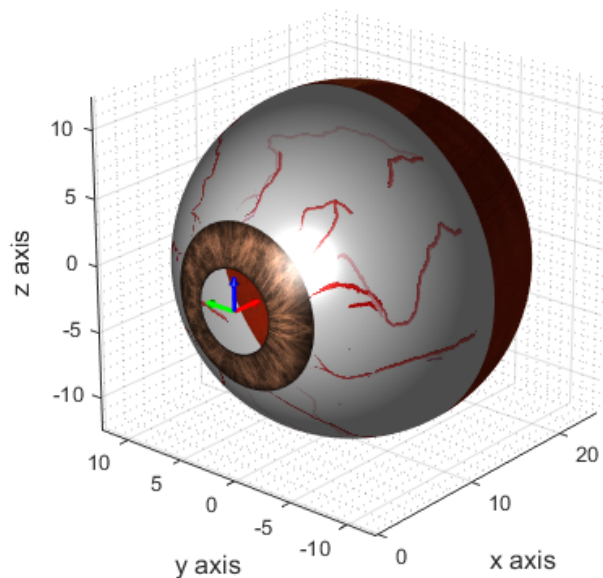


Figure C.1: A 3D view of the eye model: the colored arrows indicate the origin of the global reference and point correspondingly to the direction of the axes. X is in red, y is in green, and z is in blue.

where the x-axis points inward to the eye; z-axis points vertical up; and the corresponding y-axis points

to the left. Figure C.1 shows an image of the eye model and the corresponding axes. The center of the eye is anchored at the location such that the pupil overlaps y-z plane. All parameter settings are listed in Table C.1.

Table C.1: Eye model properties

Property	[unit]	Value
Eye center coordinates	[mm]	[12.1347;0;0]
Eye radius	[mm]	12.5
Iris radius	[mm]	6
Pupil radius	[mm]	3

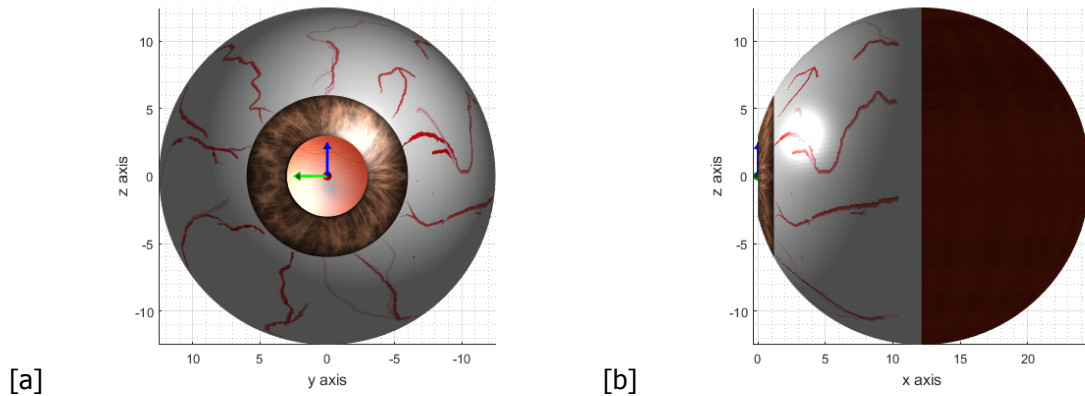


Figure C.2: [a] The front view of the eye model. [b] The side view of the eye model.

The eye model serves as the ground reference of the simulator. Target location, membrane peeling proxy, and, most important of all, penetration detection depend on this reference. Simplifying the eyeball to a perfect sphere has an advantage in the calculation of surface normal vector. E.g., the normal vector of the membrane proxy on the retina points directly to the center of the perfect sphere. With which, the peeling angle of the membrane can be calculated. However, these reference information, including the true iOCT depth, cannot be accessed by the operator. The iOCT signal has to be simulated as introduced in paper section 2.1.2.

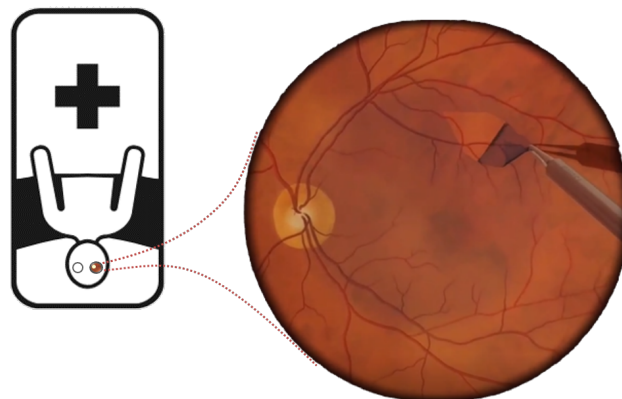


Figure C.3: At this position on the surgical table, a patient's right eye will have its optic disc showing on the left-hand side of the reader. The surgical simulation screen-shot on the right is modified from Eyesi[®] by VRmagic [2].

To provide a realistic visual effect, images of iris, eye white, and retina are employed and stitched to the spherical skeleton. It can be seen in Figure C.2 [b] the anterior eye is stitched with sclera image, while the posterior part with retina image only. Moreover, the camera perspective and the scale of the

source images are adjusted such that the relative size of the fovea and optic disc resembles real-life retinal surgery. Note, the optical disc is visible on the left-hand side to the reader, which means this is a right eye of a patient’s who lies on the surgical table with his/her head pointing towards the surgeon. Figure C.3 illustrates the position of the patient on a surgical table and a screen-shot of a commercial software specialized for surgical training – Eyesi® by VRmagic [2].

C.2. Spherical Coordinate & Target Properties

Apart from the local coordinate perspective of the simulated instrument (see Appendix B.1), a local spherical coordinate of the eye model is set up to describe the location of the ring targets and the peeling proxy. As depicted in Figure C.4, $r, \theta, and \phi$ define the spatial property of an object. The

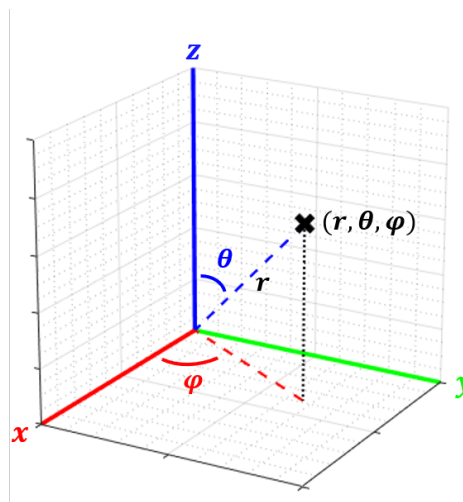


Figure C.4: The origin of the spherical coordinate is the center of the eye model. An object in this sphere is defined by three parameters: $r, \theta, and \phi$, where θ is the zenith angle and ϕ is defined as the negative azimuth angle.

property of the ring-shaped target and the criteria for a successful reach is given in this section. For how peeling proxy travels on the retina surface, please refer to Appendix C.3

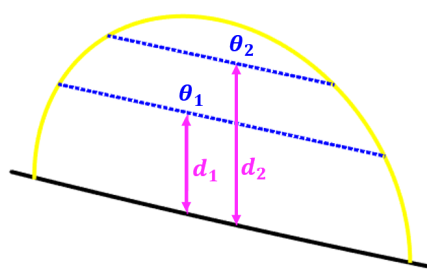


Figure C.5: Criterion for θ depends on current depth. The tolerance of θ increases as current depth decreases.

The purpose of the ring target is to motivate the participant to move the tip of the instrument to the desired location. Therefore, the physical contact between the ring and the tool tip is not taken into account. For simplicity, the orientation of the ring always aligns the lines of longitude and ring stands perpendicular to the retina surface. Table C.2 describes the algorithm used for target reaching criteria. Basically, the tool tip has to remain steady (tip velocity under $0.5mm/sec$) within the tolerance for 0.5 seconds (0.25 second was used for pilot study 1 and pilot study 2). To stay within the ring, the range

of θ changes corresponding to current depth. The closer the tool tip is to the retina, the wider the θ tolerance is. The relationship between the two variables is visualized in Figure C.5.

Table C.2: Algorithm: Target-reached Criteria

Algorithm: Target-reached Criteria	
%Transform the tooltip position into spherical coordinate	
[r, phi, theta] = Cart2Sphere(X_{tool});	
% Check ϕ	
Phi_OK = (abs(phi - Target_Phi) < phi_tolerance);	
% Check depth	
d = abs(Eye_Radius - r);	
d_OK = (d < Target_Radius);	
% Check d-dependent θ	
width = sqrt(Target_Radius^2 - d^2);	
mtheta = atan(width/r);	
Theta_OK = (abs(theta - Target_Theta) < abs(mtheta));	
% Check velocity	
V_OK = V < 0.5; % [mm/s]	
% Take intersection by and operator	
WithinTarget = Phi_OK && Theta_OK && d_OK && V_OK;	

C.3. Peeling Mechanism Model

A simple model simulating peeling an elastic film off a rigid substrate [6] is employed as the model for ERM in this study. By energy balancing method, it is shown that the elastic term tends to dominant over adhesion force only under two circumstances: 1. if the membrane does not fracture even when stress approaches elastic modulus, or 2. peeling angle approaches 180 degrees (this angle has been adapted to the definition in this report). The model has the following mathematical expression:

$$\left(\frac{F}{b}\right)^2 \frac{1}{2dE} + \frac{F}{b}(1 - \cos(180 - \theta)) - R = 0 \quad (\text{C.1})$$

, where θ angle has been modified from its original form in [6] and transformed to the definition in this report. The meaning of the parameters and the value used in the membrane model are listed in Table C.3.

Table C.3: Membrane model parameter settings

Parameter	Property	[unit]	Value
b	Membrane width	[mm]	1 e-03
d	Membrane thickness	[mm]	1 e-04
F_{break}	Breaking force	[mN]	7.5
E	Young's modulus	[N/mm ²]	9 *1 e+05
R	Experimental const.	[-]	7.5

ERM is simplified as a line-shaped thin elastic substance, having a width 0.001mm and a thickness 10% of the width. The threshold of membrane force F_{break} is chosen to be the force at the perceptual limit. Based on the predefined physical dimension and breaking force, Young's modulus is chosen such that the increase of the bonding force at the attachment point becomes more sensitive after exceeding 60 degrees. As a result, the safety margin remains for peeling (i.e., the applied force subtracted by the bonding force) before breaking the membrane decreases dramatically after 60 degrees. The

experimental constant R is used as fine-tuning of the peeling model. This constant offsets the modeled minimum adhesion force. As for the travel of the membrane proxy (representing the attachment point),

Table C.4: Algorithm: Membrane peeling mechanism

Algorithm: Membrane peeling mechanism
<pre> % Calculate elongation (no compression) elongation = sqrt(current_L/Membrane_L) - 1; % [%] % Membrane force (with saturation 1.8* Max_force) F_mem = elongation * E * A; % [N] % Decrease difficulty when the membrane is short if current_L < 30%Max_length F_mem is lowered % Calculate minimum force from membrane model F_min = Ang2Peel_F(Peel_angle); % Calculate the resultant force that contributes to moving the proxy % (with saturation to keep the proxy stable) F_result = F_mem - F_min; % Calculate peeling shear force shear_theta = F_result*cos(Peel_angle)*sin(Peel_dir_ang + Peel_rel_dir); shear_phi_g = F_result*cos(Peel_angle)*cos(Peel_dir_ang + Peel_rel_dir); % Move the membrane proxy if the elongation and direction are desired if (elongation > 0) && (shear_phi_g > 0) && (cos(Peel_rel_dir) > 0) Theta_hat = Theta - shear_theta; % + theta is downwards Phi_hat = Phi - shear_phi_g; % + phi is to the right side travel = sqrt(shear_theta^2 + shear_phi_g^2)*Eye_Radius; Membrane_L_hat = Membrane_L + travel; Path_L_hat = Path_L + travel; % Break Mechanism (Length complete or Force break) if (Membrane_L > Max_length) (F_mem > Max_force) if Membrane_L > Max_length Break = 1; elseif F_mem > Max_force Break = 2; </pre>

no tissue dynamics is considered. The algorithm for peeling is summarized in Table C.4. First, the applied force is calculated using the square root of the elongation and discounted when the membrane is 30% of its maximum length. Note, this formula is derived empirically to adjust the difficulty of the task.

The force contributed to moving the membrane proxy is the remaining force calculated using the subtraction of the applied force by the angle-dependent bonding force. The tangential component of this remaining force is then linearly mapped to the increment in θ - and ϕ -direction in the spherical coordinate (Appendix C.2). To limit the variability in participants' peeling behavior, the membrane proxy only travels towards the right-half side of the sphere (positive ϕ -direction). The membrane will increase its length the same amount as the travel distance. The maximum 2.2mm (2.5mm was used in pilot study 2) full membrane length is set up to regulate the number of re-grab motion. Once a membrane reaches this length, a segment is completed, and followed by 'Large Target (arb.)' to re-grab a new piece of membrane. Due to this setting, the number of 'Large Target (init.+arb.)' is at least five times more than that of 'Small Target,' which simulates a typical surgical condition.

C.4. Functions for Visualization

Two dynamic visual cues are implemented in the Vitreoretinal Simulator. Corresponding to paper section 2.1.4, Appendix C.4.1 describes the implementation of the instrument shadow for depth perception, while Appendix C.4.2 presents the color-mapping function used for force perception.

C.4.1. Instrument shadow

The shadow of the retinal pick is generated using the ray-tracing [7] technique. A point light source is placed inside the eye with the property listed in Table C.5. By using the line-sphere intersection

Table C.5: Lighting property

Property	[unit]	Value
Point light source o	[mm]	[9; 1; -6]

equations (equation B.18 and B.19), the projection of each surface point of the instrument on the inner eye surface can be traced by the vector \vec{l} described in the algorithm listed in Table C.6. Figure

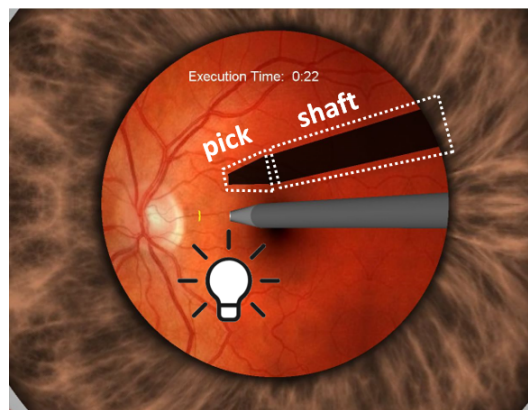


Figure C.6: A point light source is placed inside the eye. The simulated instrument is divided into two segments for implementing Matlab `surf` function.

C.6 illustrates the concept of shadow generation inside the eye. For implementation reasons, the instrument is separated into the pick- and shaft-segment. After separate projection, the shadows are stitched.

C.4.2. Membrane color

In paper section 2.2.2, Figure 7 shows the outcome of the peeling model. On the right side of the figure is the color bar of the force mapping. The RGB color is obtained by the transformation function presented in Table C.7. Note, the threshold in the exponential transformation function is set to $7mN$ ($0.5mN$ below the breaking threshold) to achieve obvious warning for the participants with no medical background. Together with the constant in the denominator, these constants are selected empirically. In the last step of the algorithm, the color was not taken square root in pilot study 2. It is adjusted to take the square root of the value so that the color changes more rapidly around the threshold.

Table C.6: Algorithm: Instrument shadow projection

Algorithm: Instrument shadow projection
<pre> % Divide 3D instrument into two segments (pick and shaft) % Select sectional points for later projection % Project these points into shadow points o = light_cneter; c = eye_center; for k = 1:size(shadowpoints,2) l = (shadowpoints(:,k)-o)/norm(shadowpoints(:,k)-o); d = -(l*(o-c))+sqrt((l*(o-c)).^2-(norm(o-c))^2+Eye_Radius^2); shad = d.*l+o; % Generate two black surfaces for pick and shaft % Stitch the two segments into one </pre>

Table C.7: Function: Membrane force-color mapping

Function: Membrane color maooining
<pre> function Mem_RGB = membrane_color(F_mem) % Force threshold is empirically set cutoff_force = 7*1e-3; % [mN] denominator = 1.5*1e-3; % [mN] % Exponential mapping color_ratio = exp((F_mem-cutoff_force)/denominator)^2; % Saturation if color_ratio >1;color_ratio = 1;end % RGB output Mem_RGB = [0.75*sqrt(color_ratio); 0; 1-0.75*sqrt(color_ratio)]; </pre>

D

Virtual Fixture Design Options

In this appendix, several haptic assistance design options are visualized with illustrations. They are introduced in chronological order of the design process.

D.1. Filtering Simulated iOCT

Corresponding to paper section 3, the virtual fixture starts by filtering the noisy iOCT measurement. A linear weighted moving average filter is employed. The window size is chosen as 250 sample points, where under the 1000Hz sampling rate, the window traces back to 5 ZOH signals. Figure D.1 depicts the result of filtering the simulated iOCT sensor information. However, both signals cannot facilitate a

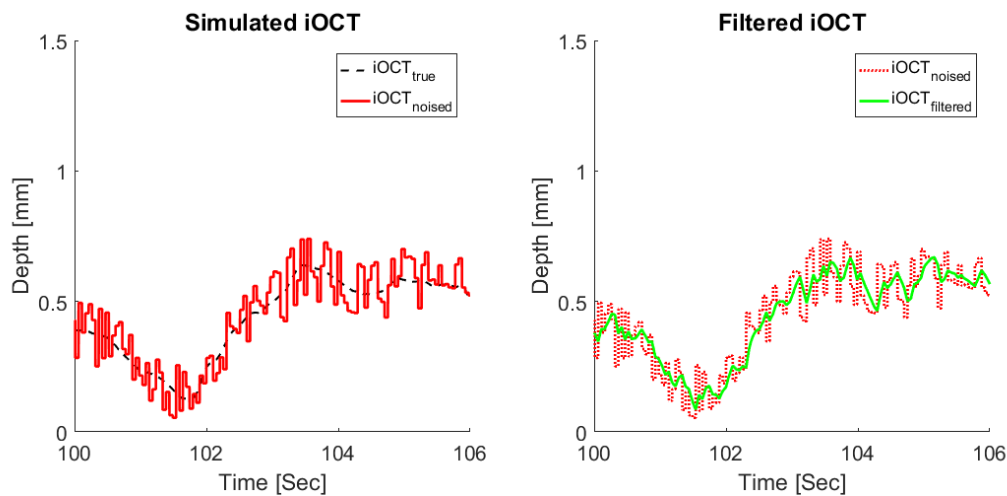


Figure D.1: On the left side of the figure shows the simulated noisy iOCT measurement as opposed to the simulated true iOCT depth. While the outcome after moving-averaging the simulated noisy iOCT depth is illustrated on the right.

traditional virtual fixture. For the unfiltered signal leads to a vibrating wall with 20Hz , and the filtered signal has little phase lag that leads to contact instability [8, 9].

D.2. Using PDD as a Passive Virtual Fixture

The filtered iOCT signal opens up design options for dampers and springs, which trades of a clear contact transition to some increasing force mapping. This idea is illustrated in Figure D.2. Corresponding to paper section 3.1, using damping as a virtual fixture is inspired by an application in Steady-Hand Eye Robot. By ramping up the damping coefficient close to the surface, a damper can be used as a Passive Virtual Fixture (PVF). The concept is depicted in Figure D.3. Note, the damping coefficient for PVF in Figure D.3 is the setting used throughout the research, which is the maximum value the

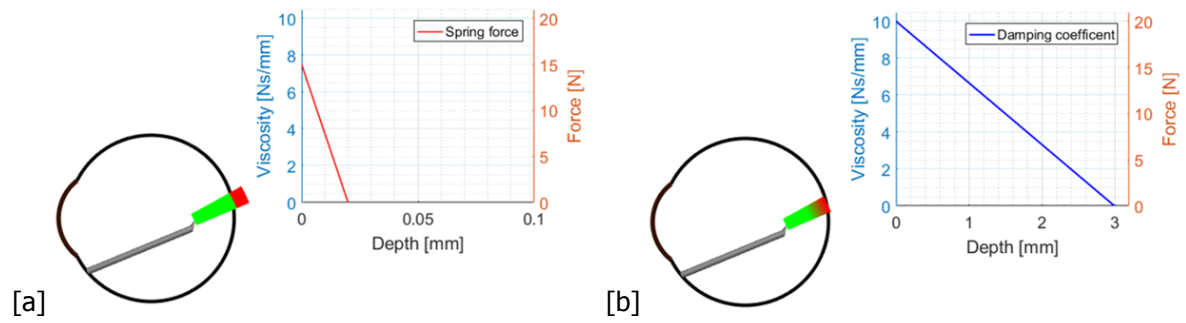


Figure D.2: [a] Traditional virtual fixture renders a wall with a stiff spring which starts slightly before the forbidden region to provide protection. Additional to the forbidden region colored in red, the green area is free from haptic feedback. [b] For a Position-Dependent Damping (PDD), the clear contact transition is replaced by a warning range that increases damping coefficient when approaching the forbidden region.

Needle Steering Haptic Master can achieve before instability due to the noise in the encoders of the device (which is amplified since there is no tachometer for velocity measurement). The maximum value $10Ns/mm$ Laurens used can only be achieved in 1D (the translational direction of the master device), while in 3D, the maximum value is around $3Ns/mm$. The comparison made in Figure D.3 adjust the maximum value of PDD to $5Ns/mm$, but the slope is kept as the original setting [10].

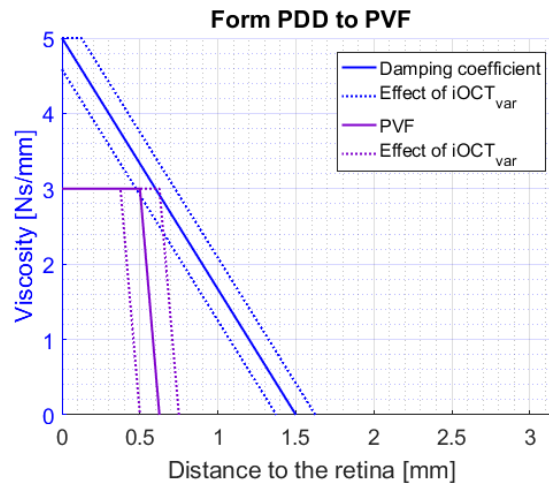


Figure D.3: A comparison between the passive virtual fixture and the linear position-dependent damping.

D.3. Active Sense vs. Passive Sense of Distance

Corresponding to Appendix F, in pilot study 1 (b), an Active Sense (AS) of distance is tested against a Passive Sense (PS) of distance in the target reaching task. Figure D.4 illustrates the principle of an AS. While Figure D.5 illustrates the principle of a PS.

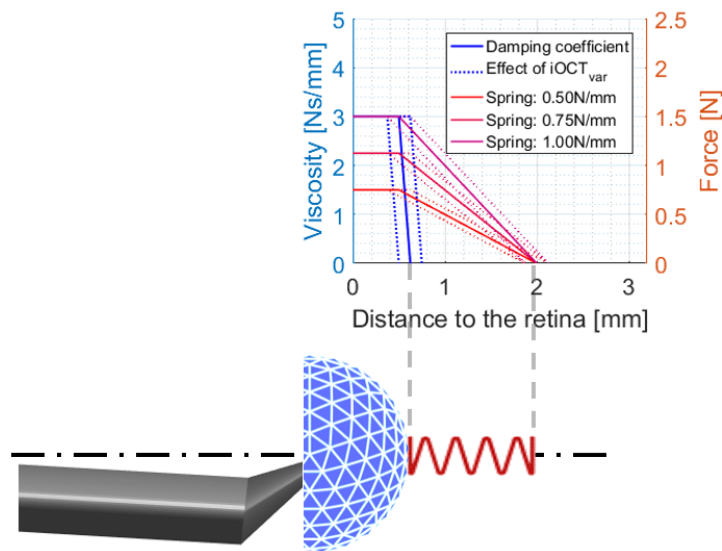


Figure D.4: The active sense consists of the passive virtual fixture (depicted as the blue sphere) and a spring extending from the PVF surface.

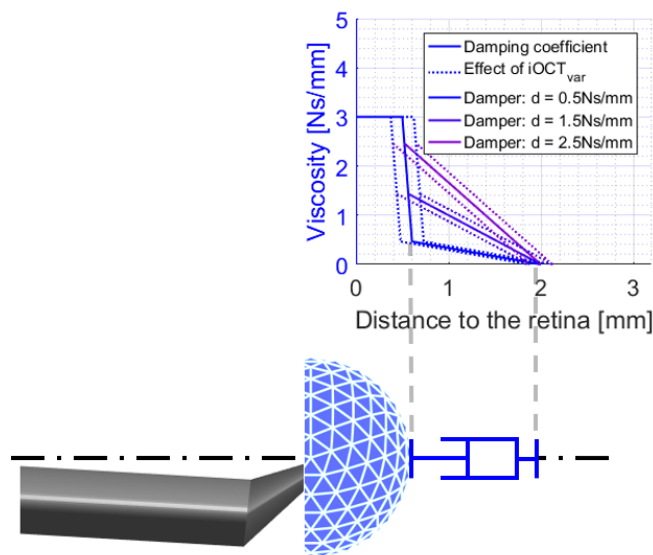


Figure D.5: The passive sense consists of the passive virtual fixture (depicted as the blue sphere) and a damper extending from the PVF surface.

D.4. Soft PVF + Active Sense of Distance

The design options tested in pilot study 2 (Appendix G) are illustrated in Figure D.6.

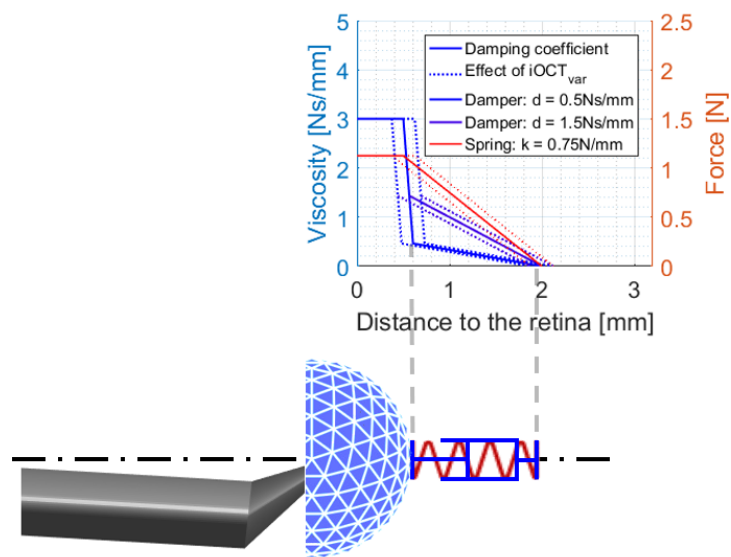
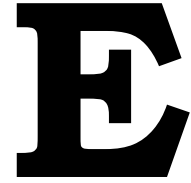


Figure D.6: This method is a combination of AS and PS, where the spring alone is tested with two combinations with two different values of damper.



Extensive Metrics & Results

Extensive metrics and the corresponding results that are not relevant for discussion in the thesis paper are discussed in this appendix. Appendix E.2 is a table listing the result of the paired sample t-test performed for all the metrics used in this research.

E.1. Extensive Metrics

- Segment Completion Rate [%]

The segment completion rate is used to reflect how likely can a piece of membrane reach the 2.2mm full segment length. It is calculated with dividing the number of the 2.2mm segments by the total fragment number of the peeling trace (i.e., the attempts of peeling). A significant difference with a large effect size is observed, from Baseline (M=65.17, SD=9.55) to VF (M=72.26, SD=7.57), with $t(15) = 3.20, p = 0.0059, d = 0.8$, which is a desirable result showing the virtual fixture is helpful for peeling.

- Safety Margin [mm]

The safety margin is a metric reflecting the performance of the target reaching task. It is the perpendicular distance of the tool tip to the retinal surface at the point where the reaching criteria are met. The larger the safety margin, the safer the retina is. Corresponding to Laurens' result [10], the safety margin of 'Large Target' shows no significant difference. However, with the effect of iOCT variance, no difference is observed in 'Small Target,' which is different from Laurens' observation in the haptic assistance without noise effect. Figure E.1 depicts the result of the safety margin for both target-reaching tasks.

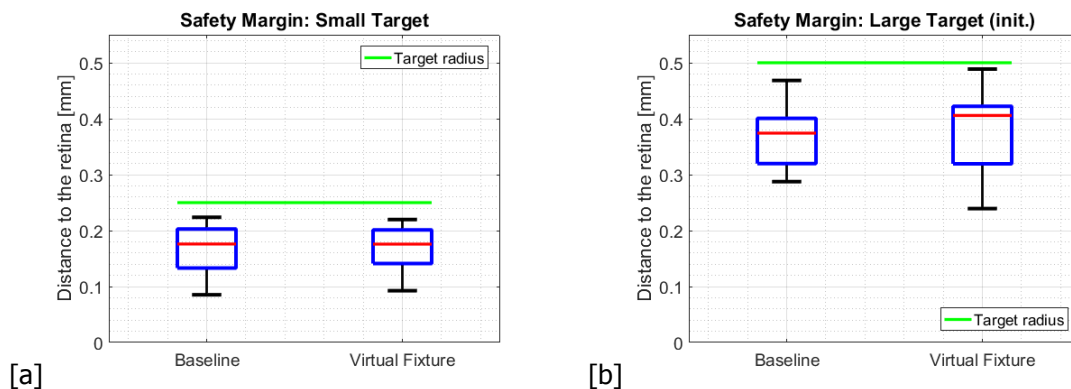


Figure E.1: [a] The averaged safety margin of reaching a small target (sample size = 16). [b] The averaged safety margin of reaching a large target (sample size = 9).

E.2. Complete Paired Sample t-test Table

Small Target		Baseline	Virtual Fixture			
		M (SD)	M (SD)	p – value t(15)	Cohen’s d	Effect size r ²
Puncture Rate	(%)	3.4722 (7.5564)	4.1667 (7.4536)	0.8198 t = 0.2319	0.0580	0.0598 ²
T _{completion}	(Sec)	11.0311 (3.8194)	13.6238 (6.7623)	0.1121 t = 1.6878	0.4219	0.3995 ²
T _{approach}	(Sec)	6.1482 (2.7488)	5.1391 (1.7846)	0.054 t = 2.0904	0.5226	0.4750 ²
T _{precise}	(Sec)	4.8830 (1.6468)	8.4847 (5.9240)	0.02 * t = 2.6031	0.6508	0.5578 ²
Safety Margin	(mm)	0.1701 (0.0436)	0.1694 (0.0394)	0.9497 t = 0.0641	0.0160	0.0166 ²
Large Target		Baseline	Virtual Fixture			
		M (SD)	M (SD)	p – value t(15)	Cohen’s d	Effect size r ²
Puncture Rate (Large)	(%)	10.4986 (8.7915)	1.0802 (1.9512)	5.26e-04 *** t = 4.3910	1.0977	0.75 ²
Large Target (Initial Position)				p – value t(8)		
Puncture Rate	(%)	5.2800 (9.6529)	0 (0)	0.1394 ^f t = 1.6410	0.5470	0.5018 ²
T _{completion}	(Sec)	11.5466 (3.3662)	11.6875 (2.0384)	0.8878 t = 0.1456	0.0485	0.0514 ²
T _{approach}	(Sec)	7.0342 (2.5913)	6.9112 (1.7630)	0.8586 t = 0.1840	0.0613	0.0649 ²
T _{precise}	(Sec)	4.5123 (1.4142)	4.7763 (0.7260)	0.6547 t = 0.4645	0.1548	0.1620 ²
Safety Margin	(mm)	0.3677 (0.0594)	0.3812 (0.0754)	0.6236 t = 0.5104	0.1701	0.1776 ²
Large Target (Arbitrary Position)				p – value t(15)		
Puncture Rate	(%)	14.4048 (12.4082)	1.3715 (2.4958)	8.18e-04 *** t = 4.1717	1.0429	0.7329 ²
Membrane Peeling		Baseline	Virtual Fixture			
		M (SD)	M (SD)	p – value t(1,15)	Cohen’s d	Effect size r ²
OCT Depth AVG	(mm)	0.6307 (0.1953)	0.6032 (0.2009)	0.3324 t = 1.0017	0.2504	0.2504 ²
OCT Depth STD	(mm)	0.2762 (0.1149)	0.2290 (0.0915)	0.0037 ** t = 3.4298	0.8574	0.6630 ²
Peeling Angle (AVG)	(deg)	29.0347 (6.5806)	27.3076 (6.9515)	0.1098 t = 1.6999	0.4250	0.4019 ²
Peeling Angle (STD)	(deg)	9.7761 (1.9713)	8.6368 (1.7348)	0.0094 ** t = 2.9771	0.7443	0.6094 ²
Peeling Force (AVG)	(mN)	4.8983 (0.2383)	4.9393 (0.2908)	0.3434 t = 0.9784	0.2446	0.2449 ²
Peeling Force (STD)	(mN)	0.5969 (0.1212)	0.5405 (0.1024)	0.0010 ** t = 4.0549	1.0137	0.7231 ²
Puncture Rate	(%)	8.7089 (5.9809)	3.9215 (4.7954)	0.0042 ** t = 3.3739	0.8435	0.6569 ²
Segment Completion Rate	(%)	65.1736 (9.546)	72.2619 (7.5652)	0.0059 ** t = 3.2023	0.8006	0.6372 ²
T _{peeling}	(Sec)	75.5067 (11.4830)	71.5780 (14.5025)	0.0315 * t = 2.3713	0.5928	0.5222 ²
Overall		Baseline	Virtual Fixture			
		M (SD)	M (SD)	p – value t(1,15)	Cohen’s d	Effect size r ²
Puncture Rate (overall)	(%)	9.6132 (6.8189)	2.7996 (2.9448)	8.9e-05 *** t = 5.3006	1.3251	0.8074 ²
T _{execution}	(Sec)	149.1209 (48.9609)	126.1862 (28.4806)	0.0133 * t = 2.8063	0.7016	0.5867 ²
Workload	(-)	61.6354 (9.7784)	54.3687 (12.1978)	0.0079 ** t = 3.0625	0.7656	0.6203 ²

f: Although the original data set passed the Kolmogorov-Smirnov normality test, the puncture rates of VF condition are all zeros (pushed to one side). Additionally, a rank transformed t-test is performed, and the result: t(8) = 2.4954, p = 0.0372* is obtained

P < 0.05 *
P < 0.01 **
P < 0.001 ***

E.3. Experimental Replay

Figure E.2 is a video demonstrating the recorded motion of the third trial of subject 11. The haptic feedback due to the support of the virtual fixture is visualized in the red line at the tip of the retinal pick.

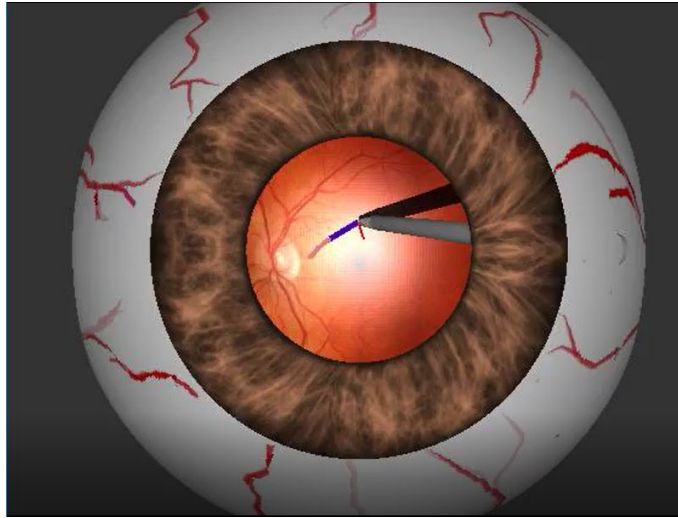


Figure E.2: An experimental replay of the third trial of subject 11. The time scale is ten times faster than real time. (This is an mp4 file that can only be viewed in the digital version of the report, please refer to TU Delft online repository.)

F

Pilot Study I

This appendix presents the first pilot study conducted in this research. The pilot study consists of two parts, which only focus on the Target Reaching Task. All participants go through two parts during the experiment. Pilot study 1 (a) and (b) use basically the same simulation platform of Laurens' work [10]. The only difference is that the haptic force feedback has been extended to 3D and the ring target is generated randomly within the target region.

Five participants participated in this pilot study. Unfortunately, the data of the first participant was incomplete, and thus removed from the analysis. Four of the participants are all right-handed male, with mean age: 25.75 years. The criterion of this experiment is not having medical training for retinal surgery.

F.1. Objective

1. Part (a): Quantification of the perceptual limit performing Target Reaching task under baseline condition to determine the proper size for:
 - Small Target – should be around the limit where the puncture rate and the completion time are expected to be higher.
 - Large Target – should be larger than small target and should have a difference in difficulty compared to the small ring.

Note, variation between participants is expected, so the selection is made conservatively.

2. Part (b): A first selection round between two haptic assistance candidates. The effect of three different gain values for each candidate is tested.
 - Active Sense (AS) of distance – a spring extended from the virtual fixture, which provides force feedback based on position. Therefore, the sense of distance is active in the sense that it can be sensed in static.
 - Passive Sense (PS) of distance – a damper extended from the virtual fixture, which provides force feedback based on velocity. Contrary to active sense, force feedback reflecting distance can only be felt during motion.

F.2. Experimental Design

The material used in this pilot study is identical to the final experiment, except that the Vitreoretinal Simulator only includes the target reaching task. The camera zoom is the same as Laurens' setting [10], which is smaller than that in the final experiment.

A new ring-shaped target is randomly generated within the range $(\theta, \phi) = (90 \pm 6.25^\circ, \pm 6.25^\circ)$ on the spherical coordinate of the eye model (Appendix C.2). The task is to consecutively reach several targets with different conditions (six haptic conditions and baseline). The subjects undergo the experiment first by completing part (a) then continue on part (b) after a break in between. The experimental

procedure and the conditions for the two parts are summarized in the following subsection. For detailed descriptions of the pilot study, please refer to Appendix H.1.

F.2.1. Part (a): Perceptual limit

Under baseline condition (with no haptic feedback), the participants are asked to place the tool tip position within the space of a series of ring-shaped targets, which differ in size. From the largest radius to the smallest are 0.6mm , 0.5mm , ..., 0.2mm . Task condition is the same for all participants. In each trial, they start from 0.6mm target, and after three accumulated successful reaches, the ring shrinks in size. If a penetration is made, the run will count as a puncture instead of accumulating as a successful reach. Until the 0.2mm level is completed, a trial ends. Six repetitions for each level are obtained by each participant performing two trials.

F.2.2. Part (b): Active Sense(AS) vs. Passive Sense(PS)

Similar to part (a), the participants are asked to reach the target from a randomized location but this time the ring size is fixed to 0.3mm , and the conditions are all with haptic assistance. A virtual fixture with extended active sense is tested against a virtual fixture with extended passive sense. Three different gain values are tested for each haptic assistance method. The six different haptic conditions being tested are:

Virtual fixture (3Ns/mm damper) + either

- | | |
|------------------------------------|---------------------------------------|
| (1) AS – 0.50N/mm spring, | (4) PS – 2.5Ns/mm damper, |
| (2) AS – 0.75N/mm spring, | (5) PS – 1.5Ns/mm damper, or |
| (3) AS – 1.00N/mm spring, | (6) PS – 0.5Ns/mm damper. |

Since the scope of this pilot study does not cover optimizing the gain value for each method, the condition does not require randomization with a Latin square. Therefore, the subject number is chosen to be four, just to balance the order of having active and passive sense. Subject 1 and 4 undergo (1), (2), and (3) then (4), (5), and (6). While subject 2 and 3 undergo the reverse order: (4), (5), and (6) then (1), (2), and (3). To better visualize the experimental procedure, two arrows are plotted in Figure F.6: AS conditions are in red and PS conditions are in blue.

F.3. Metrics & Data Analysis

The metrics used in this pilot study are: the puncture rate and completion time (overall/precise/approach) which are all defined in the thesis paper. Moreover, individual reaching behavior of Target Reaching (paper section 2.2.1) is validated by inspecting individual velocity profile.

Due to data corruption of participant number five, only four subject data are analyzed. For part (a), one outlier is removed to meet the same amount of repetition (5x) as part (b) has. The outlier criteria are based on maximum approach time, which happens when the subject idles. The calculated metrics of each condition are averaged over five repetitions.

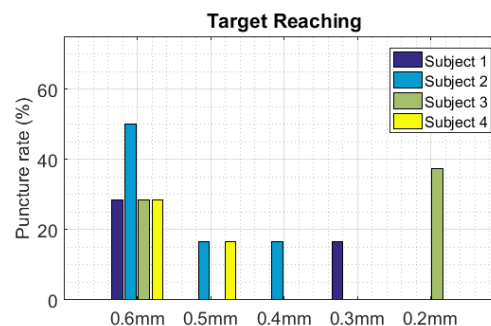


Figure F.1: Puncture rate of target reaching with different ring sizes under baseline condition.

F.4. Main Results

F.4.1. Objective 1

The perceptual limit is observed to be $0.3mm$ in terms of precise phase time. Therefore, the small target can be any value below $0.3mm$ while the large target should be larger than $0.4mm$.

F.4.2. Additional findings

Additional findings of pilot study 1 are the observation of learning effect and the establishment of precise and approach phase. As depicted in Figure F.1, the puncture rate of reaching the largest target is observed to be the largest. This unexpected result is due to learning effect. Since the targets are not generated with randomized size, the largest target is given when the subjects are still learning. By visual inspection, the completion time for different sizes of target rings also show no trend (see Figure F.2), which is different than expected. According to Fitts' law, the time needed for smaller targets should be longer. Based on Laurens' study [10], a further inspection is possible by defining the precise

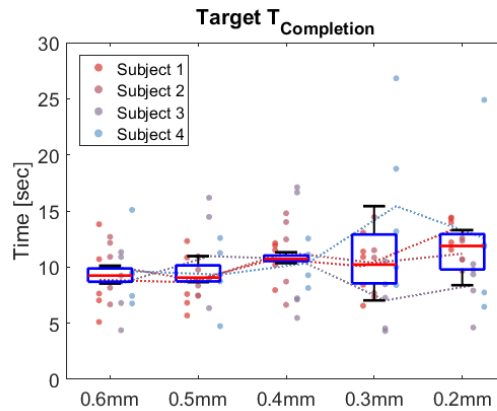


Figure F.2: The completion time of reaching targets with different sizes under baseline condition.

and approach phase based on the $1.5mm$ separation of the distance to the retina. Figure F.3 depicts the two detailed phase of completion time. The slowing down in motion can be observed in individual raw data given in Appendix F.5. A repeated measures ANOVA is performed, and a difference between

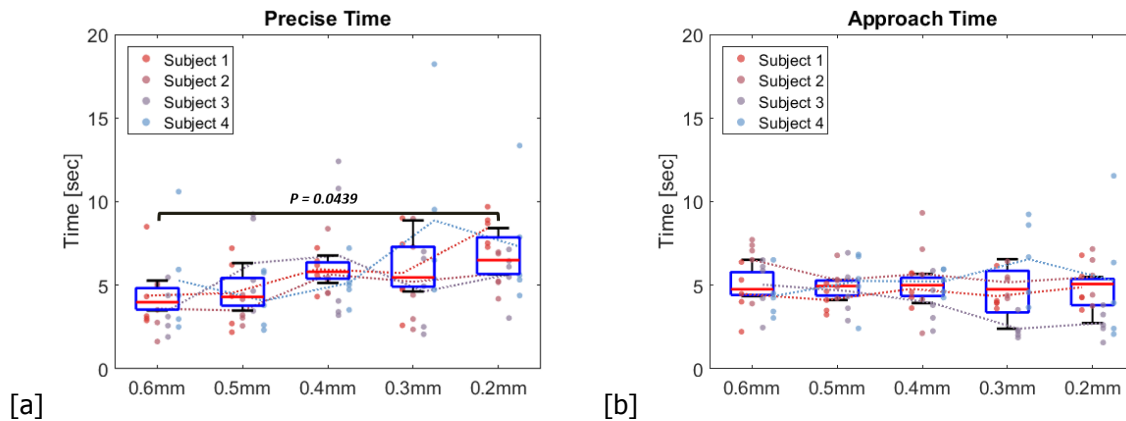


Figure F.3: [a] Precise time of reaching targets with different sizes. [b] Approach time of reaching targets with different sizes.

$0.6mm$ target and $0.2mm$ target is observed, which infers precise phase time is a robust (against the noise caused by the imperfection in the experimental set-up) metric reflecting the performance of target reaching. The perceptual limit for baseline condition is selected based on the standard deviation of precise time. Depicted in Figure F.4, a slightly higher value is observed in $0.3mm$ by visual inspection. This value appears to be the point where some subjects start to reach their limit and thus increasing the

standard deviation of precise phase time. While in 0.2mm ring size, the standard deviation decrease back to normal level for the task becomes relatively hard for every subject.

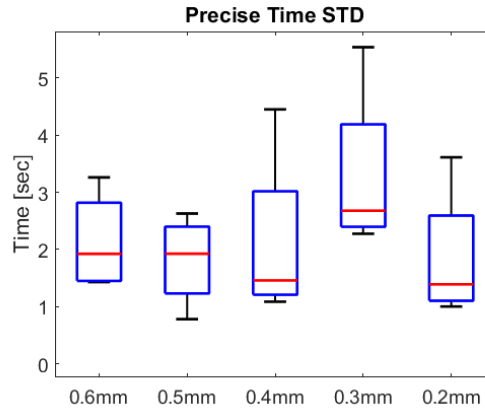


Figure F.4: The standard deviation of the execution time in precise phase under baseline condition.

F.4.3. Objective 2

In general, with the aid of active sense, the subjects performed better than with passive sense. The subjects only puncture when supported with passive sense. While the puncture rate is 0% for all participants under active sense condition. The puncture rate of pilot study 1 (b) is depicted in Figure F.5. The results of the completion time, approach time, and precise time are depicted in Figure F.6,

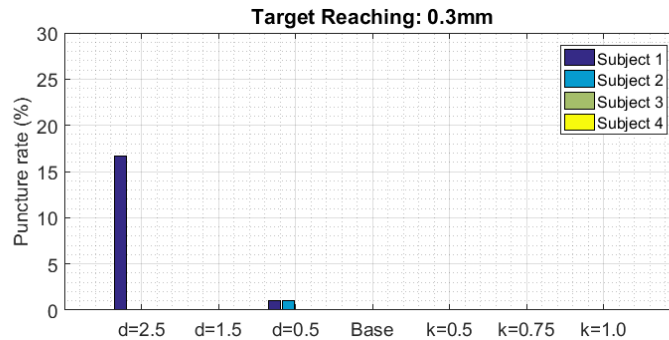


Figure F.5: Puncture rate of target reaching with different haptic conditions.

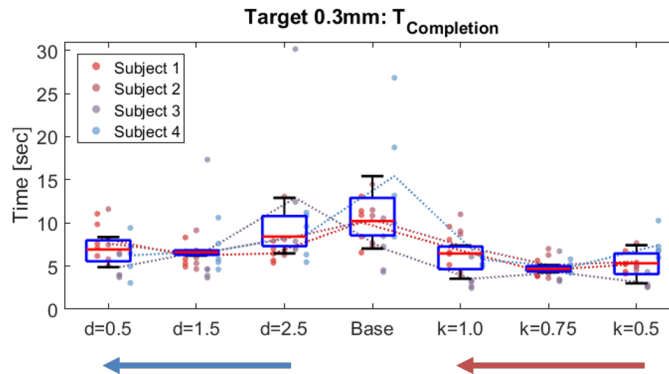


Figure F.6: The completion time of 0.3mm target reaching with different haptic conditions. The arrows illustrate the order of how the gains are given.

F.7, and F.8.

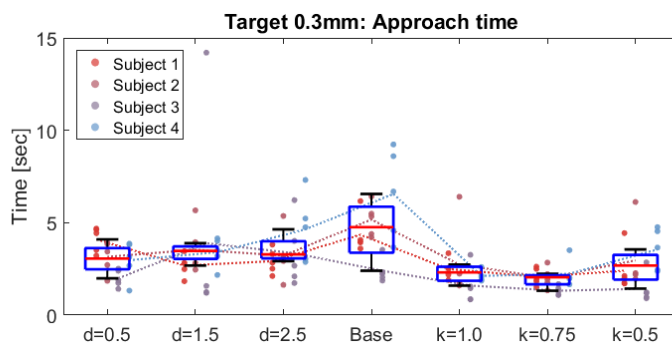


Figure F.7: The approach phase time of 0.3mm target reaching with different haptic conditions.

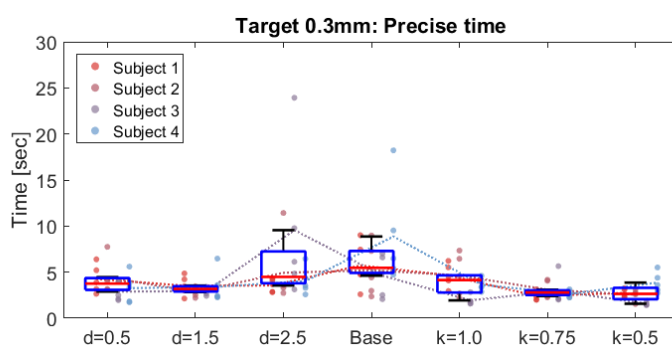


Figure F.8: The precise phase time of 0.3mm target reaching with different haptic conditions.

The effects are observed to be small by visual inspection. Additionally, the statistical power is insufficient (due to limited sample number) to draw any conclusion between the gain difference.

F.5. Individual Reaching Profile

The individual velocity profile of reaching targets with several ring sizes are depicted in the following figures. The target radius is visualized in green lines and the 1.5mm separation in dash lines.

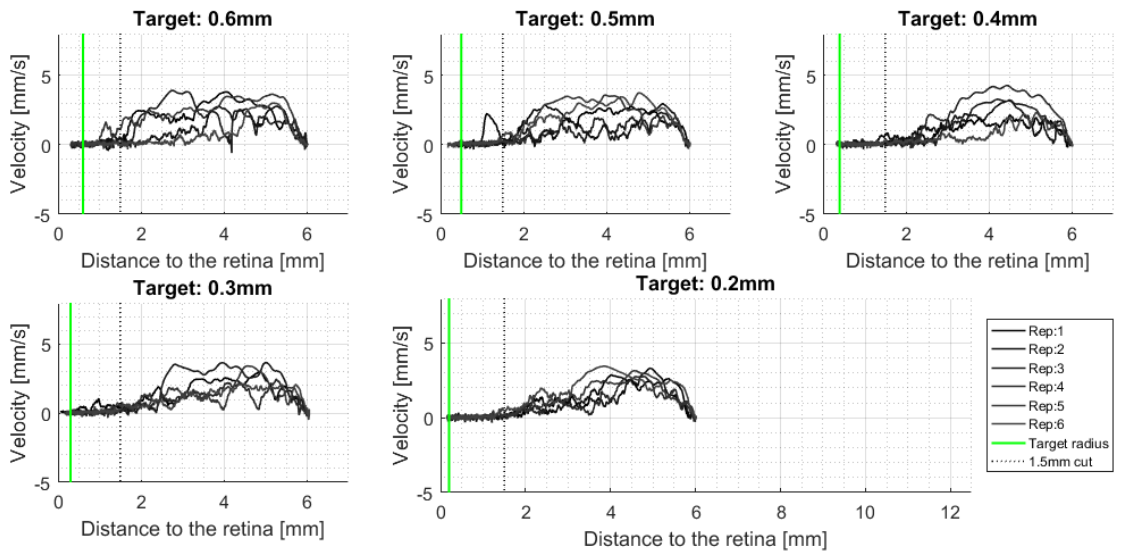


Figure F.9: Subject 1: Velocity profile in pilot study 1 (a).

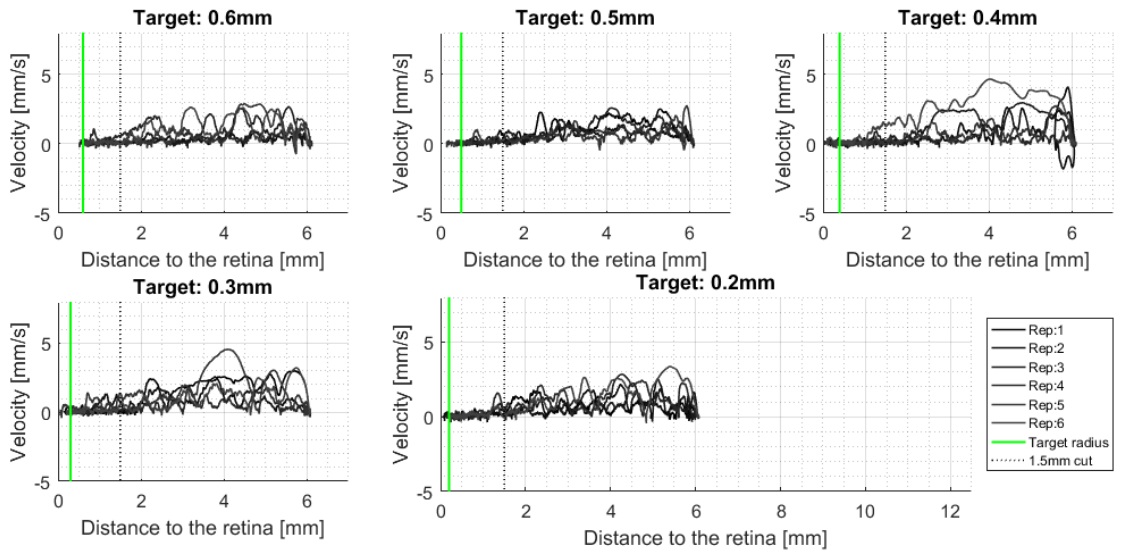


Figure F.10: Subject 2: Velocity profile in pilot study 1 (a).

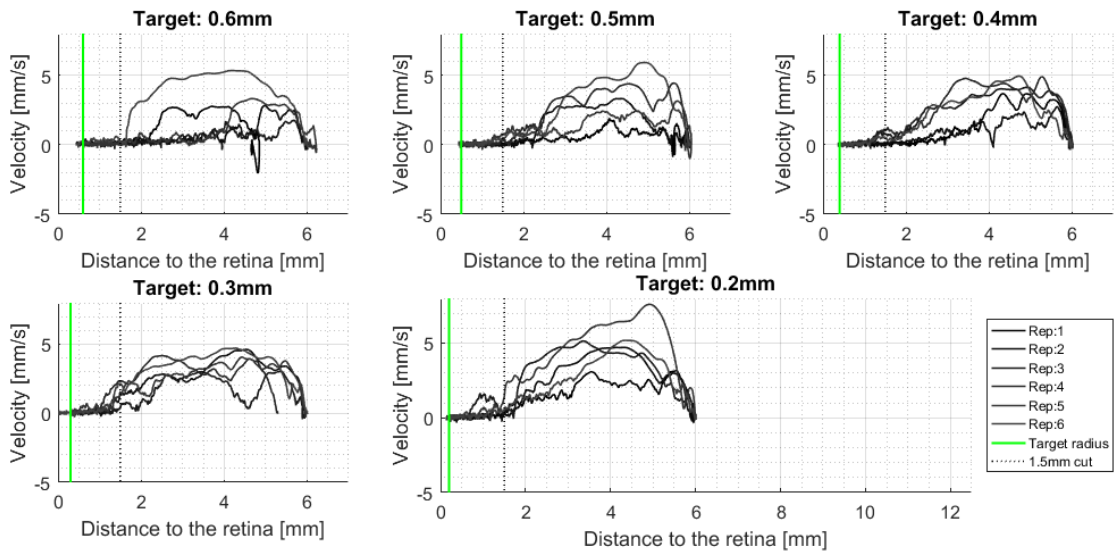


Figure F.11: Subject 3: Velocity profile in pilot study 1 (a).

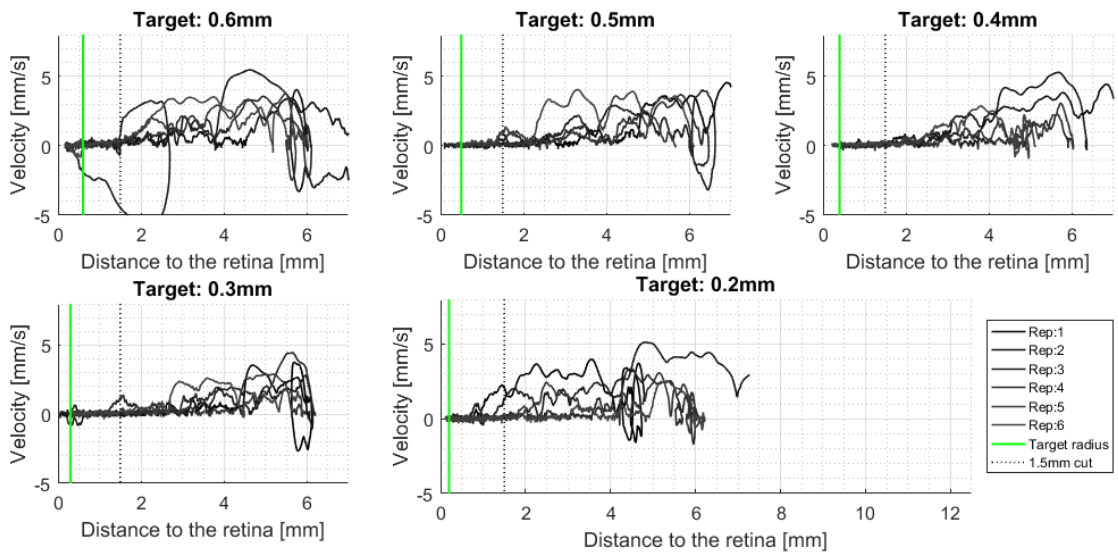


Figure F.12: Subject 4: Velocity profile in pilot study 1 (a).

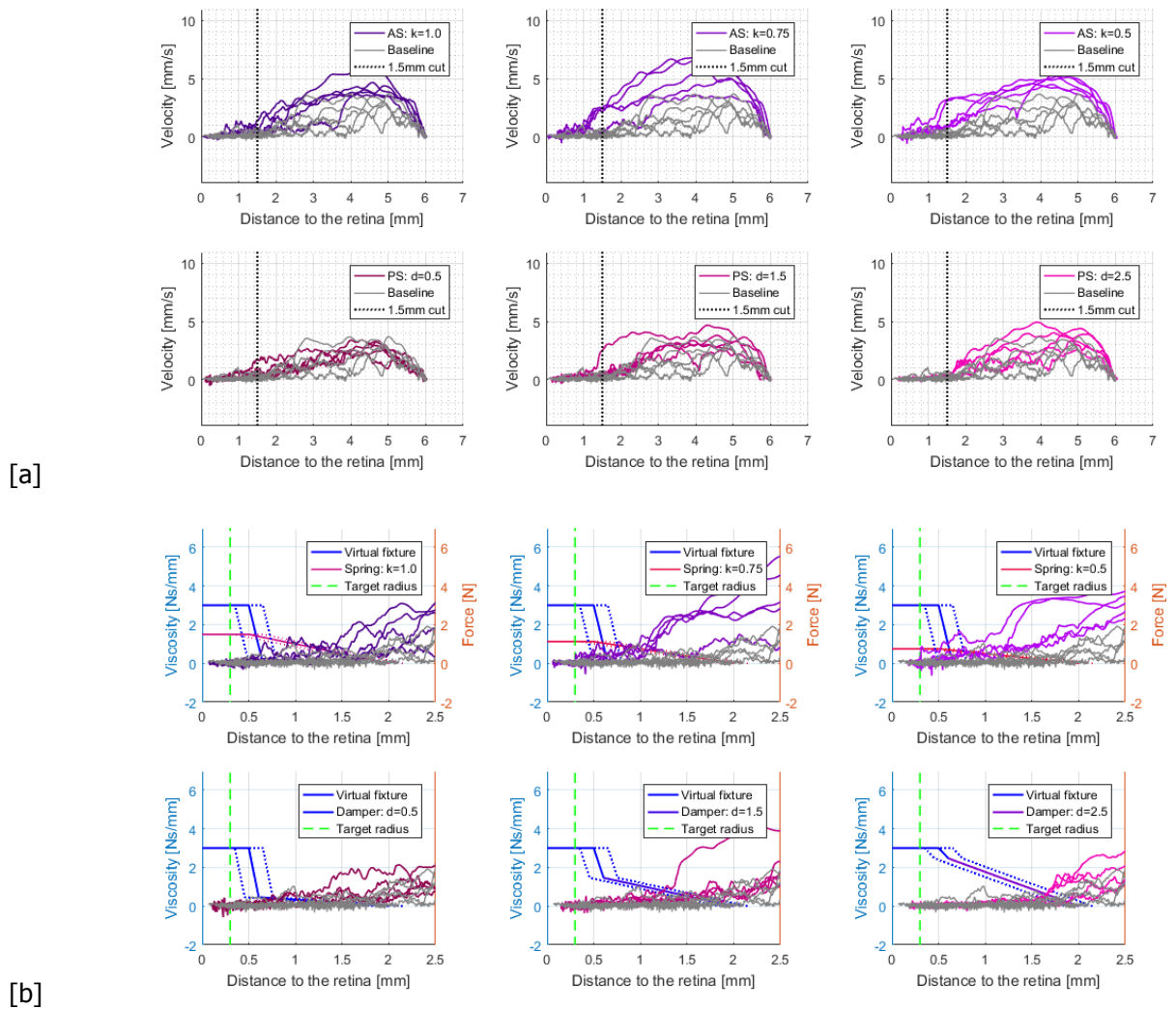


Figure F.13: Subject 1: [a] Velocity profile in pilot study 1 (b). [b] A zoom in of [a] with the 0.3mm target and haptic assistance visualized. The baseline condition in pilot 1 (a) is plotted as gray lines for comparison.

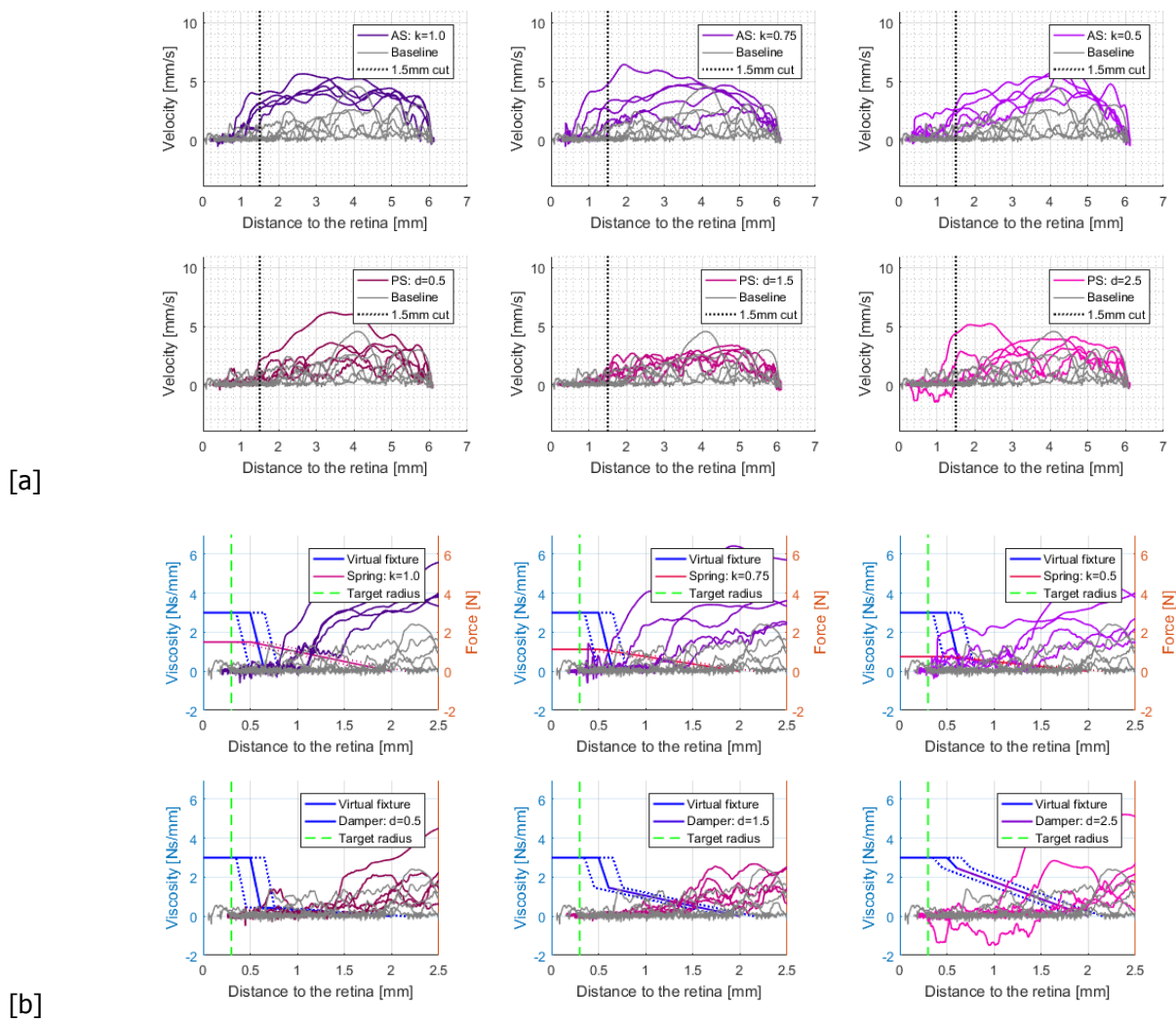


Figure F.14: Subject 1: [a] Velocity profile in pilot study 1 (b). [b] A zoom in of [a] with the 0.3mm target and haptic assistance visualized. The baseline condition in pilot 1 (a) is plotted as gray lines for comparison.

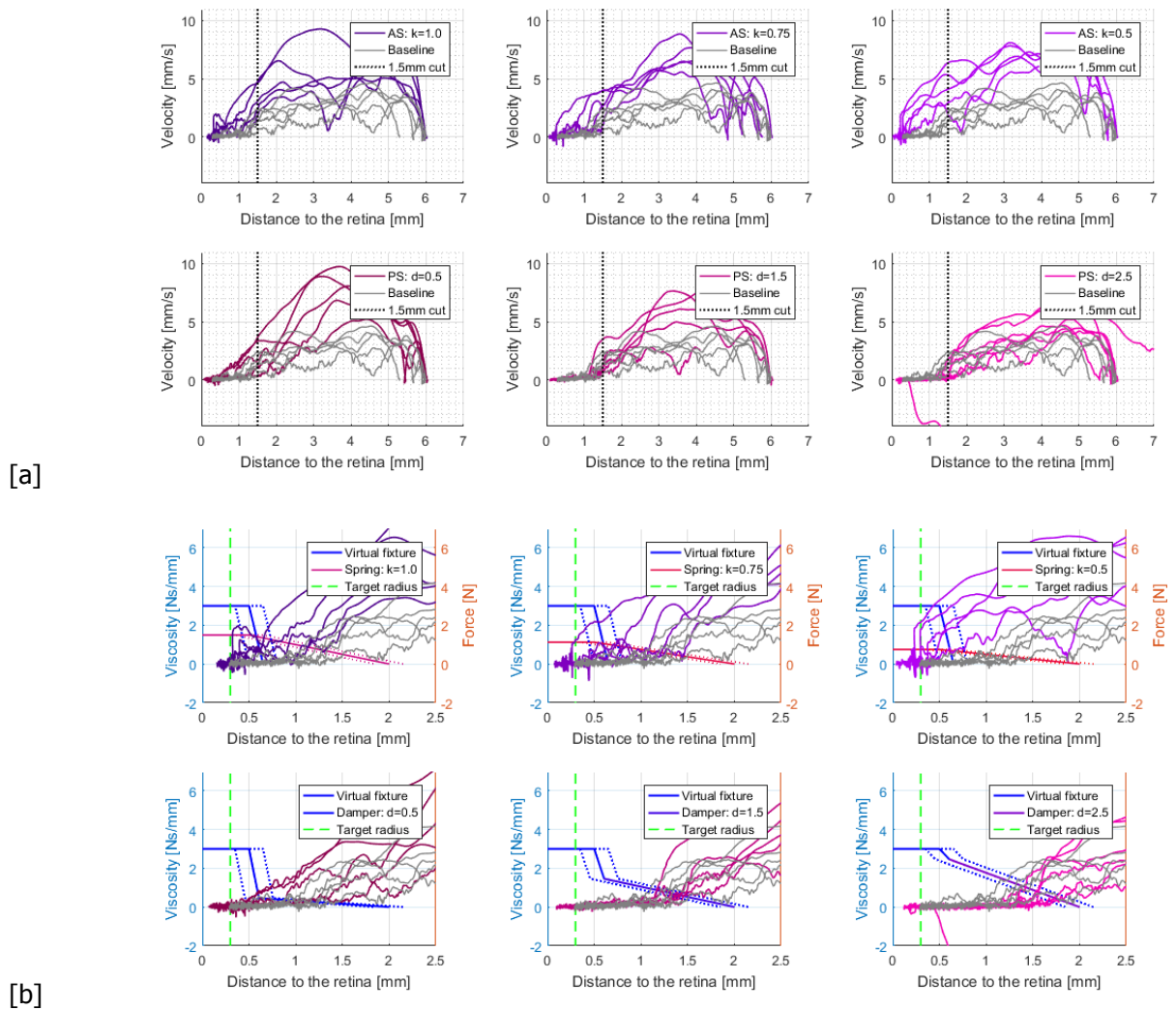


Figure F.15: Subject 3: [a] Velocity profile in pilot study 1 (b). [b] A zoom in of [a] with the 0.3mm target and haptic assistance visualized. The baseline condition in pilot 1 (a) is plotted as gray lines for comparison.

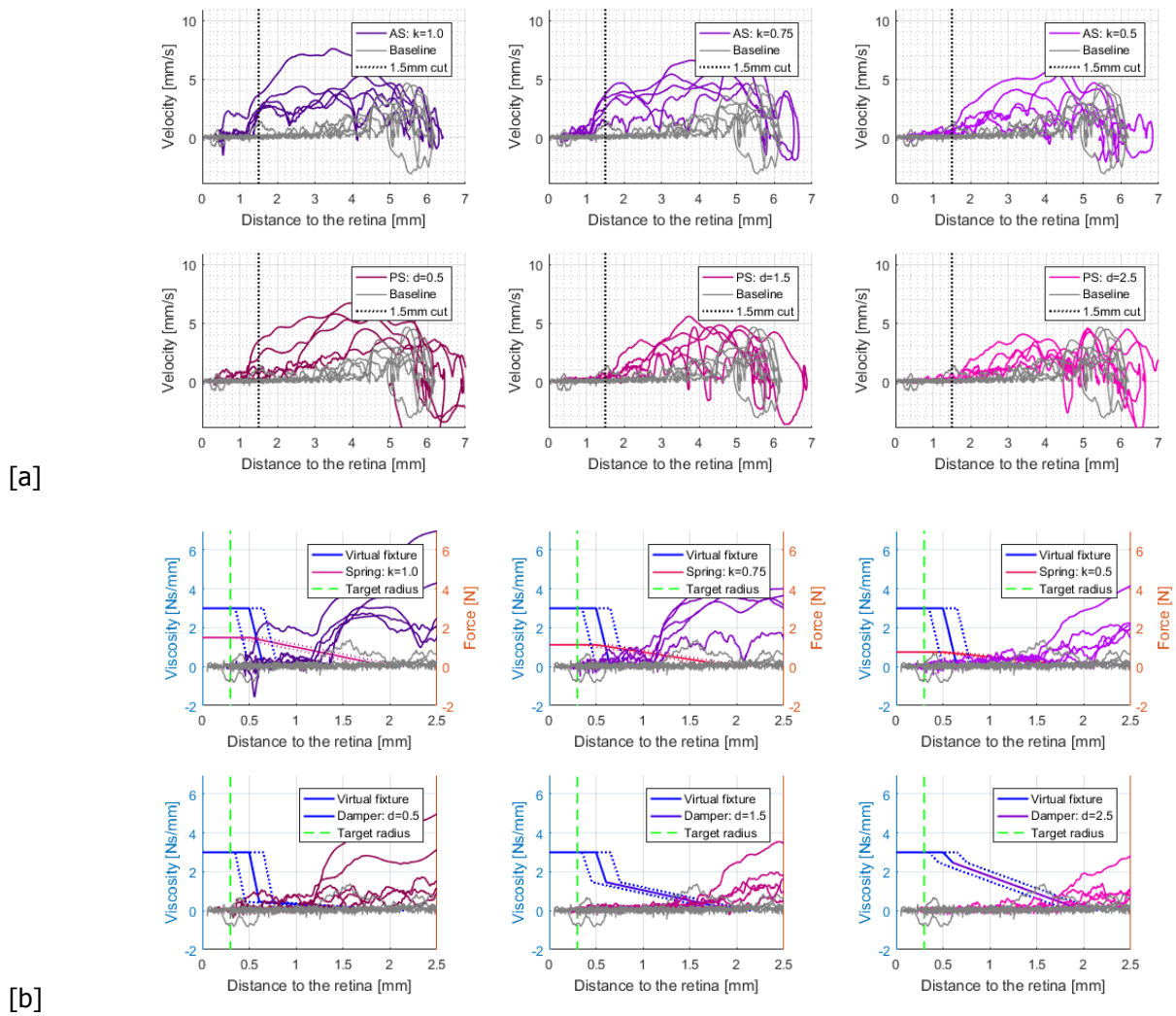


Figure F.16: Subject 4: [a] Velocity profile in pilot study 1 (b). [b] A zoom in of [a] with the 0.3mm target and haptic assistance visualized. The baseline condition in pilot 1 (a) is plotted as gray lines for comparison.



Pilot Study II

This appendix presents the last pilot study conducted before the final experiment. The experimental set-up and protocol are similar to that in the final experiment except for the model parameters in the peeling model is slightly different. Three haptic assistive methods are tested with the baseline condition. Four participants (2 male, 2 female, mean age: 28.75 years, one left-hander) participated in the experiment. The criteria for the participant of this experiment are not having previous experience on the needle steering haptic device nor medical training for retinal surgery.

G.1. Objective

1. Final selection of the virtual fixture design from the three candidates.
2. Evaluate if the task difficulty for baseline condition is appropriate for participants to complete training within 30 minutes.
3. Final testing for experimental protocol and data acquisition.

G.2. Experimental Condition & Order

virtual fixture with extended active sense is tested against a virtual fixture with extended passive sense. Three different gain values are tested for each haptic assistance method. The six different haptic conditions being tested are:

Virtual fixture (3Ns/mm damper) + either

- (1) $P - 0.75N/mm$ spring
- (2) $PD_w - 0.75N/mm$ spring + $0.5Ns/mm$ damper, or
- (3) $PD_s - 0.75N/mm$ spring + $0.5Ns/mm$ damper.

Experimental conditions are given in two orders: Baseline, (1)P, (2)PD_w, then (3)PD_s, or Baseline, (3)PD_s, (2)PD_w, then (1)P. Besides the training under the baseline condition at the beginning of the experiment, short training for each haptic condition is given before the start of the two measurement trials.

G.3. Metrics & Data Analysis

In this pilot study, the metrics used for the target reaching tasks are identical to the ones in the final experiment, which are the puncture rate and completion time (overall/precise/approach). As for the metrics used for '(Membrane) Peeling,' all of which are identical to the metrics used in the final experiment.

Due to an error in the program, subject 1 and 4 didn't switch from PDs to PD_w. Instead, they underwent PDs twice. Therefore, only the data of subject 2 and 3 are analyzed. The calculated metrics are averaged over two trials in each condition.

G.4. Results

- Due to the insufficient number of participants, the final virtual fixture method is chosen to be PDs, a relatively conservative method.
- The task is found to be too difficult for training. The peeling model is, later on, adjusted in the final experiment.
- The scoreboard gamification is tested to be successful in terms of motivating participants.

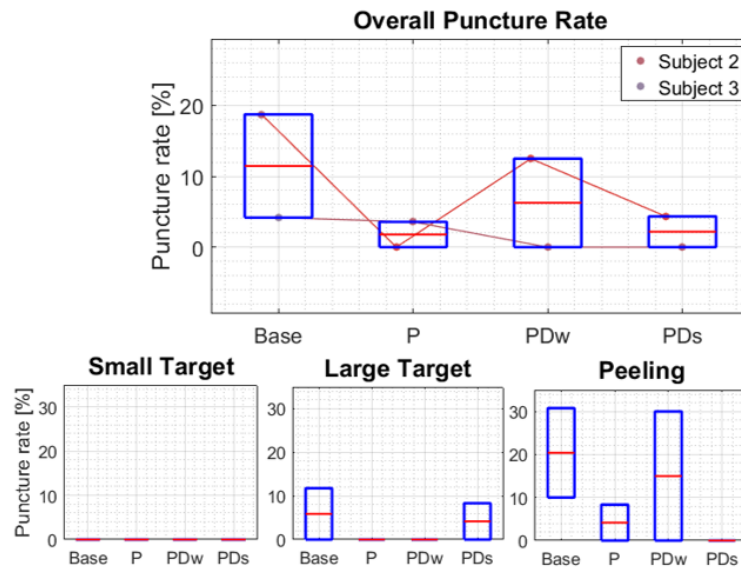


Figure G.1: The upper box plot shows the overall puncture rate of the two subjects. The mean values from the two trials in the four conditions of each participant are linked. The overall puncture rate can be broken down into the puncture rates of the three sub-tasks. Depicted from left to right are 'Small Target,' 'Large Target,' and 'Peeling.' The red line in the box plot represents the median.

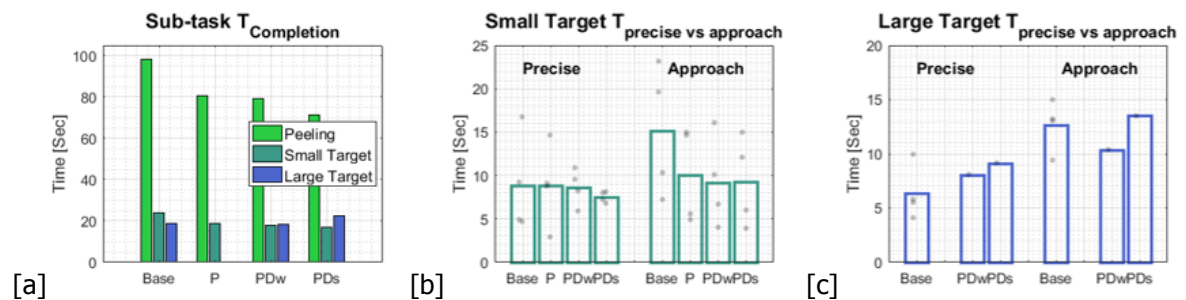


Figure G.2: [a] Depicts completion time for each sub-task under the four conditions. [b] Bar plots of precise/approach phase time for 'Small Target,' where data of the two subjects are plotted as gray dots (sample size = 2*2 for each condition). [c] Bar plots of precise/approach phase time for 'Large Target.' Note, the sample size is smaller than 'Small Target' since one of the subjects didn't penetrate the retina during peeling.

G.5. Individual Peeling Raw Data

The following figures are individual peeling data for all subjects in all experimental conditions. In this experiment, the participants performed two trials for each condition. The plots read the same way as in the thesis paper, except for the visualization of the current peeling angle is removed, leaving only peeling trace history.

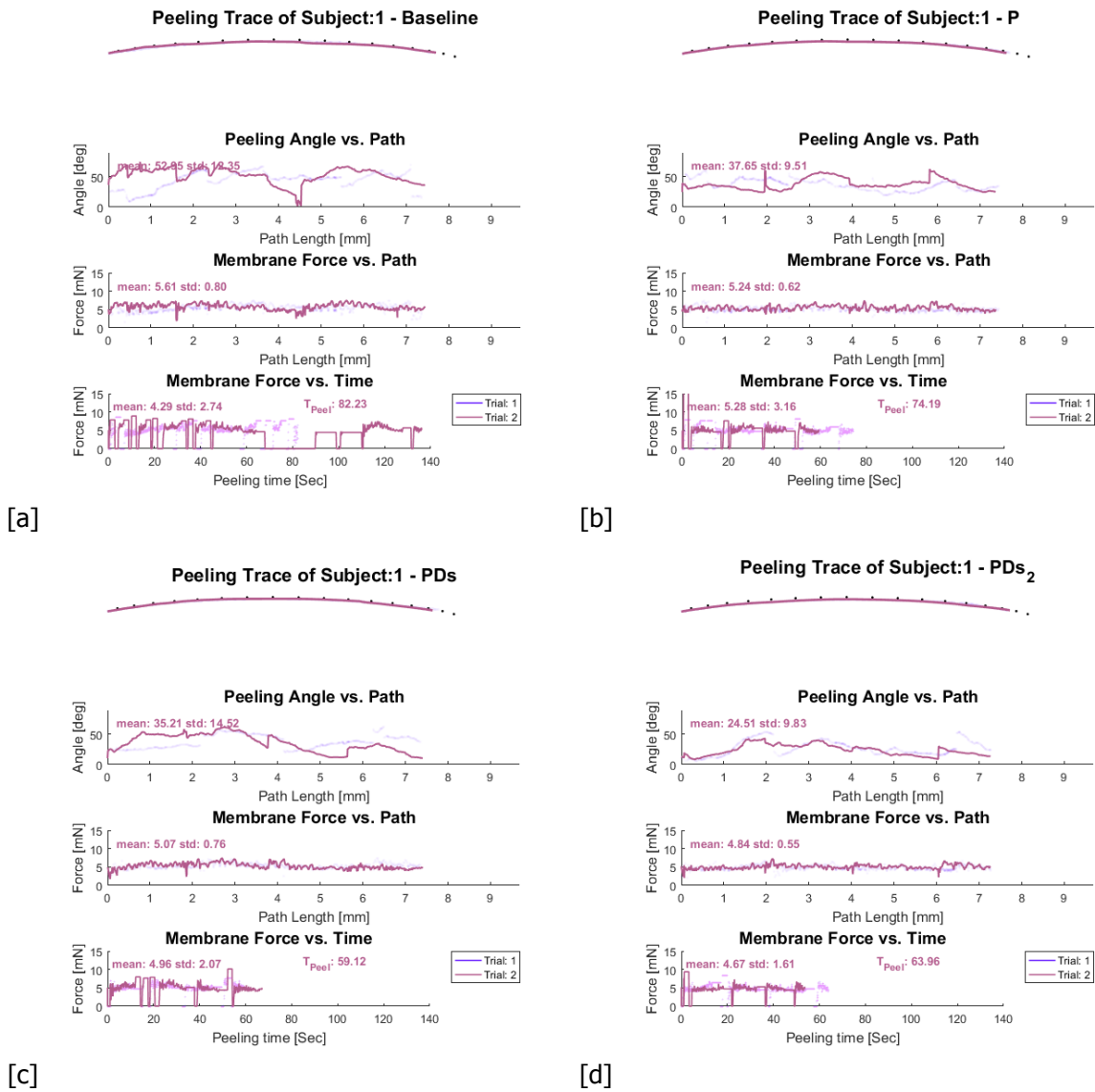


Figure G.3: Subject 1: [a] Peeling data under the baseline condition. [b] Bar plots of precise/approach phase time for ted in gray dots (sample size = 16*3). [c] Bar pl

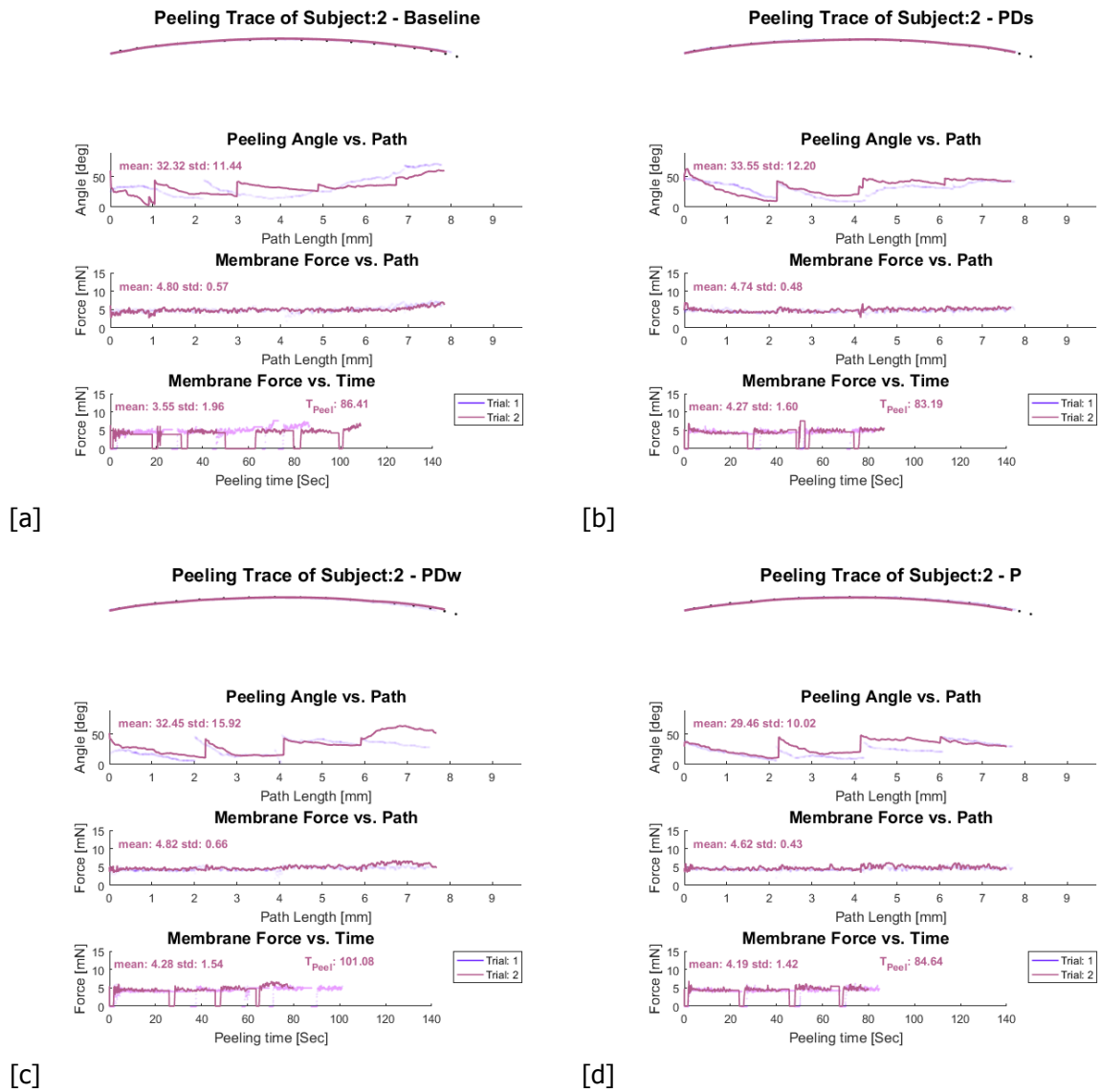


Figure G.4: Subject 2: [a] Peeling data under the baseline condition. [b] Peeling data under the 'PDs' condition. [c] Peeling data under the 'PDw' condition. [d] Peeling data under the 'P' condition.

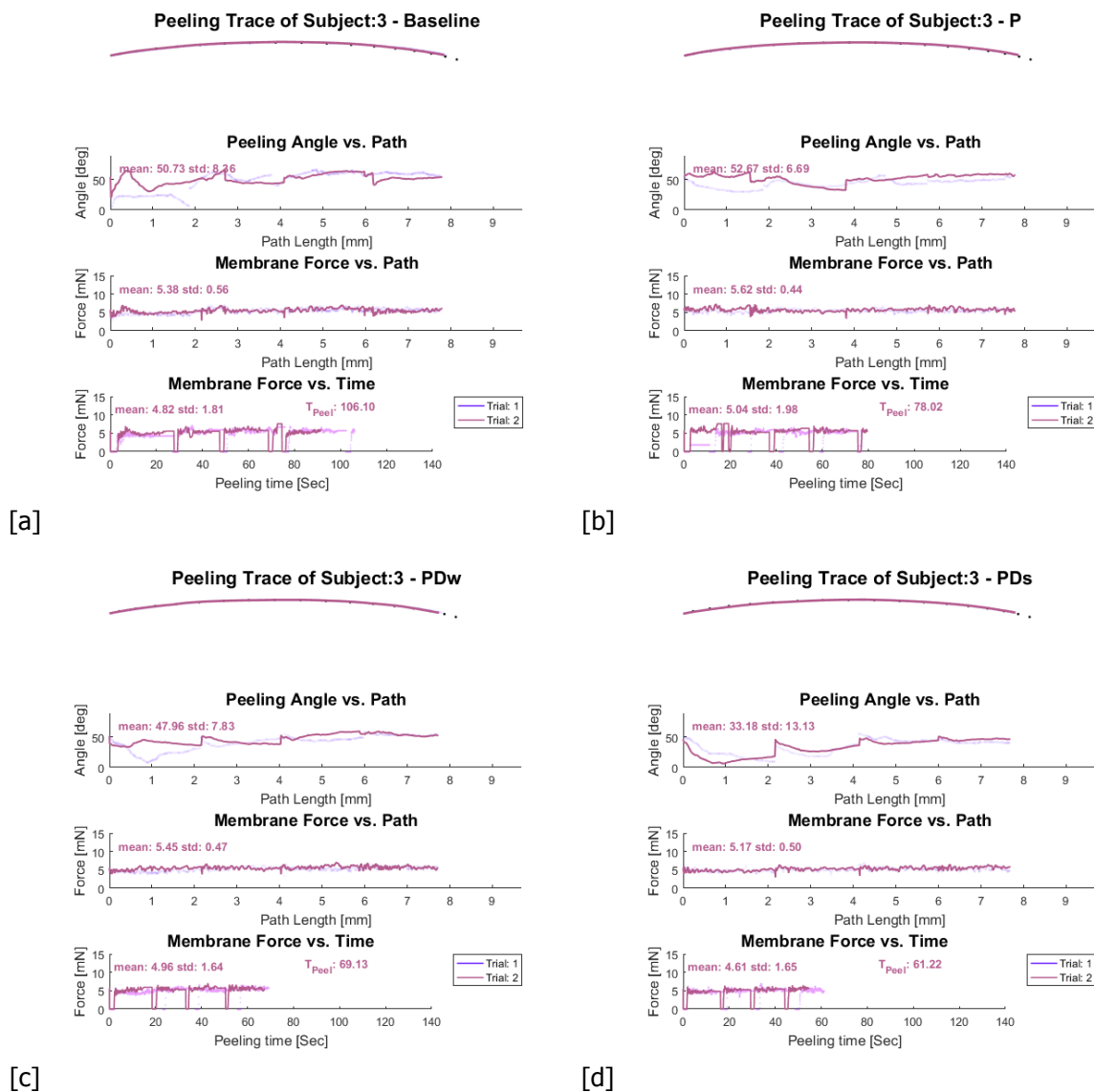
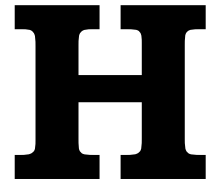


Figure G.5: Subject 3: [a] Peeling data under the baseline condition. [b] Peeling data under the 'P' condition. [c] Peeling data under the 'PDw' condition. [d] Peeling data under the 'PDS' condition.



Informed Consent Forms

This Appendix lists the informed consents that have been used throughout the study. They are pilot study 1 (a) and (b) in Appendix [H.1](#), pilot study 2 Appendix [H.2](#), and the final experiment in Appendix [H.3](#). The personal information sheet is given in Appendix [H.4](#).

H.1. Pilot Study I

HUMAN SUBJECT RESEARCH: INFORMED CONSENT

For a study investigating Haptic Feedback for Tele-operated Vitreoretinal Surgery

Date 06-08-2018, Version Pilot I. 1.0

Before agreeing to participate in this study it is important that the information in this document is carefully read and understood. This document will describe the purpose, procedures, risks and possible discomforts of this experiment.

Location of the experiment

Delft University of Technology
Department of Mechanical Engineering
Mekelweg 2, Delft
Cognitive Robotics Lab, Room 34 F-0-220

Study background

Vitreoretinal surgery (surgery that takes place in the posterior eye) remains one of the most challenging procedures now clinically in practice. It requires precise and accurate motion control and extremely high hand-eye coordination. Moreover, the delicate and fragile nature of human eye not only makes any scratch on the retina impermissible but deprives the force feeling when interacting with eye tissue. The goal of this research is to investigate whether haptic feedback can aid retinal surgery. The participant will be asked to control a needle steering haptic master to perform simulated task (computer program) that resembles retinal surgery.

Study goal

The purpose of this pilot study is to (1) quantify the perceptual limitation of performing an eye surgery on the simulator without haptic feedback; and (2) identify which range of haptic feedback gain yields a better result.

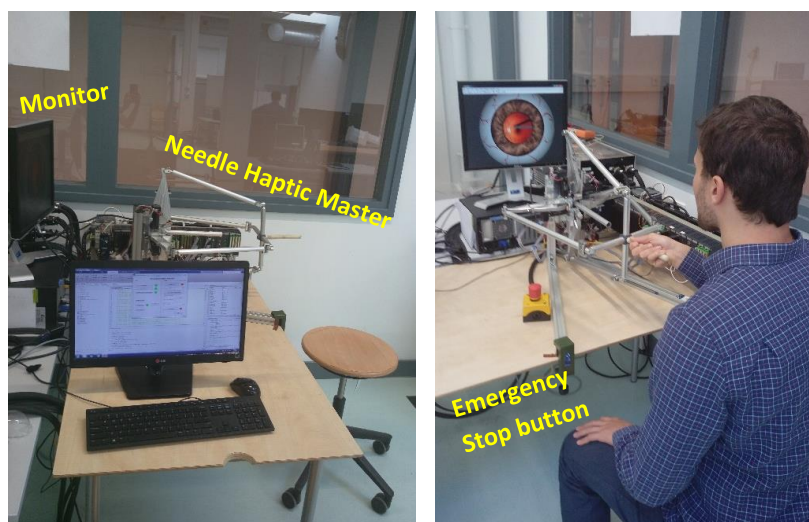


Figure 1: Experimental setup overview



Delft
Haptics
Lab



Cognitive
Robotics

PRECEYES

Procedure

Before starting the experiment, you will be asked to carefully read and sign this consent form as well as to fill out some personal details. Including familiarization with the simulator, the total length will be approximately one hour.

0. Familiarization

During this phase, you will be provided with introduction about the haptic device and the eye surgery simulator. A setup overview is shown in figure 1. The seat is adjustable such that you can manipulate the handle in the most comfortable position you like.

Following up are two tasks in this pilot study:

1. Perceptual limits

In this task you have to finish reaching six different sizes (from large to small) of yellow ring-shaped targets with the instrument pick as depicted in figure 2. Every time the target is successfully reached three times, the size (radius) of the ring shrinks. Note that there will be no haptics feedback during this task. The only visual cues are the relative position of the pick and target and the shadow of the pick. Penetrating the retina is not permitted; however, if you do so the device will reset to its initial position and restart a new run. Please release your hand from the handle when initializing (you shall see an image like figure 3).

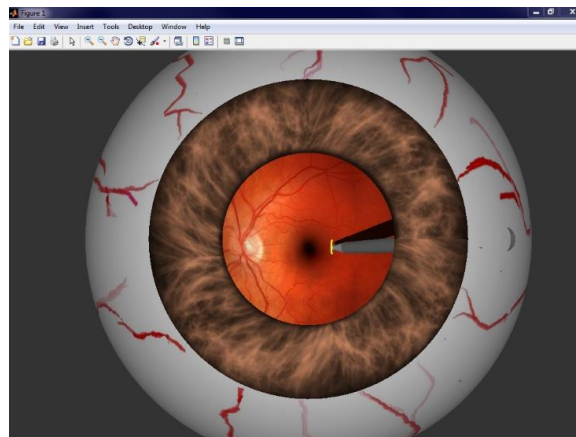


Figure 2: Image of the eye surgery simulator during target reaching task

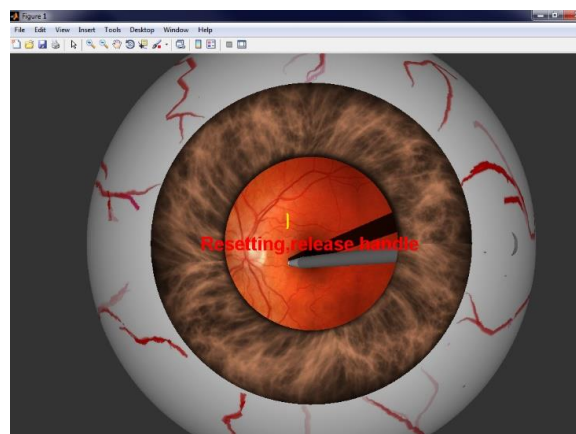


Figure 3: Text display when penetrating the retina

2. Haptic gain tuning

Similar to task 1, during this task you are still reaching the ring target but with a fixed size. Two testing haptic shared control methods will be provided. For each of them, three different gains of feedback will be tested (from weak to strong). Before recording data, complete explanation and training of the two haptic feedback methods will be provided.

Risks

Risks associated with the study are small. The movement of the shoulder is only in the order of a few centimetres and the handle is protected from making larger movements. Before participating in the study, the researcher will assess whether you are capable of finishing the study.

Participation is voluntary!

Your participation in the study is voluntary. If you agree on participating in the study, you have the right to withdraw at any time (also during the study). There is no need to have a legitimate reason to do so.

Confidentiality

Your personal details and data are fully confidential. People not authorised to access your details will not have the opportunity to do so. The experimental results will be statistically analysed and published in a Master thesis, and potentially be used in a scientific publication as while. When the results of the study get published, it is impossible to trace these back to you.

Contact information

Should you have any questions concerning the experiment, please contact the researcher:

Tse-Kang Shen (Stan)

T: +31649327103

E: T.shen@student.tudelft.nl

I have read and understood the information provided above.

I give permission to process the data for the purposes described above.

I voluntarily agree to participate in this experiment.

Name:

Date:

Signature of the participant:

H.2. Pilot Study II

HUMAN SUBJECT RESEARCH: INFORMED CONSENT

For a study investigating Haptic Feedback for Tele-operated Vitreoretinal Surgery

Date 14-08-2018, Version Pilot II. 1.0

Before agreeing to participate in this study it is important that the information in this document is carefully read and understood. This document will describe the purpose, procedures, risks and possible discomforts of this experiment.

Location of the experiment

Delft University of Technology
Department of Mechanical Engineering
Mekelweg 2, Delft
Cognitive Robotics Lab, Room 34 F-0-220

Study background

Vitreoretinal surgery (surgery that takes place in the posterior eye) remains one of the most challenging procedures now clinically in practice. It requires precise and accurate motion control and extremely high hand-eye coordination. Moreover, the delicate and fragile nature of human eye not only makes any scratch on the retina impermissible but deprives the force feeling when interacting with eye tissue. The goal of this research is to investigate whether haptic feedback can aid retinal surgery. The participant will be asked to control a needle steering haptic master to perform simulated task (computer program) that resembles retinal surgery.

Study goal

The purpose of this pilot study is to (1) acquire baseline performance of participants performing simulated membrane peeling surgery without haptic feedback; and (2) compare three different types of haptic feedback.

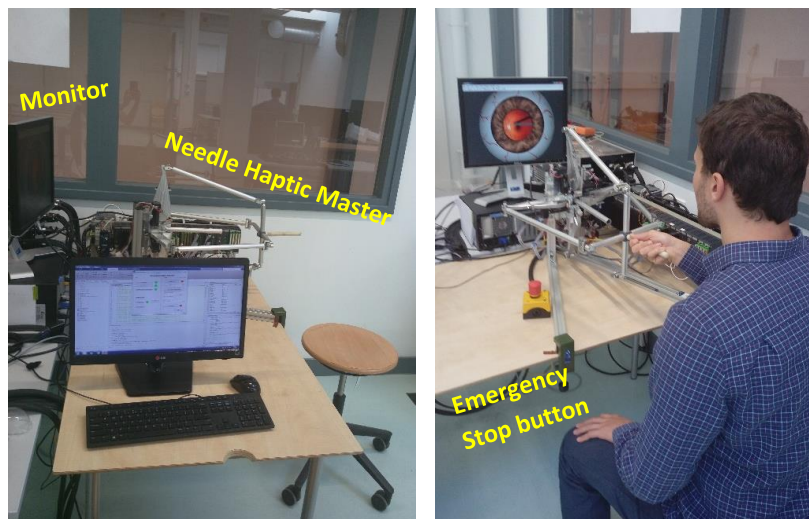


Figure 1: Experimental setup overview

Procedure

Before starting the experiment, you will be asked to carefully read and sign this consent form as well as to fill out some personal details. Including familiarization with the simulator, the total length will be approximately one hour.

0. Familiarization

To begin, you will be provided with introduction about the haptic device and the eye surgery simulator. A setup overview is shown in figure 1. It is this phase that you could adjust your seat to a proper height so that you can manipulate the handle in the most comfortable manner you like.

Following up is a training before the real experiment starts:

1. Training

To complete training session, you have to acquire sufficient high score (based on the performance metrics in the simulator) at least once without haptic feedback to show that you are familiar with both the device and the task. The task is a simplified epiretinal membrane peeling.

A standard procedure has three phases: (1) Initiate an initial flap; (2) Peel the membrane until the root of the membrane reaches goal position; however, during (2), the membrane will break if you apply excessive force. In this case, you have to (3) re-grab the flap.

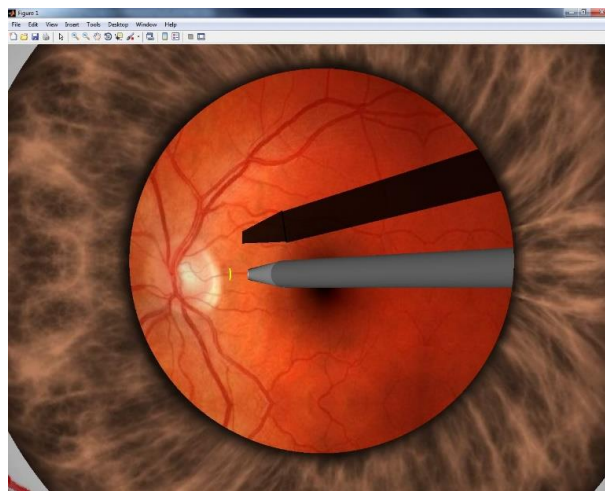


Figure 2: Reaching a small target during Flap Init phase

(1) Flap Initiation

As shown in fig.2, initiating a flap of the membrane is simplified as reaching a small ring-shaped target located at a fixed position. Every new trial starts with this task.

(2) Membrane Peeling

Every time a ring-shaped target is reached, the task enters peeling phase. Fig.3 shows the suggested circular peeling trajectory and the goal. You are asked to peel the membrane according to this path. A performance metric is displayed on the screen to provide immediate feedback to the participant. Four key elements determine the score:

- (1) **Peeling angle:** The angle between the membrane and the spherical eye surface has to be kept as small as possible (you can relate this mechanism to peeling off dried white glue on your hand if you had this experience in your childhood), otherwise the score will not accumulate.
- (2) **Time:** The longer you pull a thin membrane attached to the retina, the higher the risk you damage it. Therefore, the score leaks away as time goes by.
- (3) **Puncture:** Any puncture during the surgery will be penalized with a 10-point deduction. It might seem frustrating at first glance but if you think of how serious penetrating a patient's retina in real life could be, it is very mercy.
- (4) **Complete full length in each peel:** A 25-point bonus will be granted if you make a 2.5mm full length membrane during each peeling. The trajectory is designed such that a participant has four chances to complete a 2.5mm full length peeling. (See fig.4)

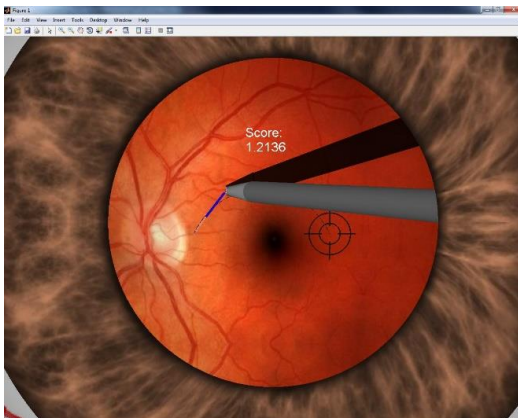


Figure 3: Image of peeling phase

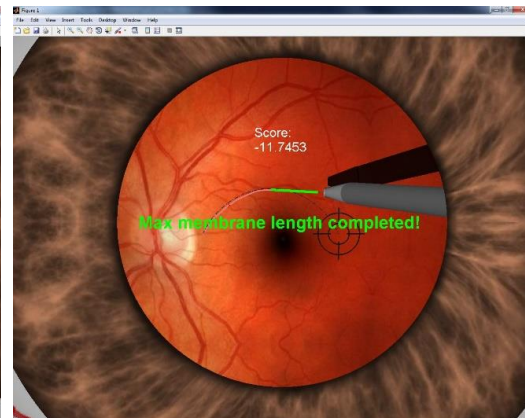


Figure 4: Image showing full membrane length is reached

(3) Re-grab phase

As mentioned earlier, any penetration (see fig.5) or dropping the membrane due to excessive force leads to re-grab phase. In this phase, the ring target will be larger than Flap Init phase. Once the large target is reached, you are back to peeling phase and continue to pursue the goal.

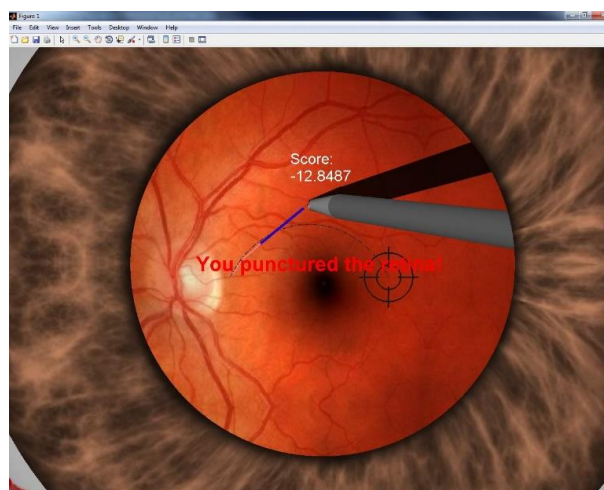


Figure 5: Release the handle if you penetrate the retina

2. Epiretinal Membrane Peeling

Similar to training, all you have to do is to take enough break and give your best shots in real experiment. After the first two trials, you will be provided with three different haptic feedback and complete four trials for each condition.

Risks

Risks associated with the study are small. The movement of the shoulder is only in the order of a few centimetres and the handle is protected from making larger movements. Before participating in the study, the researcher will assess whether you are capable of finishing the study.

Participation is voluntary!

Your participation in the study is voluntary. If you agree on participating in the study, you have the right to withdraw at any time (also during the study). There is no need to have a legitimate reason to do so.

Confidentiality

Your personal details and data are fully confidential. People not authorised to access your details will not have the opportunity to do so. The experimental results will be statistically analysed and published in a Master thesis, and potentially be used in a scientific publication as while. When the results of the study get published, it is impossible to trace these back to you.

Contact information

Should you have any questions concerning the experiment, please contact the researcher:

Tse-Kang Shen (Stan)

T: +31649327103

E: T.shen@student.tudelft.nl

I have read and understood the information provided above.

I give permission to process the data for the purposes described above.

I voluntarily agree to participate in this experiment.

Name:

Date:

Signature of the participant:

H.3. Final Experiment

HUMAN SUBJECT RESEARCH: INFORMED CONSENT

For a study investigating Haptic Feedback for Tele-operated Vitreoretinal Surgery

Date 28-08-2018, Version Final Exp. 1.0

Before agreeing to participate in this study it is important that the information in this document is carefully read and understood. This document will describe the purpose, procedures, risks and possible discomforts of this experiment.

Location of the experiment

Delft University of Technology
Department of Mechanical Engineering
Mekelweg 2, Delft
Cognitive Robotics Lab, Room 34 F-0-220

Study background

Vitreoretinal surgery (surgery taken place in the posterior eye) remains one of the most challenging procedures now in clinical practice. It requires precise and accurate motion control and extremely high hand-eye coordination. Moreover, the delicate and fragile nature of human eye not only makes any scratch on the retina impermissible but deprives the force feeling when interacting with eye tissue. The goal of this research is to investigate whether haptic feedback can aid retinal surgery. The participant will be asked to control a needle steering haptic master (see figure.1) to perform simulated task (computer program) that resembles retinal surgery.

Study goal

The purpose of this experiment is to compare the outcome of participants performing a simulated membrane peeling surgery between a proposed haptic shared control method and the baseline (no haptic feedback).

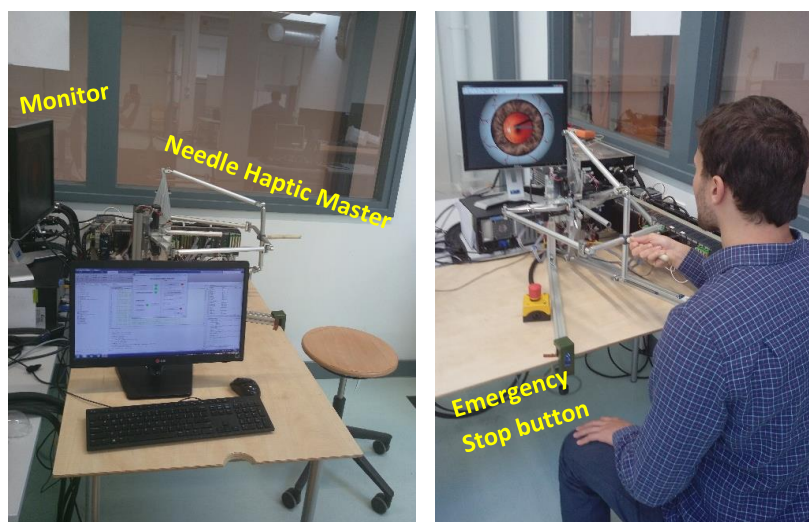


Figure 1: Experimental setup overview



Procedure

Before starting the experiment, you will be asked to carefully read and sign this consent form as well as to fill out some personal details. Including familiarization with the simulator, the total time will be around 60 – 80 minutes depending on the training time each participant needs.

0. Familiarization

To begin, you will be provided with introduction about the haptic master device and the eye surgery simulator. A setup overview is shown in figure 1. It is this phase that you could adjust your seat to a proper height so that you can manipulate the handle in the most comfortable manner you like.

Following up is a training session before the real experiment starts:

1. Training

Depending on the group assigned, you will start the training with or without haptic feedback. To complete the training session, you have to practice for at least 20 minutes and complete one task within 2:30 minutes. The task is a simplified version of epiretinal membrane peeling.

A standard procedure of which has three phases: (1) Initiate an initial flap; (2) Peel the membrane until the root of the membrane reaches goal position; however, during (2), the membrane will break if you apply excessive force. In this case, you have to (3) re-grab the flap.

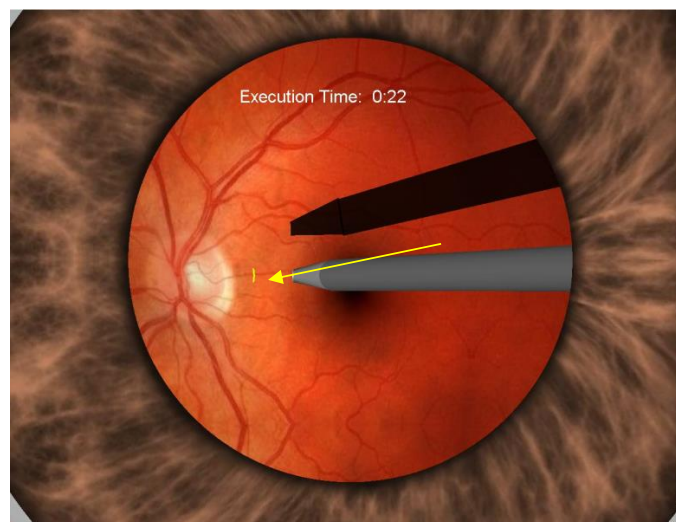


Figure 2: Reaching a small target during *Flap Init* phase. The yellow arrow indicates the motion you have to make so as to reach the ring-shaped target. You will not see the arrow in the simulator.

(1) Flap Initiation

As shown in figure 2, initiating a flap of the membrane is simplified as reaching a small ring-shaped target located at a fixed position. Every new trial starts with this task.

(2) Membrane Peeling

Every time a ring-shaped target is reached, the task enters peeling phase. First, you should notice that a suggested circular trajectory and the goal appear. You are asked to peel the membrane following this path. Also, as shown in figure 3, there are visualized data at the lower part of the screen. These numbers are present to speed up the learning process for peeling motion.

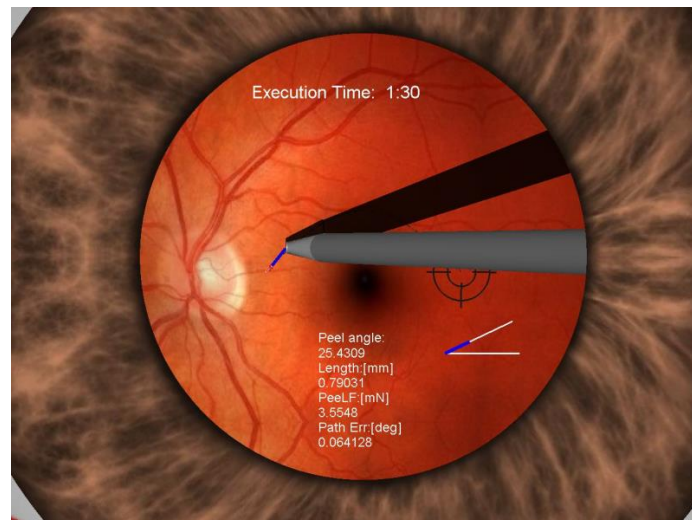


Figure 3: Visual support you will have once entering peeling phase (only provided every other training trial). From top to bottom are: Peeling angle, Membrane length, Membrane force, and the deviation from suggestion path (in spherical coordinate). On the left you see a visualization of current peeling angle, membrane length and membrane force.

The goal of training session is to learn how to use the shadow of the tool and the color of the membrane as useful visual feedback for membrane peeling task. However, the visualized information will not be displayed in real task. Therefore, you will only be provided with these additional visual supports every other trial during training, until you are able to complete the task within 2:30 minutes without support.

(3) Re-grab phase

As mentioned earlier, any penetration (see fig.4) or dropping the membrane due to excessive force leads to re-grab phase. In this phase, the ring target will be larger than Flap Init phase. Once the large target is reached, you are back to peeling phase and continue to pursue the goal.

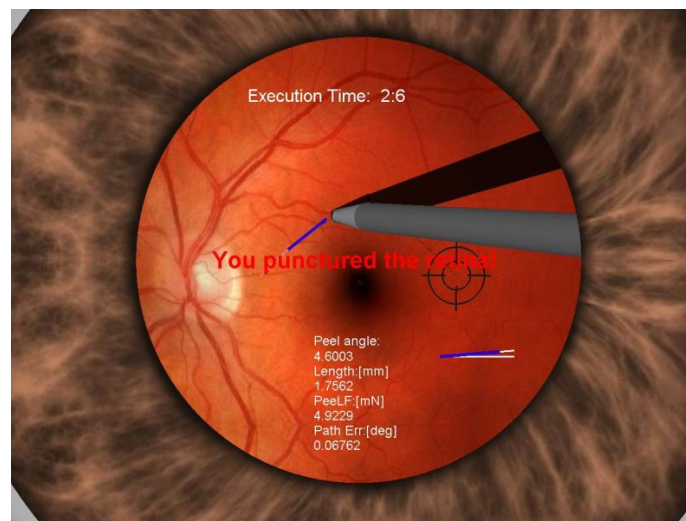


Figure 4: Release the handle if you penetrate the retina

2. Epiretinal Membrane Peeling

Similar to training, all you have to do is to take enough break and perform at your best. After every two trials, you will switch a condition (alternates between HSC and baseline). You will complete 6 trials for each condition in total.

A performance metric is displayed on the screen to provide immediate feedback to the participant about how well the procedure is going on. Five key elements determine the score:

- (1) **Peeling angle:** The angle between the membrane and the spherical eye surface has to be kept as small as possible (you can relate this mechanism to peeling off dried white glue on your hand if you had this experience in your childhood), otherwise the score will not accumulate.
- (2) **Time:** The longer you pull a thin membrane attached to the retina, the higher the risk you damage it. Therefore, the score leaks away as time goes by.
- (3) **Path error:** You are required to peel the membrane according to a circular path. The more deviation the root of the membrane is to the suggested path, the less score you are likely to accumulate.
- (4) **Puncture:** Any puncture during the surgery will be penalized with a 10-point deduction. It might seem frustrating at first glance but if you think of how serious penetrating a patient's retina in real life could be, it is very mercy.
- (5) **Complete full length in each peel:** A 25-point bonus will be granted if you make a 2.2mm full length membrane during each peeling. The trajectory is designed such that a participant has five chances to complete a 2.2 mm full length peeling. (See fig.4)

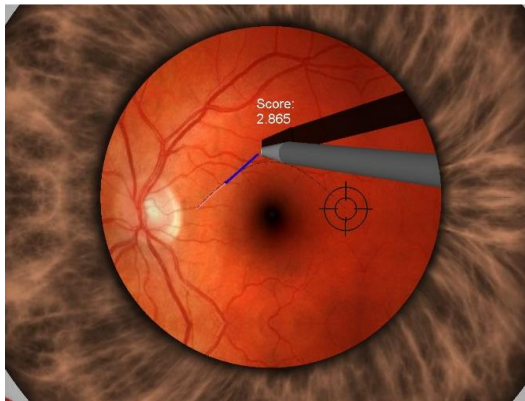


Figure 5: Image of peeling phase

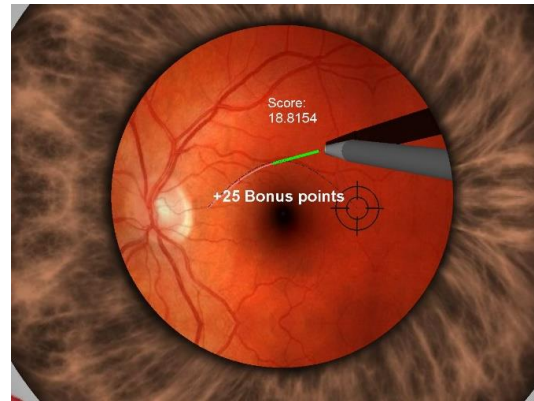


Figure 6: Image showing full membrane length is reached

Risks

Risks associated with the study are small. The movement of the shoulder is only in the order of a few centimetres and the handle is protected from making larger movements. All electronics and moving or fragile parts are covered. Before participating in the study, the researcher will assess whether you are capable of finishing the study.

Participation is voluntary!

Your participation in the study is voluntary. If you agree on participating in the study, you have the right to withdraw at any time (also during the study). There is no need to have a legitimate reason to do so.

Confidentiality

Your personal details and data are fully confidential. People not authorised to access your details will not have the opportunity to do so. The experimental results will be statistically analysed and published in a Master thesis, and potentially be used in a scientific publication as well. When the results of the study get published, it is impossible to trace these back to you.

Contact information

Should you have any questions concerning the experiment, please contact the researcher:

Tse-Kang Shen (Stan)

T: +31649327103

E: T.shen@student.tudelft.nl

*I have read and understood the information provided above.
I give permission to process the data for the purposes described above.
I voluntarily agree to participate in this experiment.*

Name:

Date:

Signature of the participant:

H.4. Personal Information Sheet



Participant Personal Information

This information is confidential and will not be made available to third parties.

Personal information

Participant number :
 Age :
 Gender : M / F
 Dominant arm : Right / Left
 Experienced with the Needle Steering Haptic Device : Yes / No
 Experiment participated : Pilot 1 / Pilot 2 / Final

Start experiment :
 Training time :
 End experiment :
 Total experiment time :

